RSC Advances

REVIEW

View Article Online
View Journal | View Issue

Open Access Article. Published on 22 July 2025. Downloaded on 10/28/2025 10:32:42 AM.
This article is licensed under a Creative Commons Attribution-NonCommercial 3.0 Unported Licence.

Check for updates

Cite this: *RSC Adv.*, 2025, **15**, 26138

Biophotonic (nano)structures: from fundamentals to emerging applications

Masoomeh Amoozadeh,[a] Amirali Hariri,[b] Atefeh Zarepour,[cd] Arezoo Khosravi,[ef] Siavash Iravani *[g] and Ali Zarrabi *[h]

Biophotonics is a dynamic interdisciplinary field that merges biology, photonics, and optics to explore and manipulate biological systems through light. Its applications are particularly prominent in medical diagnostics, imaging, and therapy. Key uses of biophotonic (nano)structures include enhancing medical imaging and enabling biosensing to detect disease markers. In therapeutic contexts, these nanostructures show significant promise in photothermal and photodynamic therapies, improving imaging contrast and allowing for real-time monitoring of cellular processes. However, the field faces challenges such as fabrication complexities, scalability, biocompatibility, and integration with existing technologies. For instance, limited biocompatibility can lead to adverse immune responses or toxicity, hindering their safe use *in vivo*, while scalability issues restrict the mass production of nanostructures with consistent quality, both of which are critical for clinical translation. Moreover, integrating these materials with existing medical devices or workflows often requires redesigning current platforms, slowing down adoption. Despite these obstacles, the future of biophotonics appears promising, especially with advancements in nanotechnology, including 3D printing and self-assembly, which could streamline production. The potential integration of biophotonic nanostructures with emerging technologies like wearable devices and point-of-care diagnostics could revolutionize healthcare by facilitating continuous health monitoring and rapid disease detection. This review aims to provide a thorough examination of biophotonic nanostructures and their emerging applications in disease diagnosis, imaging, and therapy. Additionally, it will address the challenges and future directions of biophotonic research, enhancing our understanding of how these innovative technologies can tackle critical issues in modern medicine and deepen our knowledge of complex biological systems.

Received 10th May 2025
Accepted 14th July 2025

DOI: 10.1039/d5ra03288a

rsc.li/rsc-advances

1 Introduction

The convergence of nanotechnology, photonics, and biology has led to significant breakthroughs in science and technology, leading to the emergence of the interdisciplinary field of biophotonics.[1] Optical detection is at the core of biophotonics, enabling the identification and monitoring of biological signals with high sensitivity, specificity, and spatial resolution. By capturing real-time signals from biomolecular markers, cells, pathogens, and tissues, optical detection facilitates early diagnosis and effective management of diseases, including cancer and infectious disorders. This rapidly growing domain utilizes the interaction of light with biological systems, opening new frontiers for probing, imaging, diagnosing, and treating complex biological processes. Unlike conventional detection methods, optical techniques overcome the light–matter interactions such as fluorescence, reflectance, and scattering, providing a non-invasive and label-free alternative for studying biological systems.[2,3]

The history of biophotonics is deeply rooted in the development of optical detection and imaging technologies. The advent of fluorescence microscopy in the early 20th century marked a turning point, allowing scientists to visualize biological processes with unprecedented detail. Subsequent innovations in laser technology and spectroscopy further expanded the capabilities of optical methods, enabling researchers to study

[a]Department of Chemistry, University of Isfahan, Isfahan 81746, Iran
[b]Department of Pharmaceutical Biotechnology, School of Pharmacy and Pharmaceutical Sciences, Isfahan University of Medical Sciences, Isfahan, 8174673461, Iran
[c]Department of Biology, Faculty of Arts and Sciences, Kocaeli University, İzmit, Kocaeli, 41001, Türkiye
[d]Department of Research Analytics, Saveetha Dental College and Hospitals, Saveetha Institute of Medical and Technical Sciences, Saveetha University, Chennai 600 077, India
[e]Department of Genetics and Bioengineering, Faculty of Engineering and Natural Sciences, Istanbul Okan University, Istanbul 34959, Türkiye
[f]Graduate School of Biotechnology and Bioengineering, Yuan Ze University, Taoyuan 320315, Taiwan
[g]Independent Researcher, W Nazar ST, Boostan Ave, Isfahan, Iran. E-mail: siavashira@gmail.com
[h]Department of Biomedical Engineering, Faculty of Engineering and Natural Sciences, Istinye University, Istanbul 34396, Türkiye. E-mail: alizarrabi@gmail.com

© 2025 The Author(s). Published by the Royal Society of Chemistry

Open Access Article. Published on 22 July 2025. Downloaded on 10/28/2025 10:32:42 AM.
This article is licensed under a Creative Commons Attribution-NonCommercial 3.0 Unported Licence.

dynamic biological processes in real-time.[4,5] Biophotonic nanostructures are engineered materials with at least one dimension in the nanometer range that exhibit unique properties, including enhanced optical behavior, high surface-to-volume ratios, and quantum confinement effects, which enable precise manipulation of light–matter interactions.[6] Unlike their bulk counterparts, nanostructures allow the design of highly specialized optical systems capable of probing biological entities with exceptional sensitivity and specificity. Indeed, by integrating nanoscale materials and devices with photonic principles, transformative tools are prepared for tackling critical challenges in optoelectronics as well as the healthcare and environmental monitoring. The applications of these nanostructures range from real-time visualization of cellular processes to the development of advanced therapeutic modalities, enabling non-invasive imaging, ultra-sensitive biosensing, and targeted therapeutic delivery.[4,7] In this context, nanoscale materials, such as quantum dots (QDs), metallic nanoparticles (NPs), and photonic crystals, provide exceptional optical properties such as surface plasmon resonance (SPR), localized electromagnetic field enhancement, and photonic bandgap effects that have proven instrumental in biomedical imaging, sensing, and therapy.[7–12] Biophotonic nanostructures (Table 1) have significantly enhanced the capabilities of optical detection systems. For instance, plasmonic NPs amplify electromagnetic fields at their surfaces, enabling highly sensitive detection of biomolecules through techniques like surface-enhanced Raman spectroscopy (SERS).[13,14] QDs, known for their size-dependent photoluminescence, are widely used as fluorescent probes for imaging intracellular processes with unparalleled spatial and temporal resolution.[15,16] Photonic crystals, with their ability to manipulate light propagation, have been employed in designing advanced optical filters and biosensors.[17,18] Plasmonic NPs have revolutionized optical sensing techniques, enabling real-time detection of biomolecular interactions with femtomolar sensitivity. Similarly, photonic crystals have been employed for designing biosensors capable of detecting trace amounts of biomarkers in complex biological environments.[19,20] In imaging, QDs have enabled multiplexed fluorescence imaging, providing insights into cellular dynamics and molecular interactions.[21,22] Furthermore, tissue-based lasers, utilizing the scattering properties of biological tissues, have demonstrated potential for distinguishing between healthy and malignant tissues.[23,24] The laser-emission-

Table 1 Comparison of biophotonic nanostructures for biomedical applications

Nanostructure type	Examples	Advantages	Limitations	Key applications	Ref.
Plasmonic NPs	AuNPs, AgNPs	High photothermal conversion efficiency; tunable LSPR; strong field enhancement	Phototoxicity; limited penetration depth; aggregation in biological fluids	Photothermal therapy, SERS biosensing, photoacoustic imaging	48 and 49
Upconversion NPs (UCNPs)	NaYF4: Yb, Er/Tm doped UCNPs	Anti-stokes emission; deep tissue penetration; photostability	Low quantum yield; complex synthesis; surface quenching	Deep-tissue imaging, photodynamic therapy	50 and 51
QDs	CdSe/ZnS, InP/ZnS	Size-tunable emission; high brightness; multiplex imaging	Cytotoxicity (heavy metals); blinking; clearance issues	Fluorescence imaging, targeted diagnostics	8 and 52
Photonic crystals	2D or 3D periodic dielectric structures	Wavelength-selective reflection; structural color; label-free detection	Difficult fabrication; angle-dependent signal	Optical biosensing, real-time analyte monitoring	53 and 54
DNA nanostructures	DNA origami, DNA wires	Precise programmability; biocompatibility; responsive design	Nuclease degradation; stability *in vivo*	Förster resonance energy transfer (FRET) sensors, smart drug delivery, logic-gate biosensing	6 and 55
Organic fluorescent dyes	Cy5, Alexa Fluor, IR-800	Established biolabels; high quantum yield; available in near-infrared (NIR)	Photobleaching; nonspecific binding; short circulation time	Fluorescence-guided surgery, immunofluorescence	55
Carbon-based nanostructures	Carbon dots, CNTs, graphene QDs	Low toxicity; stable fluorescence; biodegradability	Surface functionalization needed; limited control over emission properties	Multimodal imaging, photothermal therapy (PTT)/photodynamic therapy (PDT) platforms	56
Polymeric nanostructures	Conjugated polymer NPs (CPNs)	High brightness; tunable emission; good stability in aqueous media	Batch-to-batch variation; lower tissue penetration in visible range	Optical tracking, imaging-guided delivery	57
MXene nanostructures	$Ti_3C_2T_x$ nanosheets	Strong photothermal effect; excellent NIR absorption	Oxidation instability; potential cytotoxicity	NIR-II PTT, hybrid imaging-therapy	58
Hybrid structures	Core–shell Au@UCNPs, DNA-AuNP hybrids	Multifunctionality; synergistic optical behavior	Complex fabrication; reproducibility issues	Theranostics, biosensing, dual-modality imaging	59

Open Access Article. Published on 22 July 2025. Downloaded on 10/28/2025 10:32:42 AM.
This article is licensed under a Creative Commons Attribution-NonCommercial 3.0 Unported Licence.

based microscope (LEM) is an innovative tool that combines high-resolution imaging with precise detection of tumor biomarkers, facilitating early cancer diagnosis.[24,25] In therapeutic applications, biophotonic nanostructures have shown promise in photodynamic therapy, where photosensitizer-loaded NPs generate reactive oxygen species upon light activation, selectively killing cancer cells.[26,27] Additionally, optogenetics—a technique that combines light-sensitive proteins with optical stimulation—has revolutionized neuroscience by enabling precise control of neural activity.[28,29] One of the important points in this context is the selection of materials that have a key role in defining the performance and functionality of biophotonic nanostructures. Conventional materials like silica, glass, and polymeric nanowires have been widely employed in the fabrication of optical waveguides, sensors, and fiber-optic devices. These materials offer excellent transparency, mechanical strength, and ease of fabrication, that render them appropriate for different applications, including deep-tissue imaging and fiber-optic bioimplants.[30–34]

Despite these advancements, several limitations remain in the development and application of biophotonic nanostructures. One major challenge is the scalability and cost-effectiveness of nanomaterial synthesis, particularly for clinical translation. Ensuring long-term biocompatibility and stability of biophotonic devices in complex biological environments is another critical issue. Indeed, the limited biocompatibility and biodegradability of these materials pose challenges for *in vivo* applications. Moreover, the integration of these devices into existing medical workflows requires standardized protocols and rigorous validation.[35] Recent innovations in material science and device fabrication have addressed some of these challenges. For instance, researchers have explored naturally derived biomaterials, such as DNA, proteins, silk, and polysaccharides, which exhibit remarkable optical properties, biological compatibility, and degradability.[36–38] Green fluorescent protein (GFP) and riboflavin have been employed as gain media in biological lasers, while silk-based photonic structures have demonstrated potential for creating biocompatible optical devices.[39–43] The integration of biophotonic nanostructures with biological entities, such as cells, viruses, and tissues, has opened new avenues for designing hybrid systems.[44–46] These bio-inspired and biologically derived materials enable the construction of photonic devices that seamlessly interface with living systems, enhancing their functionality and adaptability for biomedical applications.[46] The development of self-assembled nanostructures and 3D-printed biocompatible materials has paved the way for scalable and customizable biophotonic devices. Hybrid systems that combine plasmonic NPs with responsive polymers offer tunable optical properties, enhancing their functionality for targeted diagnostics and therapy.[47]

The aim of this review is to provide an overview about the recent advancements and emerging applications of biophotonic nanostructures *via* focusing on their applications in disease diagnosis, imaging, and therapy. To this aim, the integration of biophotonic nanostructures in optoelectronics has been explored *via* highlighting their contributions to light-emitting diodes (LEDs), photodetectors, and other photonic devices. Furthermore, the challenges associated with their design, synthesis, and clinical translation have been discussed, offering insights into potential future directions for this rapidly evolving field. By bridging the gap between photonics, biology, and materials science, biophotonic nanostructures hold immense potential for developing healthcare and advancing our understanding of complex biological systems. Through this review, we aim to highlight the transformative impact of these nanostructures on science and technology, emphasizing their role in addressing some of the most pressing challenges in modern medicine.

2 Biophotonic nanostructures: synthesis, photophysical properties, and structure–function relationships

2.1 Synthesis

The synthesis of biophotonic nanostructures necessitates precise control over size, shape, composition, crystallinity, and surface chemistry to fulfill the dual demands of optical functionality and biological compatibility. Each class of nanomaterial employed in biophotonics, including plasmonic NPs, QDs, upconversion NPs (UCNPs), carbon-based dots, and MXenes, requires tailored synthetic protocols that ensure reproducibility, scalability, and biofunctionality. This section reviews the most advanced and widely adopted synthesis methods used for each of these materials, highlighting their critical chemical parameters, fabrication mechanisms, and post-synthesis modifications relevant to biomedical applications.

2.1.1 Plasmonic NPs: gold and silver. Gold (Au) and silver (Ag) NPs are primarily synthesized *via* wet chemical reduction, with meticulous control over nucleation and growth kinetics. The classical methods employ trisodium citrate to reduce $HAuCl_4$ at boiling temperatures, yielding spherical AuNPs in the 10–40 nm range. This process allows partial control over particle size *via* pH and reactant ratio adjustment. For anisotropic shapes such as nanorods, nanostars, and triangular prisms, seed-mediated growth in the presence of surfactants like cetyltrimethylammonium bromide (CTAB) is used.[60] In this method, small spherical seeds (~2–4 nm) are first prepared, followed by their overgrowth in a growth solution containing Au ions, ascorbic acid (a mild reducing agent), and shape-directing additives such as Ag^+ ions to modulate the aspect ratio and induce anisotropy.[61] Shape-controlled synthesis of AgNPs is similarly achieved using polyol processes where ethylene glycol acts as both reducing agent and solvent, with polyvinylpyrrolidone (PVP) serving as a stabilizer. pH, temperature, and ion concentration critically influence morphology.[62] Post-synthesis, ligand exchange is essential for biomedical utility, as CTAB is cytotoxic. AuNPs are often functionalized *via* thiol-terminated polyethylene glycol (PEG-SH), antibodies, or oligonucleotides, using robust Au–S bonds for stability in physiological environments.[63–65]

 © 2025 The Author(s). Published by the Royal Society of Chemistry

Open Access Article. Published on 22 July 2025. Downloaded on 10/28/2025 10:32:42 AM. This article is licensed under a Creative Commons Attribution-NonCommercial 3.0 Unported Licence.

2.1.2 Quantum dots (QDs). Quantum dots (QDs) such as CdSe/ZnS or InP/ZnSe are typically synthesized by hot-injection colloidal methods, in which organometallic precursors are rapidly introduced into coordinating solvents at elevated temperatures (220–300 °C). For CdSe synthesis, a selenium precursor dissolved in trioctylphosphine (TOP) is injected into a mixture containing cadmium oleate and trioctylphosphine oxide (TOPO). Size control is achieved by adjusting growth time and precursor ratios, which directly influence the quantum confinement and emission wavelength.[66,67] To enhance stability and quantum yield, QDs are often coated with a ZnS shell *via* successive ion layer adsorption and reaction (SILAR) methods. This core–shell architecture reduces surface trap states and prevents photobleaching. Environmentally benign QDs (*e.g.*, InP) are now preferred for clinical translation due to the reduced toxicity of indium compared to cadmium.[68,69] For aqueous solubility and biocompatibility, ligand exchange with hydrophilic molecules (*e.g.*, mercaptoacetic acid, dihydrolipoic acid) or polymer encapsulation using amphiphilic block copolymers (*e.g.*, PMAO) is employed. These surface treatments improve circulation time and enable bio-conjugation.

2.1.3 Upconversion NPs (UCNPs). In UCNPs, such as $NaYF_4$ doped with Yb^{3+} and Er^{3+} or Tm^{3+}, high-temperature (typically 300–330 °C) thermal decomposition of lanthanide trifluoroacetate precursors in hydrophobic solvents like oleic acid and 1-octadecene is used as the most traditional fabrication method. This yields monodisperse, highly crystalline particles with hexagonal (β-phase) structure, known for superior upconversion efficiency compared to the cubic (α-phase).[70–72] To enhance luminescence and reduce surface quenching, an inert shell layer (*e.g.*, $NaYF_4$) is grown epitaxially around the core using the same decomposition approach or solvothermal methods. This core–shell structure increases quantum yield by shielding sensitizer-activator pairs from surface defects and water molecules.[70,71] In a recent study by Xu *et al.* (2024), a facile one-pot solvothermal synthesis method was developed for the large-scale production of biocompatible, water-soluble UCNPs composed of $NaYF_4$ co-doped with Yb^{3+} and Er^{3+} ions. The procedure began by preparing a reaction mixture containing lanthanide oleates (derived from Y^{3+}, Yb^{3+}, and Er^{3+} nitrates) and sodium fluoride (NaF) as the fluorine source, all dispersed in 1-octadecene (ODE) as the high-boiling non-polar solvent. To impart water dispersibility and improve biocompatibility, poly(ethylene glycol) bis(carboxymethyl) ether (HOOC–PEG–COOH) was introduced as a functional surfactant during the synthesis. This PEG ligand enabled simultaneous surface passivation and aqueous compatibility, circumventing the need for post-synthesis ligand exchange.[72] The reaction was carried out under a nitrogen atmosphere and involved a three-stage heating protocol: initial heating at 135 °C for 1 hour ensured complete solubilization and precursor complexation; followed by 200 °C for 30 minutes to promote nucleation; and a final 310 °C for 1 hour to facilitate full crystallization of the hexagonal β-phase $NaYF_4$ nanocrystals. This *in situ* surface PEGylation approach enhanced colloidal stability through covalent coordination between the carboxylic acid groups and surface lanthanide ions, while the long hydrophilic PEG chains prevented aggregation and reduced opsonization. The resulting NPs exhibited a uniform spherical morphology with an average size of ∼50 nm as confirmed by TEM, high crystallinity as indicated by XRD, and consistent water dispersibility with excellent stability in physiological media such as PBS and NaCl solutions. Notably, this synthesis method allowed batch-scale fabrication of up to 40 grams per run with minimal purification steps, marking a significant advancement in the scalable production of UCNPs for biomedical applications.[72] UCNPs are rendered water-dispersible using silica coating (Stöber method), ligand oxidation, or amphiphilic polymer wrapping, followed by surface modification with targeting ligands (*e.g.*, folic acid, peptides). Their non-blinking, narrow-band emission under NIR excitation makes them ideal for deep-tissue imaging.[71,72]

2.1.4 Carbon dots and graphene QDs. Carbon dots (CDs) and graphene QDs (GQDs) are synthesized *via* bottom-up carbonization of organic precursors under hydrothermal, solvothermal, or microwave-assisted conditions. Common feedstocks include citric acid, ethylenediamine, glucose, and even biomass waste. A standard method involves heating a citric acid/ethylenediamine mixture at 180 °C for 6–8 hours in a Teflon-lined autoclave, yielding blue-emissive nitrogen-doped CDs.[73,74] The emission properties of CDs depend on surface functional groups, heteroatom doping (N, S, P), and degree of graphitization. Post-synthetic passivation with PEG or PEI improves quantum yield and biological compatibility. GQDs are typically derived by oxidative cleavage of graphene oxide sheets, using concentrated HNO_3 or $KMnO_4/H_2SO_4$ treatment followed by ultrasonication and filtration.[73,74] A novel and innovative approach for synthesizing carbon-based QDs involves the use of pulsed laser ablation in liquid (PLAL), which has gained increasing attention due to its simplicity, environmental friendliness, and ability to produce high-purity nanomaterials. In this top-down laser-based method, a high-intensity pulsed laser—typically a Nd: YAG system—is focused on a solid carbonaceous target (such as graphite rods or graphene oxide films) immersed in a liquid medium. The rapid energy deposition at the solid–liquid interface induces localized plasma formation, explosive evaporation, and subsequent nucleation of carbon nanostructures. The process enables precise control over the particle size (generally in the 2–10 nm range), crystallinity, and surface functionality of the generated carbon or graphene QDs. The choice of liquid environment, laser wavelength and pulse duration, and irradiation parameters allows fine-tuning of optical properties such as fluorescence wavelength and quantum yield—making this method particularly attractive for biomedical imaging and sensing.[75] An excellent demonstration of this technique was provided by Zhang *et al.* In their study, GQDs were synthesized from graphite rods using a nanosecond-pulsed Nd: YAG laser in deionized water, with varying laser fluence to control dot size and emission characteristics. The resulting GQDs exhibited narrow size distribution (∼3–5 nm), blue-green fluorescence, and high stability under UV excitation. Spectroscopic analysis (UV-vis, FTIR, Raman) confirmed sp^2 carbon networks with surface hydroxyl and

Open Access Article. Published on 22 July 2025. Downloaded on 10/28/2025 10:32:42 AM. This article is licensed under a Creative Commons Attribution-NonCommercial 3.0 Unported Licence.

carboxyl groups, enhancing water dispersibility. Notably, this PLAL approach enabled label-free, excitation-wavelength-tunable photoluminescence, suitable for imaging and sensing applications. Their findings underscore the potential of PLAL as a scalable, clean, and customizable method for QD fabrication with minimal environmental impact and high biomedical compatibility.[74,75]

2.1.5 MXenes. The conventional approach for MXene synthesis involves chemical etching with hydrofluoric acid (HF) or *in situ* generated HF, such as using a LiF + HCl mixture. In this method, Ti_3AlC_2 powder is immersed in the etchant to remove the Al layers, resulting in multilayered $Ti_3C_2T_x$ structures. To achieve few-layer or monolayer MXene sheets, the etched material undergoes intercalation with organic solvents such as dimethyl sulfoxide (DMSO) or tetramethylammonium hydroxide (TMAOH), followed by mild sonication to delaminate the layers. This yields colloidally stable suspensions of $Ti_3C_2T_x$ flakes with high surface area, suitable for a range of applications including drug delivery, biosensing, and photothermal therapy.[76–78] However, the reliance on HF presents serious health, environmental, and scalability challenges, prompting the development of alternative synthesis methods. One such innovative and safer method is electrochemical etching, which avoids the use of fluoride-based reagents. Besides, a fluoride-free electrochemical route was used in a recent study to synthesize $Ti_3C_2T_x$ MXenes. Their protocol employed a three-electrode system comprising Ti_3AlC_2 as the working electrode, a platinum counter electrode, and Ag/AgCl as the reference electrode in a 1 M ammonium chloride (NH_4Cl) electrolyte. Under a constant current density of 7.8 mA cm^{-2}, anodic oxidation facilitated the selective removal of Al atoms from the MAX structure. This method effectively preserved the integrity of the Ti_3C_2 basal planes, minimized environmental risk, and resulted in high-purity, delaminated MXene sheets. Subsequent intercalation with TMAOH and bath sonication yielded few-layer nanosheets with excellent dispersion in water.[79,80] Characterization of the resulting MXenes confirmed the complete etching of Al (*via* XRD), high electrical conductivity (~10 000 S m^{-1}), and large lateral dimensions (1–2 μm) as observed under TEM. Importantly, cytocompatibility assays using NIH-3T3 cells revealed >90% viability at concentrations up to 200 μg mL^{-1}, and zeta potential measurements demonstrated sustained colloidal stability for several weeks. These features underscore the potential of electrochemically synthesized MXenes for biomedical applications such as bioelectronics, imaging, and drug delivery systems.[79] Surface functionalization plays a pivotal role in the biomedical deployment of MXenes. During synthesis, surface terminations such as –OH, –O, and –F are naturally introduced, imparting hydrophilicity and reactivity. Further surface engineering techniques—such as PEGylation, protein adsorption (*e.g.*, albumin), or covalent conjugation with targeting ligands—enhance biocompatibility, extend blood circulation time, and enable specific targeting. Additionally, the intrinsic NIR absorption capability and photothermal conversion efficiency of MXenes position them as ideal candidates for photothermal cancer therapy, while their redox-active surfaces support ROS scavenging and biosensing functions.[79,80] Overall, the versatility in synthesis routes and functionalization strategies allows MXenes to be tailored for precise biomedical roles, ranging from imaging agents and drug carriers to phototherapeutic and diagnostic platforms.

2.2 Photophysical properties of biophotonic nanostructures

The photophysical properties of nanostructures define their interaction with electromagnetic radiation, influencing how they absorb, scatter, emit, and convert light. In biophotonics, understanding and engineering these properties is essential for developing systems for imaging, sensing, and therapeutic intervention. Each nanostructure class—plasmonic NPs, QDs, UCNPs, carbon-based nanodots (CDs/GQDs), and MXenes—exhibits unique optical behaviors governed by their electronic structure, geometry, and surface chemistry. For instance, plasmonic NPs (PNPs), particularly those composed of Au and Ag, exhibit localized surface plasmon resonance (LSPR). This phenomenon arises from the collective oscillation of conduction-band electrons in response to an external electromagnetic field. The resonance leads to intense light absorption and scattering at specific wavelengths, which are tunable by modifying particle shape, size, aspect ratio, and surrounding dielectric environment.[81] Spherical AuNPs typically display LSPR peaks around 520–530 nm. As the size increases (>50 nm), scattering dominates absorption. Au nanorods (AuNRs) exhibit two plasmon bands—transverse and longitudinal. By increasing the aspect ratio (length/diameter), the longitudinal band can be shifted deep into the NIR region (~700–1100 nm), which is essential for biological transparency windows. Au nanostars and nanocages, characterized by sharp tips and hollow interiors respectively, further amplify local electromagnetic fields through the "lightning rod" effect, enhancing applications in SERS and photothermal conversion.[82–84] The dielectric sensitivity of LSPR enables refractive index sensing with limits of detection down to 10^{-7} RIU. Additionally, these nanostructures can serve as heat transducers for PTT. Upon NIR excitation, absorbed energy is dissipated non-radiatively as heat, raising local temperatures to induce hyperthermia in diseased tissues. Notably, LSPR linewidths are narrower in AgNPs compared to AuNPs, resulting in sharper optical features, although Ag's poor stability in biological environments limits its utility.[85,86]

In the case of QDs, as the size reduces to the exciton Bohr radius, the energy levels discretize, resulting in a blue shift of emission. For instance, CdSe QDs ranging from 2 to 6 nm can emit across the visible spectrum (~450–650 nm). InP, a cadmium-free alternative, shows similar confinement properties and is gaining attention due to its lower cytotoxicity.[87] The core–shell architecture (*e.g.*, CdSe/ZnS) enhances quantum yield (QY) and photostability by passivating surface trap states. ZnS or CdS shells create a potential barrier for electrons and holes, preventing non-radiative recombination. Typical photoluminescence quantum yields reach 60–90% in optimized QDs.[88,89] QDs exhibit high absorption cross-sections (~10^{-14} cm^2), enabling efficient excitation with low light doses. Their narrow emission spectra and resistance to photobleaching make them ideal for multiplexed bioimaging. Additionally,

 © 2025 The Author(s). Published by the Royal Society of Chemistry

Open Access Article. Published on 22 July 2025. Downloaded on 10/28/2025 10:32:42 AM. This article is licensed under a Creative Commons Attribution-NonCommercial 3.0 Unported Licence.

blinking, a stochastic switching between emissive and non-emissive states, has been mitigated by thick-shell designs and core/alloy/shell strategies.[90,91] Surface ligands critically influence QD photophysics. Ligand exchange with thiol- or amine-terminated molecules imparts aqueous solubility and allows for bio-conjugation; however, improper exchange can reduce QY due to partial loss of passivation, necessitating careful optimization.[92]

UCNPs convert low-energy NIR photons into higher-energy visible or UV emission through nonlinear multiphoton absorption. This process is mediated by sensitizer ions (commonly Yb^{3+}) that absorb 980 nm or 808 nm light and transfer energy sequentially to activator ions (*e.g.*, Er^{3+}, Tm^{3+}, Ho^{3+}), leading to anti-stokes emission.[93,94] Emission spectra are composed of discrete narrow bands, such as green (~540 nm), red (~660 nm), or blue (~480 nm), depending on the activator. The β-phase hexagonal $NaYF_4$ is the most efficient host crystal, offering low phonon energy and high upconversion efficiency. Upconversion is sensitive to dopant concentration, so that excessive activator ions result in cross-relaxation quenching, while inadequate levels limit energy transfer efficiency. Therefore, an optimal ratio (*e.g.*, 20% Yb^{3+}, 2% Er^{3+}) is usually required.[95,96] Core–shell engineering is vital to mitigate surface quenching. Coating with inert $NaYF_4$ or $NaGdF_4$ shells increases emission intensity by 10–50 fold. Shells also enable multifunctionality, such as MRI contrast when Gd^{3+} is used.[97,98] UCNPs exhibit exceptional photostability, negligible autofluorescence, and deep tissue penetration due to NIR excitation, making them superior to QDs or organic dyes in long-term imaging and photo-triggered drug release.

CDs and GQDs display unique fluorescence originating from π–π transitions*, surface state emissions, and molecular fluorophores. Their emission is typically excitation-wavelength-dependent, a result of size heterogeneity and diverse surface traps.[99,100] CDs show tunable emission from blue to red, with quantum yields ranging from 10–80% depending on the synthesis method, precursor, and passivation. Nitrogen doping enhances QY by introducing mid-gap states that facilitate radiative recombination. CDs are resistant to photobleaching and exhibit strong two-photon absorption, useful for deep tissue imaging.[101,102] GQDs, derived from graphene oxide, exhibit intrinsic quantum confinement and edge effect-induced luminescence. Their planar sp^2 domains offer higher conductivity and robustness. Unlike CDs, GQDs can display structured, excitation-independent emission.[103,104] Photostability of CDs/GQDs is enhanced by surface passivation with polyethylene glycol (PEG), polyethylenimine (PEI), or other polymers. Their biocompatibility, rapid renal clearance, and easy surface modification make them promising candidates for targeted imaging and photodynamic therapy.[105]

Unlike conventional fluorescent NPs, MXenes do not rely on bandgap emission but exhibit strong broadband absorption across the UV-NIR range, stemming from free-carrier absorption and metallic conductivity.[106] Photothermal conversion efficiency (PCE) of MXenes, particularly $Ti_3C_2T_x$, can exceed 40% under 808 nm irradiation. This is attributed to their high NIR absorbance, high extinction coefficients (~10^9 M^{-1} cm^{-1}), and strong electron–phonon coupling. These features make MXenes ideal for photothermal therapy and optoacoustic imaging.[107,108] MXenes also serve as fluorescence quenchers due to their wide energy band and electron-donating surface. This property enables their application in FRET-based biosensors, where interaction with a fluorescent probe modulates signal.[109] However, MXenes have some challenges as well. For instance, the stability is a challenge; since MXenes can oxidize in aqueous media, leading to degradation. Antioxidant coatings or encapsulation with polymers (*e.g.*, polydopamine) can mitigate this. Their surfaces can be functionalized with PEG, albumin, or targeting ligands for improved circulation and cellular uptake. Table 2 shows a summary of different photonic compounds, their properties, and applications.

3 Biophotonic nanostructures in optoelectronics

3.1 Biophotonic and LEDs

LED have emerged as a superior alternative to incandescent and fluorescent lamps, offering unparalleled advantages in terms of energy efficiency, luminous output, and durability. Their growing dominance in both consumer and industrial markets over the past two decades has been driven by the adoption of innovative designs, such as widely utilization of blue LED chip combined with green and red light-emitting phosphors.[110] This setup operates by partially absorbing blue light through the phosphor, while the unabsorbed portion is transmitted directly. However, the environmental impact of rare-earth-based phosphors and the absence of effective recycling methods have driven growing interest in exploring organic and biological alternatives for LED development.[111]

Sensing mechanisms with bio-LEDs typically involve modulation of the light emission in response to biochemical changes. The integration of bio-recognition elements—such as pH-responsive dyes, enzymatic substrates, or redox-active layers—onto the emission surface allows the LED output to reflect specific biological cues. These interactions alter emission intensity, spectral characteristics, or lifetime through changes in refractive index, energy transfer efficiency, or photonic interference patterns. In advanced configurations, closed-loop circuits couple emission with feedback sensors, enabling real-time quantification of analytes like glucose, lactate, or reactive oxygen species.[112,113] In the context of bioimaging, bio-LEDs serve as precision illumination sources embedded in flexible or implantable platforms. Their ability to emit within the visible and NIR windows permits imaging at variable tissue depths while minimizing background scattering. When aligned with contrast-enhancing agents—such as QDs or lanthanide nanoprobes—the emitted light enhances imaging resolution and signal stability. Pulsed or modulated LED arrays can further support high-speed fluorescence imaging or structured illumination techniques, improving visualization of dynamic cellular processes.[112,114]

Hagen *et al.* first demonstrated the incorporation of biomaterials into LED systems in 2006 by employing DNA films

Open Access Article. Published on 22 July 2025. Downloaded on 10/28/2025 10:32:42 AM.
This article is licensed under a Creative Commons Attribution-NonCommercial 3.0 Unported Licence.

Table 2 Photonic properties and biomedical application of different types of different nanostructures

Types of nanomaterial	Size (nm)	Emission type	Excitation	Quantum yield	Photostability	Penetration depth	Toxicity concerns	Key applications	Ref.
Plasmonic NPs	10–100	Photoluminescence, plasmon-enhanced fluorescence, surface-enhanced Raman scattering, and heat	Visible/NIR	N/A (non-emissive)	Moderate	Low	Low (Au), high (Ag)	PTT, SERS, biosensing, drug delivery	48 and 49
QDs	2–10	Photoluminescence	UV-visible	High (60–90%)	High	Low-Moderate	High	Bioimaging, FRET, diagnostics, LEDs, solar cells, PDT	50 and 51
UCNPs	20–80	Upconversion luminescence	NIR (980/808 nm)	Moderate	Excellent	High	Low	Deep-tissue imaging, PDT, NIR-triggered drug delivery, upconversion lasers	8 and 52
CDs/GQDs	3–10	Fluorescence	UV-visible	Moderate	Good	Low	Low	Imaging, biosensors, photocatalysis, drug delivery, PDT	58
MXenes	100–1000	Fluorescence quenchers, photothermal conversion	NIR	N/A	Low	Moderate	Moderate	PTT, biosensing and imaging, antibacterial coatings, drug delivery, energy storage	109

as electron-blocking layers in organic light-emitting diodes (OLEDs), which significantly enhanced luminous efficiency.[115] This milestone marked the beginning of a new era in the use of biological components in electronic and photonic devices. In OLEDs, biomaterials have been employed both as white-emitting composite materials and as functional elements for enhancing luminous control. Recent research is advancing the frontiers of bio-LED technology, expanding its applications to include biological recognition and environmental responsiveness.[116] One key advancement in bio-LED technology involves leveraging organic dyes for energy transfer *via* FRET. Despite the promise of this mechanism, random dye distribution within films has historically hindered energy transfer efficiency. To overcome this, Benson *et al.*, introduced a bovine serum albumin (BSA) hydrogel framework, which precisely binds red, green, and blue dyes at discrete sites.[116] This arrangement regulates the spatial distribution of dyes, maintaining high local concentrations while preventing aggregation and quenching. By varying the molar ratios of the dyes, a stable white-emitting LED was achieved, capable of functioning in both dry and wet environments.

BSA hydrogels also exhibit remarkable adaptability to environmental stimuli such as pH, temperature, and ligand presence. Changes in these conditions alter the gel's swelling behavior, modifying the distances between donor and acceptor dyes and thereby disrupting FRET efficiency. As a result, the color of emitted light can be dynamically tuned, ranging from red in acidic conditions to white in neutral pH and green in basic environments. This versatility underscores the potential of bio-LEDs in applications requiring dynamic color modulation and responsiveness, opening new avenues for innovation in lighting and sensing technologies.[117,118]

Fluorescent proteins, a unique class of organic dyes, have also garnered significant attention for their role in biological and organic LED advancements. Efficient energy transfer in such systems depends heavily on the design of protein-based packaging.[119] Two primary approaches used in this context are included multilayered cascade coatings and micropatterned single-layer coatings of fluorescent proteins.[120,121] However, these methods are often hindered by labor-intensive fabrication processes and suboptimal light outcoupling in thicker layers. To address these challenges, Aguino *et al.*, engineered a single white fluorescent protein (FP) emitter vi linking the blue-, green-, and red-emitting proteins, expressed recombinantly in *Escherichia coli* (*E. coli*), that led to the photoluminescence quantum yield of about 26% and a stable white emission. The photoluminescence was modulated *via* changing the excitation wavelength, allowing for precise control of emission peaks at 450, 510, and 610 nm. Depending on the excitation range, emission intensities could shift to favor green and blue peaks, demonstrating the versatility of this system.[122] Building on these advancements, researchers designed high-performance white LEDs by utilizing red-emitting mScarlet and green-emitting eGFP fluorescent proteins (Fig. 1). By optimizing the concentration ratios of these proteins, they achieved a maximum color-rendering index of 92, highlighting the potential of protein-based systems for superior color fidelity.[123]

 © 2025 The Author(s). Published by the Royal Society of Chemistry

Open Access Article. Published on 22 July 2025. Downloaded on 10/28/2025 10:32:42 AM.
This article is licensed under a Creative Commons Attribution-NonCommercial 3.0 Unported Licence.

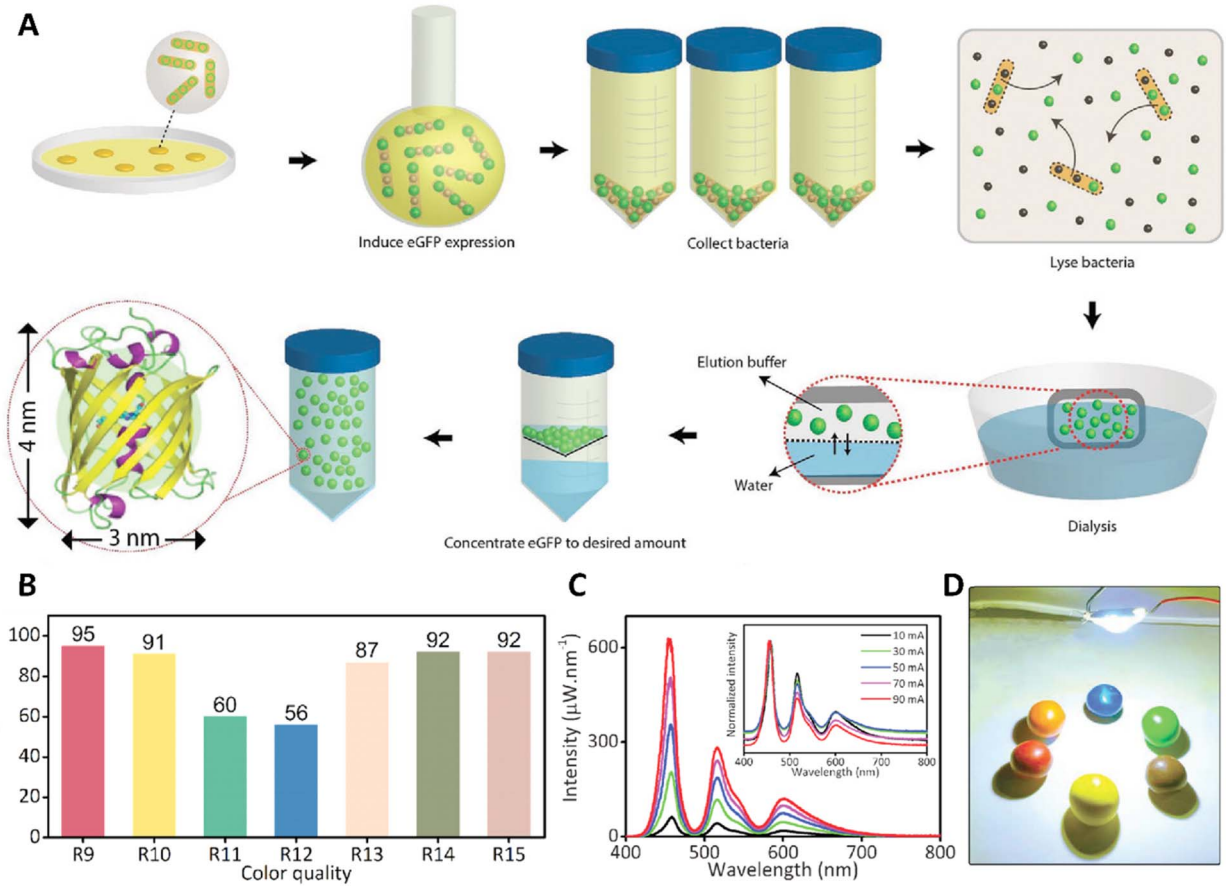

Fig. 1 (A) Schematic image related to the fabrication of eGFP and mScarlet fluorescent proteins. (B) Results of the extended CRI for the white light produced by the PLED. (C) Intensity curve related to the protein-based white LEDs (PLEDs) with the highest CRI at various injection currents (10–90 mA). (D) Image related to the illumination of objects with different colors by the PLED. Reprinted with permission from 123. Copyright 2020, WILEY-VCH Verlag GmbH & Co.

In parallel, DNA has emerged as a functional material in LED systems, serving as an electron-blocking layer to enhance luminous efficiency and luminance. By leveraging the base-pairing specificity of DNA, Back *et al.* created prismatic hexagonal rod crystals composed of single-stranded DNA (ssDNA) and Alq3. The luminescence intensity was enhanced by approximately 1.6-fold when these rods were treated with complementary DNA sequences, while mismatched DNA sequences produced minimal enhancement.[124] Furthermore, Kim *et al.* demonstrated that DNA–DNA recognition impacts not only photoluminescence intensity but also waveguide properties. By preparing solutions with complementary and mismatched DNA sequences, they observed distinct variations in intensity, underscoring the precise tunability offered by DNA-based systems. These findings reveal the broad potential of DNA and protein materials in advancing bio-LED technologies, paving the way for next-generation applications in lighting and sensing.[124]

3.2 Biophotonic and wire

Biophotonics has also ventured into the realm of molecular photonic wires (MPWs), which are sophisticated nanostructures designed for the transport of photons. Operating similarly to electrical wires but on a photonic scale, these structures are pivotal in harnessing light for advanced applications. Among MPWs, DNA-based molecular photonic wires have gained significant traction due to their flexibility and ability to spatially arrange chromophores with precision. These systems often rely on FRET for energy migration, utilizing two primary methodologies: hetero-FRET and homo-FRET. Hetero-FRET facilitates energy transfer between different donor and acceptor dyes, though its scalability is limited by the necessity for diverse dye sources. In contrast, homo-FRET offers a scalable solution by employing chains of identical-energy dyes, enabling energy transfer from high-energy donors to lower-energy acceptors. The success of this approach hinges on the arrangement and orientation of chromophores to maximize efficiency.[125]

Biowires function as nanoscale transducers and optical/electrical conduits, interfacing seamlessly with biological systems to enable precise detection, visualization, and modulation of physiological signals. Their core mechanism relies on the efficient coupling of their one-dimensional architecture with biological, electrical, or photonic inputs. In biosensing, biowires—particularly silicon nanowires (SiNWs), zinc oxide

Open Access Article. Published on 22 July 2025. Downloaded on 10/28/2025 10:32:42 AM. This article is licensed under a Creative Commons Attribution-NonCommercial 3.0 Unported Licence.

(ZnO) nanowires, and conductive polymers—act as ultra-sensitive field-effect transducers.[126] Molecular binding events at the biowire surface modulate the local charge density or electric field, leading to measurable variations in carrier transport characteristics (*e.g.*, drain current, threshold voltage shift). These interactions often occur within a Debye length, making biowires highly responsive even at femtomolar analyte concentrations. In optoelectronic sensing, biowires also function as dielectric waveguides or plasmonic resonators, where the presence of a target analyte perturbs the evanescent optical field, causing wavelength shifts or intensity modulation in guided modes.[127]

In imaging, biowires serve as directional nanophotonic structures that can guide, emit, or amplify light at cellular and subcellular resolutions. Fluorescently labeled or rare-earth doped nanowires can generate coherent emission upon excitation, while metallic biowires (*e.g.*, Au or Ag) act as nanoscale plasmonic antennas, enhancing local electromagnetic fields and fluorescence yield. Their anisotropic light propagation enables targeted illumination with reduced scattering, improving the signal-to-noise ratio and spatial resolution in dense tissue environments. Furthermore, when integrated into intracellular structures, biowires can act as intracellular optical probes, tracking dynamic processes such as membrane potential changes or ion fluxes with high spatiotemporal fidelity.[128,129] Collectively, the utility of biowires lies in their ability to integrate electronic and photonic functionality with biological systems at the nanoscale, offering multiplexed capabilities in biosensing, diagnostics, and precision therapy.

Boeneman *et al.*, demonstrated the creation of self-assembled QD-sensitized multivalent DNA photonic wires, integrating the unique photophysical properties of QDs with programmable scaffolding capabilities of DNA. These hybrid structures employed QDs as central nanoscaffolds and ultraviolet energy donors, driving sequential FRET cascades through a DNA-based system to achieve energy transfer over distances exceeding 150 Å. By arranging acceptor dyes with increasing red-shifted emissions on a complementary DNA template modified with a peptide, the system facilitated precise energy flow. This approach allowed testing configurations like intercalating dyes or multiple identical acceptor dyes utilizing homo-FRET. Notably, a structure incorporating four acceptor dyes demonstrated four-step energy transfer, though efficiency was primarily limited by acceptor dye quantum yields. These findings highlight the potential of DNA-QD hybrids for advancing photonic wire assemblies and their applications in nanotechnology.[130]

An innovative diagnostic approach was introduced in a research for acute myocardial infarction (AMI) by developing a miRNA addition probe utilizing a non-crosstalk DNA photonic wire (PW) and a clustering algorithm. Their design incorporates a three-dye DNA PW to construct a two-step FRET cascade system, enabling separate or additive analysis of two upregulated miRNAs (miR-133a and miR-208a). By employing a K-Means clustering algorithm, the system achieved 100% accuracy in diagnosing early-stage AMI in clinical serum samples across both training and validation cohorts. This method demonstrates the potential of integrating DNA photonic technologies with advanced computational algorithms for precise and early medical diagnostics.[131]

A cutting-edge DNA-based intelligent machine was established by Zhang *et al.*, *via* developing an advanced DNA-based intelligent machine that was used for imaging from the live biological samples with a high-performance, to address the major challenges in enzyme-free fluorescence biosensors. This system consisted of two primary components: a pair of double-stranded DNA probes, DP1 and DP2, along with their related single-stranded sequences (S1 to S4), which were anchored onto a long DNA wire nano-scaffold. In this configuration, S1 and S2 were labeled with a fluorophore-quencher pair—black hole quencher-3 (BHQ-3) and cyanine 5 (Cy5)—to enable a FRET process when in close proximity. The nano-scaffold also contained another DNA duplex, named WS, with single-stranded DNAs S5 and S6 (DP-WS). The second part of the system consisted of core–shell UCNPs coated with polyacrylic acid (PAA) and functionalized with DP-WS (Fig. 2). Using an 808 nm NIR light-activated biosensing technique, this DNA machine restricted nucleic acid interactions to the DNA wire nano-scaffold, leading to a 30.8-fold increase in local concentration and a 15-fold improvement in reaction rate. The system was validated with miRNA-221 as a low-abundance biomarker, demonstrating ultra-high sensitivity (limit of detection of about 62.65 fM) and exceptional specificity for the detection of hepatic tumor. Additionally, it showed remarkable imaging performance in live biological samples, from cellular assays to whole-body applications, in nude mice, highlighting its transformative potential in diagnostic and bio-imaging technologies.[132]

Nicoli *et al.*, investigated the potential of FRET within DNA origami-based photonic wires to advance nanoscale light transport. By leveraging the spatial programmability of DNA origami, they constructed a directional photonic wire comprising cyanine 3 (Cy3) dye flanked by a blue donor dye (Alexa488) and a red acceptor dye (Cy5). Their study demonstrated that homo-FRET among Cy3 dyes enhanced energy transfer to the acceptor, with the system effectively transporting energy over 16 nm. Bulk and single-molecule spectroscopy, supported by Monte Carlo simulations, confirmed the efficiency of this design. This work highlights the promise of DNA-based platforms in constructing scalable photonic circuits for future light-harvesting and dye-based applications.[133]

Lv *et al.*, presented a groundbreaking approach to DNA-based programmable gate arrays (DPGAs), marking a significant step toward general-purpose DNA computing. By utilizing single-stranded oligonucleotides as uniform transmission signals, they successfully developed large-scale DNA integrated circuits (DICs) with minimal leakage and high fidelity. Their system features a reconfigurable DPGA comprising 24 addressable dual-rail gates, capable of implementing over 100 billion distinct circuits through programmable wiring instructions. Additionally, the use of DNA origami registers facilitated directionality and asynchronous execution in cascaded DPGAs, exemplified by a quadratic equation-solving DIC with 30 logic gates and approximately 500 DNA strands. The integration of DPGAs with analog-to-digital converters further demonstrated

 © 2025 The Author(s). Published by the Royal Society of Chemistry

Open Access Article. Published on 22 July 2025. Downloaded on 10/28/2025 10:32:42 AM.
This article is licensed under a Creative Commons Attribution-NonCommercial 3.0 Unported Licence.

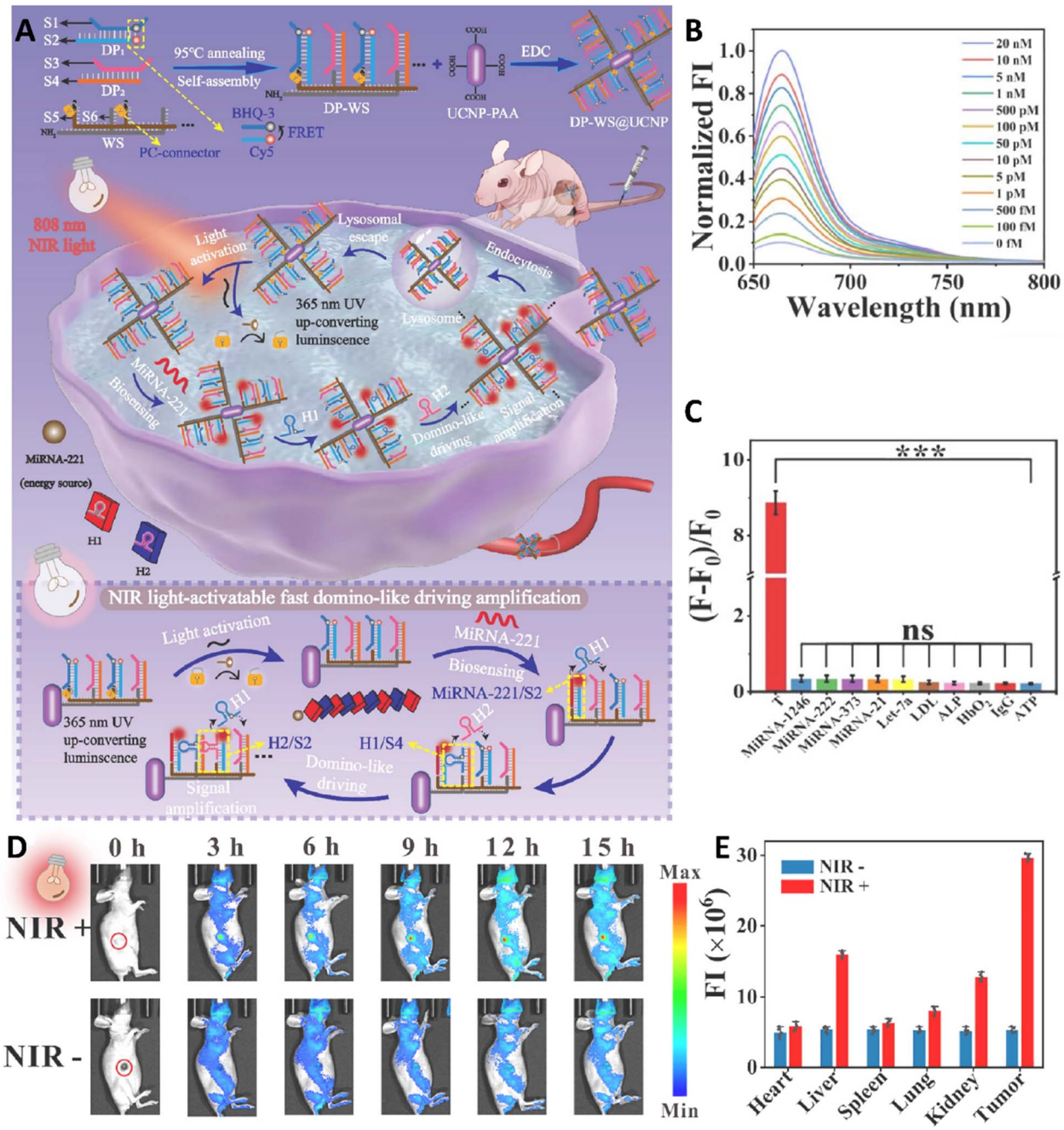

Fig. 2 (A) Schematic image related to the fabrication of DP-WS@UCNP machine and its application for high-performance imaging. (B) Fluorescence spectra of Cy5 of the DP-WS@UCNP in the presence of different concentrations of miRNA-221. (C) Result of specificity assessment of fabricated sensor (*** refer to $P < 0.001$). (D) Real-time fluorescence image of mice injected with DP-WS@UCNP during 15 h in the presence and absence of NIR irradiation. (E) Fluorescence intensity of vital organs and tumor tissue in the presence/absence of light. Reprinted with permission from 132. Copyright 2024, Elsevier B.V.

the potential for classifying disease-related microRNAs, highlighting the versatility and scalability of this innovative platform in advancing DNA computing technologies.[134]

Díaz *et al.*, explored the potential of excitonically coupled J-like cyanine dye dimers (Cy3 and Cy5) as energy transfer relayed within DNA-templated photonic wires to leverage the collective emission dipole of J-dimers and enhance FRET rates between relay dimers and remote acceptor dyes. However, under standard aqueous buffer conditions, dimer relays showed no improvement over monomer relays in energy transfer quantum yield, primarily due to nonradiative relaxation, suboptimal dye orientation within dimers, and misalignment between dimers and acceptor dyes. The researchers mitigated nonradiative losses by using viscous solvents or cooling samples, which significantly enhanced energy transfer efficiency. They concluded that achieving practical

Open Access Article. Published on 22 July 2025. Downloaded on 10/28/2025 10:32:42 AM. This article is licensed under a Creative Commons Attribution-NonCommercial 3.0 Unported Licence.

improvements in energy transfer with J-dimers would require precise control over dye orientations to fully harness their potential. This study highlights the challenges and opportunities in optimizing excitonic coupling for molecular photonic applications.[135]

Adamczyk *et al.*, demonstrated precise control of excitonic energy transfer using DNA origami as a platform to position and orient organic dyes. By independently manipulating the orientation of single donor and acceptor dyes within DNA nanostructures, they achieved a twofold increase in energy transfer efficiency. This approach highlights the potential of DNA nanotechnology for optimizing molecular exciton flow, with significant implications for applications such as artificial light-harvesting systems, energy conversion, and advanced spectroscopy. The study underscores the transformative role of DNA-based platforms in achieving high-precision molecular control for photonic applications.[136]

3.3 Biophotonic and biolaser

Biological lasers represent a groundbreaking advancement where laser technology is seamlessly merged with biological materials to produce highly tunable, precise, and intense light emissions. Unlike LEDs and fluorescence systems, lasers offer unparalleled advantages, including narrow linewidths, enhanced intensity, and superior controllability, making them indispensable for advanced nanoscale and microscale applications.[137] Bio-lasers operate on the fundamental principle of light amplification through stimulated emission within biological or bio-integrated systems. In these constructs, the gain medium is typically composed of biologically compatible fluorophores—such as fluorescent proteins (*e.g.*, GFP), synthetic dyes (*e.g.*, rhodamine derivatives), or rare-earth doped NPs —that are either embedded in tissues, coupled to cells, or encapsulated in biopolymers. Resonant feedback is provided by naturally occurring or engineered microcavities, including intracellular lipid droplets, cell membranes, or artificially introduced whispering-gallery-mode (WGM) microspheres and Fabry–Pérot cavities.[106,138] In sensing applications, bio-lasers exhibit ultra-narrow linewidths and extreme sensitivity to environmental perturbations. Slight changes in refractive index, pH, ion concentration, or biomolecular interactions near the lasing cavity result in measurable shifts in emission wavelength or intensity. For instance, binding events at the cavity surface alter local optical density, modulating the lasing threshold or emission profile. This allows real-time, label-free biosensing with high resolution and specificity.[139] In imaging, bio-lasers enable enhanced signal-to-noise ratios due to their coherent and monochromatic emission.[140] Bio-lasing constructs embedded within cells or tissues act as bright, tunable contrast agents. Unlike traditional fluorophores, lasing emissions avoid broad spectral backgrounds, providing super-resolution imaging in complex biological environments. Additionally, their emission can be tuned to penetrate deeper tissues when lasing in the NIR region.[141] For therapeutic purposes, bio-lasers have been explored in photothermal and photodynamic therapy platforms.[140] Here, the optical gain medium—especially when based on plasmonic or lanthanide-doped nanostructures—can convert absorbed laser energy into localized heat or reactive oxygen species (ROS). When pumped above lasing threshold, the intensified optical field significantly enhances therapeutic output, allowing for more precise ablation of diseased cells or activation of photosensitizers with spatial control.

Biolasers typically incorporate biological components either within the gain medium, the optical cavity, or both, enabling innovative functionalities.[142] These systems often operate in fluidic environments, where biological materials such as proteins, DNA, or enzymes interact with optical cavities like Fabry–Pérot resonators, distributed feedback cavities, or optofluidic ring resonators to amplify light signals.[143] For instance, Chen *et al.*, developed an optofluidic laser system that utilized genetically encoded fluorescent protein FRET pairs connected by tunable peptides. It was composed of two strands of peptides contained genetically encoded fluorescent proteins (eGFP and mCherry which acted as donor and acceptor, respectively) that were connected *via* a peptide with two different lengths, which were injected into an optofluidic ring resonator (OFRR). This system demonstrated a 25-fold reduction in donor laser emission when donor and acceptor fluorophores were brought into proximity, significantly outperforming conventional FRET detection methods, which achieved only a 17% reduction. This approach offers enhanced sensitivity for studying protein–protein and protein–drug interactions, paving the way for advanced applications in biochemical and biophysical research.[144]

Yuan *et al.*, introduced the concept of bioresponsive microlasers using whispering-gallery-mode (WGM) microdroplet cavities, offering a novel approach to amplify light–matter interactions at the bio-interface. These microlasers leverage interfacial energy transfer to manipulate lasing wavelengths based on molecular binding concentrations at the cavity surface. By integrating protein-based and enzymatic interactions, they achieved tunable lasing wavelengths over a broad spectral range using different donor/acceptor dye pairs. This study provided insights into how molecular interactions modulate laser emissions and opened avenues for developing smart biophotonic devices for advanced biodetection and bioimaging applications.[145] Optical resonators constructed from biological materials provide additional avenues for innovation. Protein-based microlasers, hydrogels, and crystalline nanocellulose (CNC) systems exhibited tunable properties based on environmental stimuli. For instance, CNC materials utilized self-assembly to form cholesteric liquid crystals, which can shift photonic bandgaps in response to moisture changes and enabled wavelength modulation through swelling and shrinking behaviors. Similarly, starch-based ellipsoidal microgranules demonstrated lasing wavelength shifts by altering water content or crystalline arrangements.[146] Structural changes induced by dehydration or rehydration allow these systems to tune their cavity volumes dynamically. Protein materials such as silk and squid ring teeth add another dimension of functionality through their high thermo-optic coefficients. For instance, squid ring teeth proteins exhibited thermo-refractivity nearly a hundred times greater than silica, enabling efficient optical

 © 2025 The Author(s). Published by the Royal Society of Chemistry

Open Access Article. Published on 22 July 2025. Downloaded on 10/28/2025 10:32:42 AM.
This article is licensed under a Creative Commons Attribution-NonCommercial 3.0 Unported Licence.

switching. Azosilk, a modified silk composite incorporating azobenzene moieties, responded to light exposure by altering its diffraction efficiency, creating adaptable optical patterns.[147,148] Such advancements highlight the versatility of biolasers in integrating biological structures for responsive optical control.

Recent breakthroughs in biolaser technology underscore their potential in diverse applications. For instance, genetically encoded proteins in combination with optofluidic systems enable high-performance imaging in live biological samples.[149] DNA-templated QD systems further enhance these capabilities by enabling multi-step energy transfer for broad-spectrum tunability. These advances extend the functionality of biolasers to include precise diagnostics, biosensing, and environmental monitoring, with applications spanning cellular

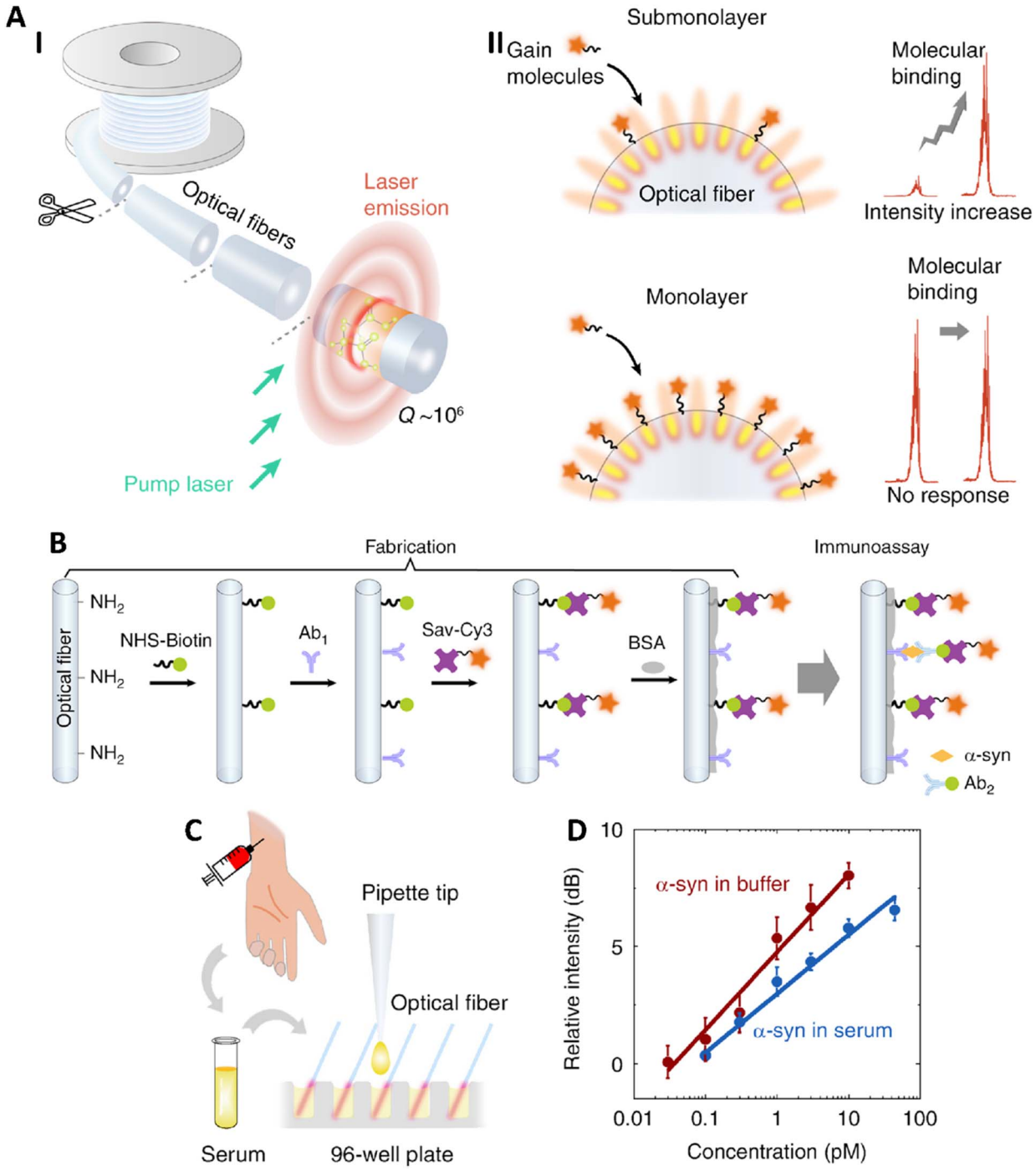

Fig. 3 (A) Schematic image related to the application of telecom optical fibers for the fabrication of submonolayer whispering-gallery biolasers (I). Differences in the intensity response of submonolayer (up) and monolayer (down) (II). Schematic images related to the fabrication of submonolayer biolaser immunosensor (B) and application of fabricated sensor for real sample (C). (D) The intensity curve related to the detection of α-syn in buffer and serum. Reprinted from 151 under the terms of the Creative Commons CC BY license. Copyright 2023 Springer Nature.

Open Access Article. Published on 22 July 2025. Downloaded on 10/28/2025 10:32:42 AM. This article is licensed under a Creative Commons Attribution-NonCommercial 3.0 Unported Licence.

imaging to whole-organism studies.[150] In another research, telecom optical fibers were used, as optical microcavities, to fabricate low-coat repeatable disposable ultrasensitive biosensors that had the capability of detecting biomarkers using whispering-gallery laser emission. It was a submonolayer biolaser that showed better performance (about 6-time magnitude advancement in limit of detection (LOD)) compared with the monolayer biolaser. The fabricated sensor was used for the detection of alpha-synuclein (α-syn), as one of the biomarkers of Parkinson's disease, in serum that showed LOD of about 0.32 pM and linear range between 0.1–100 pM. It was a sandwich-like sensor composed of optical fibers which were functionalized with biotin and antibody 1 (Ab1, named as capture antibody). Then, streptavidin-Cy3 (Sav-Cy3) were added to the media which were attached to the biotin molecules and acted as the laser gain molecules. If α-syn molecules were present in the microenvironment of the sensor, they would be captured between Ab1 and Ab2 (the detection antibody conjugated with a biotin molecule), followed by the attachment of additional Sav-Cy3 molecules, which enhanced the fluorescence signal (Fig. 3).[151]

Structural innovations also play a critical role in advancing optical resonators. Hydrogel-based microlasers, for instance, can modulate lasing properties by responding to external stimuli such as pH or temperature. Polysaccharide-based systems offer similar tunability through structural transformations. Examples include whispering gallery mode resonators that leverage protein-based secondary structures to achieve dynamic wavelength control.[152]

Collectively, these advancements highlight the transformative potential of biolasers in merging biological and synthetic materials to create responsive, efficient, and highly customizable optical systems. The convergence of DNA nanotechnology, protein engineering, and hybrid material platforms positions biolasers as a cornerstone for next-generation optical technologies. These systems redefine the capabilities of lasers in biomedical imaging, diagnostics, environmental sensing, and beyond, opening new frontiers for scientific exploration and industrial innovation.

4 Applications of biophotonic nanostructures in biomedicine

Biophotonic nanostructures have emerged as transformative tools in biomedicine due to their unique ability to manipulate light at the nanoscale. The application of biophotonic nanostructures in biomedical domain has experienced significant growth especially in imaging, diagnostics, and therapy. This progress is attributed to the non-invasive and remote nature of light-based techniques, the availability of light, and the versality of light manipulation for diagnosis, treatment, and therapy guidance.[153] In therapeutic applications, biophotonic nanostructures have shown remarkable potential in photothermal and photodynamic therapies. These properties provide superior imaging contrast and enable real-time monitoring of cellular processes, making them invaluable in both preclinical and clinical settings. Therefore, the advancements in biophotonic nanostructures continue to develop biomedical applications, offering precise, minimally invasive, and highly effective solutions for complex medical challenges.

4.1 (Bio)sensing

Biophotonic nanostructures are revolutionizing the field of sensing due to their ability to precisely interact with light, enabling highly sensitive and selective detection of chemical and biological targets. The accurate and specific identification of targeted molecules such as proteins and nucleic acids, is crucial for a wide range of applications, including disease diagnosis and drug development. The use of biophotonic structures for optical sensing of biomolecules offers valuable advantage such as fast analysis, good reproducibility, high selectivity and high sensitivity, making them indispensable tools for biomedicine.[154] Such advancements have facilitated breakthroughs in medical diagnostics, environmental monitoring, and food safety by enabling rapid, accurate, and non-invasive detection methods. Application of biophotonic structures as optical sensing platforms providing optical features like surface plasmon resonance (SPR), Raman scattering (RS), and fluorescence biosensing, that have emerged as valuable tools in the field of biomedicine.

4.1.1 Surface plasmon resonance (SPR). Surface plasmon resonance sensing has become a powerful tool for the detection of biomolecules due to its non-destructive nature and high sensitivity that could detect molecular interactions in real-time without using any label.[154,155] It is an optical phenomenon based on surface plasmons, which are collective oscillations of electrons at the interface between a metal and a dielectric, triggered by electromagnetic wave (light wave) that has garnered significant attention due to its advantages, such as low sample volume requirements, high sensitivity, and excellent reproducibility.[156] This phenomenon is sensitive to changes in the dielectric medium, which affects the refractive index. When an analyte is introduced, it alters the dielectric medium, leading to observable changes in the surface plasmon resonance. This sensitivity to changes in the surrounding medium forms the basis for the use of SPR in sensing applications.[157]

Various metals with plasmonic properties like Ag,[158] copper (Cu),[159] and aluminum,[160] as well as various metal alloys can be used for SPR based biosensing applications. Among these, Au is the most commonly used for biomedical applications. Au NPs, as a type of biophotonic material, exhibit a characteristic intense SPR band around 510–530 nm.[161] Fang *et al.* used this feature of Au NPs to design a biosensor for DNA detection (Fig. 4A). A sandwich structure was constructed for the detection of the alkaline phosphatase-related PML/RARA gene, providing specific DNA detection with a lowered limit of detection. In this structure, a Au chip was used as the probe to capture the target analyte, while AuNPs functionalized with oligonucleotides served as external labels. These NPs bind specifically to the captured analyte, resulting in an increase in SPR reflectivity. The SPR signal response indicated a linear relationship with the increasing concentration of the analyte.

 © 2025 The Author(s). Published by the Royal Society of Chemistry

Open Access Article. Published on 22 July 2025. Downloaded on 10/28/2025 10:32:42 AM.
This article is licensed under a Creative Commons Attribution-NonCommercial 3.0 Unported Licence.

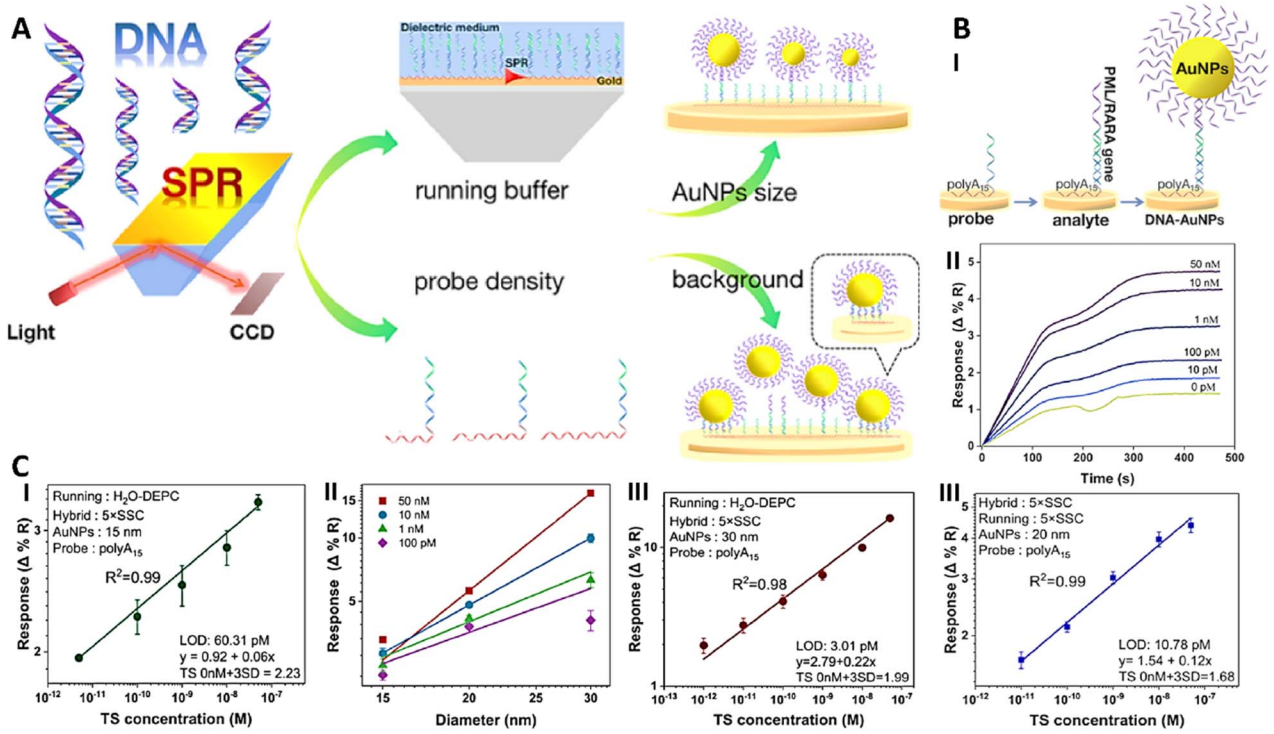

Fig. 4 (A) Schematic illustration of SPR-based DNA sensing using Au biophotonic structures. (B) Schematic image related to the sandwich structure of biosensor (I). Signal response curve of amplified concentration gradient analyte target (II) corresponding linear calibration plots (III). (C) Linearity between the amplified signal and analyte target concentration with 15 nm Au NPs (I) linearity between the AuNPs size and the amplified signal at different concentrations of target analyte (II) Linearity between the amplified signal and analyte target concentration with 30 nm AuNPs (III). Reprinted with permission from 162. Copyright 2024, American Chemical Society.

The biosensor achieved a limit of detection of 10.78 pM in the linear range between 10 pM–50 nM for the PML/RARA gene (Fig. 4B). When the external label, including AuNPs, was added, the limit of detection was significantly reduced (compared to when no external label was used). Various sizes of Au NPs (15, 20, and 30 nm) were utilized to investigate the impact of NP size on biosensor performance. The limit of detection for AuNPs with 20 nm and 30 nm diameters was significantly lower than that of 15 nm AuNPs (60.31 pM). However, there was no significant difference between the 20 nm (9.03 pM) and 30 nm (3.01 pM) AuNPs (Fig. 4C). Although larger NPs provided a lower limit of detection, this effect diminished as the analyte concentration decreased. Furthermore, increasing the thickness of the spacer layer of the probe can decrease the limit of detection from 9.03 pM to 5.53 fM and reduce the background signal. The coefficient of variation for repeatability improved from 14.89% to 3.40%, when the spacer layer was increased. In the presence of real samples, the fabricated system showed recovery rate of about 44.83, 92.98, and 103.64% for the concentrations of 10 pM, 1 nM, and 1 pM of PML/RARA gene, respectively, that confirmed the specificity and performance of utilizing this system for real sample detection.[162] This result shows that AuNPs, as biophotonic NPs, have significant SPR ability. This ability is enhanced by optimizing the size and other characteristics of the AuNPs.

SPR biosensors based on Au can be used for the detection of small biomolecules, such as microRNAs (miRNA). Detecting miRNAs is challenging due to their short sequence length, small molecular weight, and rapid degradation. Biosensors used SPR with AuNPs offer high sensitivity for miRNA detection. Liu *et al.* developed a dual-mode phase imaging surface plasmon resonance (PI-SPR) aptasensor for miRNA detection as a tumor marker. The dual-mode operation allows for a rapid sensing mode with high linearity and a real-time mode with a wide response range, enabling the user to choose the sensing mode based on desired target. The biosensor chip was coated with a Au nanofilm functionalized with an aptamer as the detecting agent. A sandwich biotin–streptavidin strategy was employed to enhance the sensing signal for real-time sensing mode by improving the surface mass density of the target. The biosensor demonstrated excellent selectivity and sensitivity for miRNA detection, providing a limit of detection of 7.14 pM at low concentrations of miRNA (50 pM to 1 nM). The PI-SPR aptasensor exhibited good accuracy and reproducibility, with recovery rates ranging from 90.0–97.0% and the coefficient of variation below 5.76%. This aptasensor successfully detected miRNA biomarkers in clinical samples with high sensitivity. Therefore, sensing with biophotonic materials like Au is useful for detecting small analytes.[156]

MXenes, as biophotonic structures, possess rich oxygen and hydroxyl functional groups along with complete metal atomic layers, giving them a unique ability to bind with biomolecules. This characteristic makes them ideal for enhancing the performance of SPR biosensors by creating an effective bio-

Open Access Article. Published on 22 July 2025. Downloaded on 10/28/2025 10:32:42 AM. This article is licensed under a Creative Commons Attribution-NonCommercial 3.0 Unported Licence.

interface.[154] For instance, Wu *et al.* developed an ultrasensitive SPR biosensor based on MXenes for detecting carcinoembryonic antigen (CEA) as a tumor marker. The ultrathin Ti_3C_2-MXene nanosheets were decorated with polyclonal *anti*-CEA antibodies (Ab_2), while a monoclonal *anti*-CEA antibody (Ab_1) decorated the Au film used as the sensing platform. A sandwiched immunocomplex was formed after introducing MXene-Ab_2 to the sensing platform, capturing the CEA. The proposed biosensor exhibited high sensitivity, with a limit of detection of 1.7 pg mL^{-1} and linear range between 10^{-11} to 10^{-6} g mL^{-1}. A linear relationship was established between the change in SPR signals and CEA concentration. Furthermore, the biosensor demonstrated good reproducibility and high specificity with recovery in the range of 93–110% with relative standard deviation (RSD) between 4.7–7.6 for detecting different concentrations of CEA in real samples. The SPR biosensor performed satisfactorily in evaluating CEA levels in human serum samples, providing good selectivity and negligible nonspecific interactions between the sensing chip and signal amplifiers, as no obvious shift was exhibited in resonant angle.[163]

In another study, Wu *et al.* reported a Ti_3C_2-MXene-based SPR biosensor that exhibited an excellent performance in detecting CEA which was composed of two different layers of MXenes; one of them (Ab_1/N–Ti_3C_2-MXene/Au film) was functionalized with Au film and monoclonal *anti*-CEA antibodies (Ab_1), and the other one (N–Ti_3C_2-MXene/HGNPs/SPA/Ab_2) was modified by hollow Au NPs (HGNPs), staphylococcal protein A (SPA), and polyclonal *anti*-CEA antibodies (Ab_2). In the presence of CEAs, these compounds were conjugated with Ab_1 and Ab_2 to fabricate sandwich structure by MXenes. As the CEA concentrations increased, the shift of the resonance angle gradually increased, resulting in a detection limit of 0.15 fM with linear range between 0.001–1000 PM. The relative standard deviation was less than 5%, demonstrating good reproducibility and stability of the sensing platform. The platform showed good stability, as after 28 days storage at 4 °C, it lost only 20% of its activity. In real serum samples, the sensing platform exhibited recoveries ranging from 91.5%–104% with relative standard deviations from 3.4% to 7.1%.[164] Therefore, the MXenes-based SPR sensing hold great potential in CEA detection with high sensitivity.

4.1.2 Surface enhanced Raman spectroscopy. Since its first report in 1974, Surface Enhanced Raman Scattering (SERS) has attracted significant interest in research. It is a powerful biosensing technique that can identify substances through their molecule-specific spectral fingerprints, allowing for the chemical identification of the single molecules.[165] It has the capability of detecting molecules at low concentrations with high sensitivity, even under physiologically relevant conditions that provides ultrahigh molecular specificity.[165,166] Moreover, SERS offers several additional benefits, including rapid and real-time detection, non-destructive analysis, powerful multiplexing and anti-interference capabilities, minimal water interference, and label-free detection ability.[166,167] These features make SERS particularly noteworthy for applications in biomedicine.

The performance of SERS is significantly influenced by the choice of substrate material, which plays a critical role in amplifying the Raman signal.[168] The primary substrate materials used for SERS are noble metals, such as Au,[169] Ag,[170] and Cu.[167] Indeed, nanostructured Au and Ag exhibit remarkable optical properties, primarily due to their surface plasmon resonance effect that makes them highly effective for SERS applications. In contrast, Cu-based substrates demonstrate inferior structural stability and limited effectiveness in SERS applications.[171]

Pazin *et al.* introduced a SERS nanobiosensor based on Au nanoislands for the precise detection of SARS-CoV-2 antigens. The Au nanoislands were deposited on glass substrates and functionalized with 4-aminothiophenol (4-ATP), as a Raman reporter, along with antibodies. Although the nanobiosensor generated SERS spectra with intense peaks at 1079, 1004, 1179, and 1141 cm^{-1}, no significant shift in peak position was detected between the SERS spectra before and after exposure to a SARS-CoV-2 antigen solution. Therefore, the resulting information visualization from the biosensor was integrated with machine learning techniques. The resulting Raman spectra were analyzed using supervised machine learning algorithms to improve the detection of SARS-CoV-2. Detection accuracies of the fabricated sensor was ranged from 96% to 100%, demonstrating its high capability for antigen detection.[172] Thus, the application of biophotonic structures of Au in SERS sensing can be effective in detecting disease agents.

Besides Au, as the main SERS substrate material, Ag can also be used as a biophotonic material with SERS properties. SERS based on Ag substrates can be employed for the early detection of cancer. Wang *et al.* utilized Ag NPs as a SERS substrate to screen the breast cancer at its early stage. The fingerprint SERS spectra resulting from Ag NPs with size between 50–60 nm were analyzed using machine learning for data mining. Fine needle aspiration samples from 78 patients were incubated with Ag NPs, and the resulting SERS spectra were analyzed using machine learning techniques. The analysis of the SERS spectra revealed notable biochemical differences among breast fibroadenoma, breast hyperplasia, and breast cancer. The diagnostic sensitivity and specificity for breast cancer, breast fibroadenoma, and breast hyperplasia were obtained as follows: 94.74%, 83.33%, 81.82% for sensitivity, and 86.96%, 100%, 94.00% for specificity, respectively, using support vector machine (SVM) algorithm. Therefore, the combination of SERS with Ag NPs and machine learning can enhance fine needle aspiration techniques for the early-stage diagnosis of breast cancer.[170]

Nowadays, semiconductor materials such as graphene, transition metal oxides, and metal–organic composites have been extensively explored for their potential as SERS substrates, demonstrating significant SERS activity.[171] Graphene-enhanced Raman scattering has garnered interest in the field of biosensing, as it can be used to detect biological processes, disease stages, and biomarkers.[168] For instance, Wang *et al.* introduced a SERS-based graphene sensing technique for detecting Alzheimer's biomarkers. In this study, a monolayer graphene was placed in contact with mouse brain tissue slices. The Raman spectra from the mouse brain tissues were collected and analyzed using machine learning classification algorithms. The spectra for mice with and without Alzheimer were measured

 © 2025 The Author(s). Published by the Royal Society of Chemistry

Open Access Article. Published on 22 July 2025. Downloaded on 10/28/2025 10:32:42 AM.
This article is licensed under a Creative Commons Attribution-NonCommercial 3.0 Unported Licence.

with and without graphene contact. The presence of graphene improved the signal-to-noise ratio of the spectra, increasing it from 53.9 to 121, due to graphene's high thermal conductivity and fluorescence quenching capability. This method achieved an accuracy of 98% in detecting Alzheimer's biomarkers in the presence of graphene, compared to 77% without graphene. This study illustrated that the application pf graphene can improve SERS-based sensing for early disease diagnosis.[173]

It was also shown in a study that the combination uses of noble metal NPs and metal–organic frameworks (MOFs) can improve the selectivity and sensitivity of molecule detection in clinical samples.[174] Chen *et al.* proposed a label-free SERS biosensor based on Au nanostars coated with MOF for the selective and ultrasensitive detection of trimetazidine in clinical samples (Fig. 5A). The core–shell biosensor functions as a molecular sieve, where Au@MOF is decorated on a silicon substrate and further modified with 1*H*,1*H*,2*H*,2*H*-perfluorodecyltriethoxysilane (PFDT-silane) to create a superhydrophobic surface that enhances the sieving capability for the small-molecule trimetazidine (TMZ) and para nitrophenyl phosphate (*p*-NTP). This biosensor selectively sieves TMZ and *p*-NTP from mixed solutions while preventing the entry of larger molecules like rhodamine G6 (RhG 6) (Fig. 5C). The Au@MOF biosensor demonstrated a much stronger SERS signal compared to Au nanostars with significantly lower limit of detection for *p*-NTP (5.25×10^{-12} for Au@MOF compare with 4.58×10^{-10} for Au nanostar) in the linear range between 10^{-9}–10^{-4} M and 10^{-11}–10^{-6} M for Au nanostars and Au@MOF, respectively (Fig. 5B). Additionally, it exhibited remarkable detection performance, achieving a limit of detection of

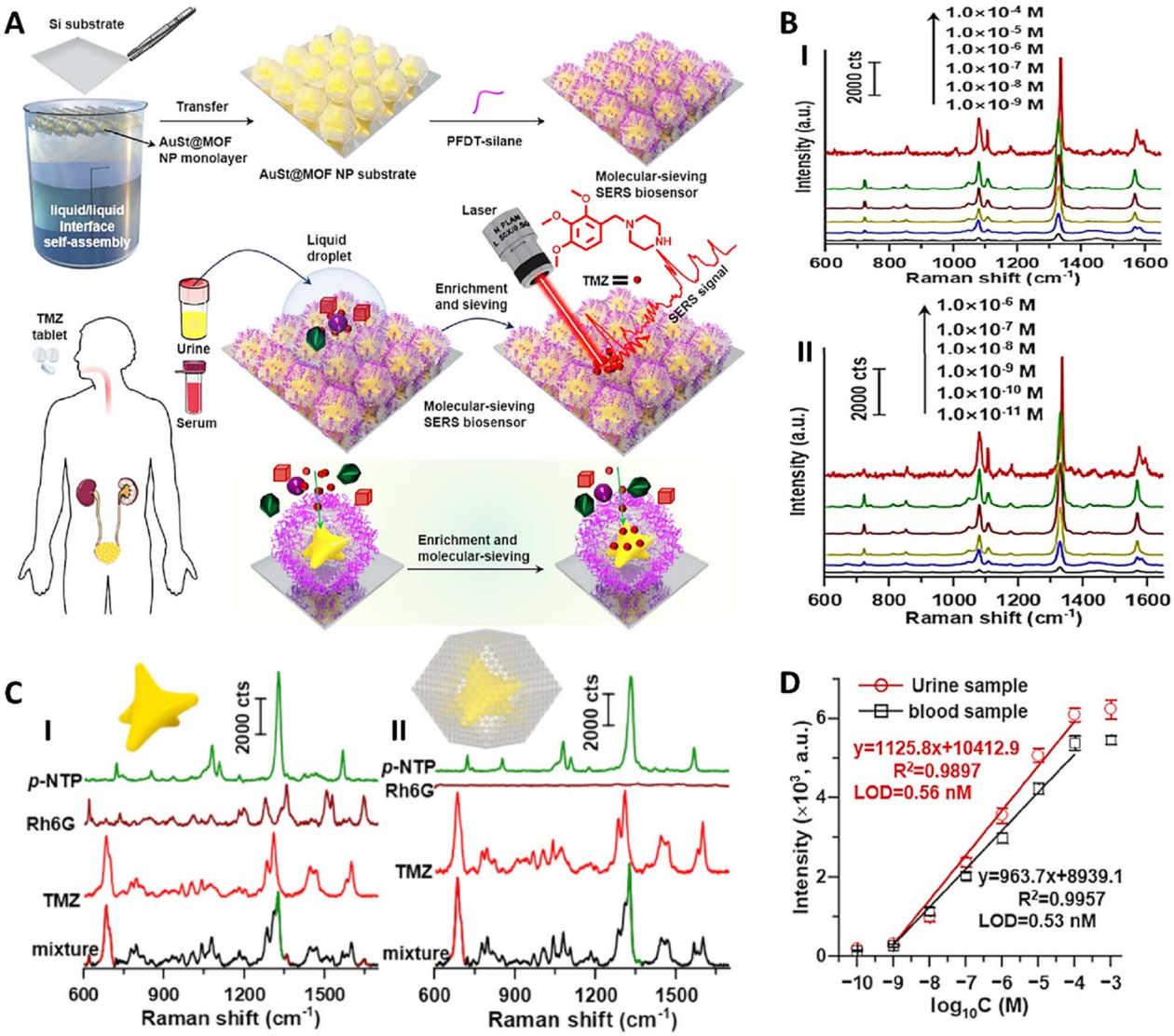

Fig. 5 (A) Schematic illustration of SERS-based DNA sensing using Au nanostars biophotonic structures. (B) SERS spectra of *p*-NTP at different concentrations by the Au nanostars (I) and Au@MOF (II). (C) SERS spectra of *p*-NTP, Rh6G, TMZ, and their mixture in the presence of Au nanostars (I) and Au@MOF (II). (D) Linearity between the amplified signal and TMZ concentration. Reprinted with permission from 165. Copyright 2024, American Chemical Society.

Open Access Article. Published on 22 July 2025. Downloaded on 10/28/2025 10:32:42 AM.
This article is licensed under a Creative Commons Attribution-NonCommercial 3.0 Unported Licence.

approximately 0.56 nM and 0.53 nM in urine and blood samples, respectively, for TMZ (Fig. 5D). This biosensing approach was successfully applied for detecting trimetazidine in a mouse model.[165]

4.1.3 Fluorescence-based systems biosensing. Sensing by fluorescence is widely used in biosensors due to its high sensitivity, simplicity, and versatility, in which fluorescence is employed as a signal transduction mechanism, enabling the detection and quantification of various biological and chemical substances. Fluorescence is a photophysical phenomenon in which certain molecules, known as fluorophores, absorb light at a specific wavelength and subsequently emit light at a longer wavelength. These fluorophores can change their intrinsic fluorescence when interacting with other elements and are employed as sensing probes in biosensor-based fluorescence applications.[175]

QDs are remarkable semiconductor fluorophore NPs that possess unique properties including narrow and tunable emission spectra, high quantum yields, and compatibility with biological molecules, such as DNA and proteins, that enables their use in various biological applications as biophotonic materials.[153] For instance, the application of QDs for nucleic acid characterization represents a significant advancement in molecular biology techniques. Hastman *et al.* reported a multiplexed biosensor based on QDs that can detect both target DNA strands and active proteolysis. In this biosensor, multiple DNA sequences are assembled around a single QD *via* peptidyl-PNA (peptide nucleic acid) linkers. The DNA sequences encoded complementary genomic sequences originating from the Ebola, influenza, and COVID-19 viruses, labeled with acceptor dyes, while a Ru(II)-modified peptide quenches the QD's photoluminescence, which is restored upon protease interaction. The dyes, including terbium (Tb) chelate, AlexaFluor647, and Cy5.5, create potential FRET cascades. The sensor employs orthogonal energy transfer processes, featuring two FRET cascades: one involving Tb → QD → AlexaFluor647 → Cy5.5, and the other using direct excitation of QD → AlexaFluor647 → Cy5.5. The ratiometric assembly of labeled DNAs and peptides allows for precise tuning of energy transfer pathways, enabling specific detection of given target(s). Additionally, the biosensor can perform logical operations, enhancing its capability to discriminate between different pathogens. This innovative design holds great potential for rapid and multiplexed pathogen detection in diagnostic applications.[176]

Besides QDs, organic dyes such as rhodamine derivatives, fluorescein, Cy3, and Cy5 are widely used as biophotonic materials due to their fluorescence properties, making them highly effective in biosensing applications.[177–180] Lamberti *et al.*

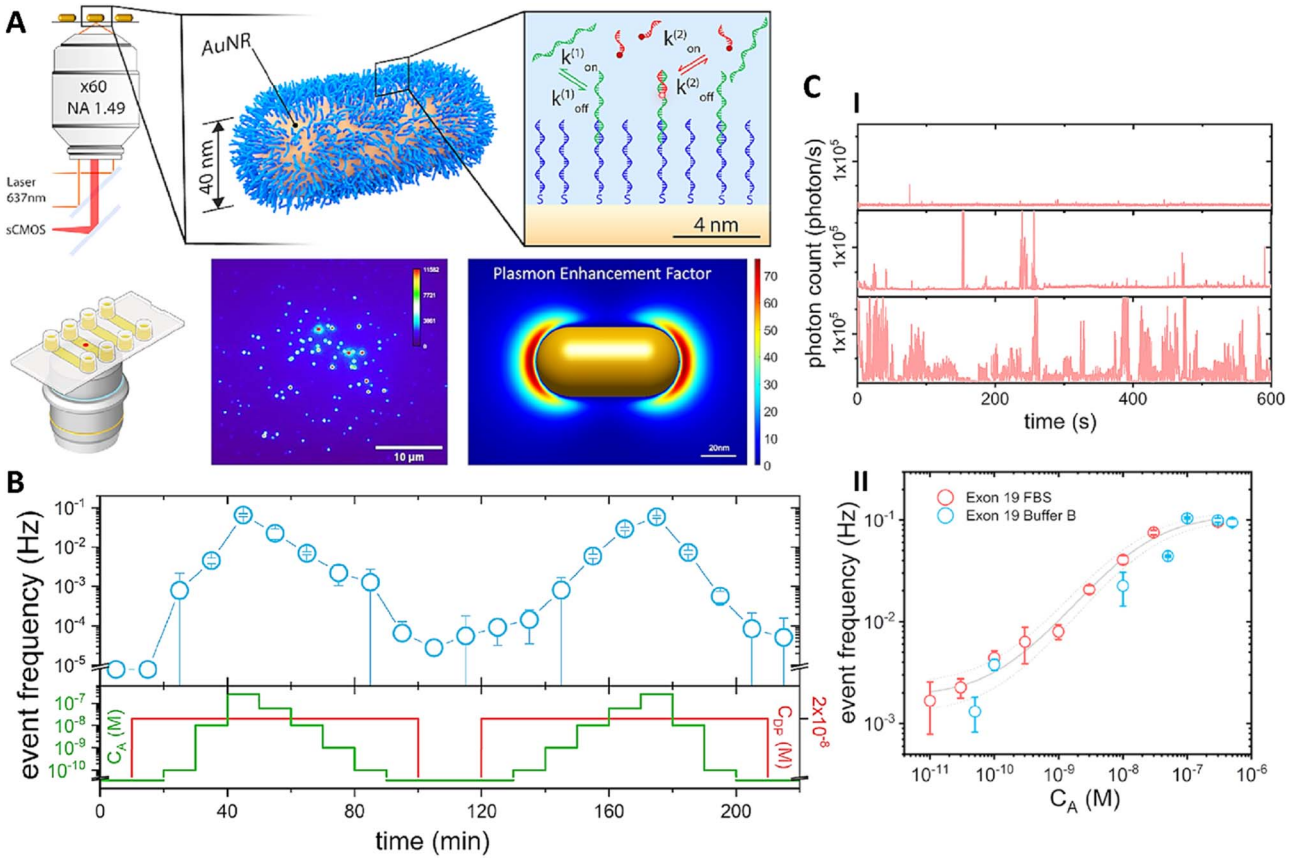

Fig. 6 (A) Schematic illustration of fluorescence-based biosensor for sensing cancer biomarker. (B) Continuous monitoring of cancer biomarkers over a duration of 3.5 hours. (C) Signal response for sensing over time at three cancer analyte concentrations (I) dose-response curve for the detection of cancer biomarker in different media (II). Reprinted from 181 under CC-BY 4.0 license. Copyright 2024, American Chemical Society.

 © 2025 The Author(s). Published by the Royal Society of Chemistry

Open Access Article. Published on 22 July 2025. Downloaded on 10/28/2025 10:32:42 AM. This article is licensed under a Creative Commons Attribution-NonCommercial 3.0 Unported Licence.

developed a biosensor based on plasmon-enhanced fluorescence that can track the concentration of tumor DNA markers (Fig. 6A). This biosensor had the capability of continuously monitoring analyte concentrations directly within biological fluids. It consisted of Au nanorods that were biofunctionalized with single-stranded DNA, as the capture probe. The AuNPs served as antennas to strongly enhance the fluorescence of detection probes. In here, fluorescence probe was a rhodamine derivative (ATTO655) that bonded weakly to the target analyte in a sandwich approach. This weak interaction allowed the probe to dissociated and reassociated dynamically, which is essential for continuous monitoring. In the presence of higher concentrations of analyte, the biosensor exhibited increased activity from individual particles (Fig. 6C(I and II)). It was able to detect cancer biomarkers in complex media such as buffers and serum without washing steps. This biosensor demonstrated continuous monitoring for cancer markers over a 3.5-h assay, varying analyte concentration from 0 to 250 nM without washing or regenerations steps (Fig. 6B). The biosensor showed high reproducibility in average response, with a limit of detection of 1 nM and a temporal resolution of 10 minutes, with a coefficient of variation of approximately 50%.[181] Therefore, this biosensor, using Au NPs, exhibited great potential in the continuous monitoring of cancer biomarkers in complex media.

UCNPs as biophotonic probes have shown promising potential in fluorescence biosensing. However, their low fluorescence intensity has limited their sensitivity, ranging only from picomolar to femtomolar levels. Ma *et al.* developed a fluorescence-based sensing method using UCNPs with ultrasensitive capability to detect the SARS-CoV-2 N-gene. This FRET probe was composed of core–shell UCNPs ($NaGdF_4$:Yb^{3+}, Er^{3+}@$NaGdF_4$) linked to an Au–Au dimer. The dimer, by generating a stronger electromagnetic field compared to single Au NPs, could transfer energy more effectively to the UCNPs, leading to more effective detection of the target gene. This system exhibited excellent sensing efficacy for detecting the SAR-CoV gene. A linear correlation between signal intensity and the concentration of target DNA was observed *in vitro*, ranging from 2 aM to 2 fM, with a limit of detection around 4 aM. Additionally, in clinical samples, the signal luminescence intensity increased from 18% to 51% as the concentration of the target increased from 25 aM to 2.5 fM. This detection was carried out in 30 minutes without the need to amplify the target DNA. Therefore, UCNPs, as biophotonic structure exhibited rapid and sensitive sensing of biomolecules.[182]

One application of biophotonic materials is the design of point-of-care diagnostic methods. Recently, point-of-care diagnostics have gained importance in biomedical applications due to their ease of use, elimination of the need for trained personnel, and the ability to conduct tests directly near patients, resulting in immediate analysis, which is crucial for timely disease diagnosis. Devices integrating biophotonic materials can promptly detect and record signals, enabling rapid clinical sensing and self-testing. In particular, chemiluminescent materials are well-suited for point-of-care applications, as they do not require an external light source for excitation. Zhu *et al.* proposed a point-of-care, rapid, and user-friendly testing platform using a chemiluminescent probe to detect liver injury directly from whole blood. This strategy employed Schaap's dioxane derivative, as the chemiluminescent probe, biothiols, as biomarkers of liver injury, and α-cyclodextrin to enhance the chemiluminescence signal. The method successfully detected biothiols levels in the living cells of mouse models. Additionally, it produced clear signal readout in whole blood samples.[183]

Using biophotonic materials as biolaser offers significant advantages for biosensing applications. For instance, a smart, protein-based biolaser was designed for the detection of protein conformational changes. This biolaser was composed of an organic laser dye embedded within a silk fibroin matrix. The dye, serving as the optical gain medium, was doped into the silk protein to construct a microcavity laser. The laser output was strongly influenced by conformational changes in the silk structure. Silk fibroin exhibited two distinct conformations, and the transition between them altered the refractive index at 540 nm from 1.55 to 1.58. As a result, the microsphere biolaser demonstrated high sensitivity to conformational changes in proteins and presented a promising tool for monitoring such transformations.[147]

DNA photonic nanowires are nanoscale structures designed to facilitate energy transfer, most commonly *via* FRET. Their capabilities-such as high information storage potential and long-range resonance energy transfer-make them suitable for applications in sensing, monitoring, and DNA computing, surpassing the limitations of conventional molecular beacons. According to these interesting features, DNA photonic nanowires were employed for the detection of the thrombin biomarker. A FRET cascade was constructed using fluorophores FAM, Cy3, and Cy5. FAM was positioned in the input region, while Cy5 and Cy3 were located in the bridge and output regions, respectively. Energy was transferred from FAM (a green donor dye) to Cy3 (a red acceptor dye) through Cy5. Detection was enabled by a specific aptamer targeting thrombin. In the presence of thrombin, the FRET cascade was disrupted, resulting in a high signal-to-background ratio (F_{FAM}/F_{Cy5}). This sensing strategy demonstrated a high sensitivity for thrombin detection, with a detection limit of 2.7 nM. By modifying the aptamer, this approach can be adapted for the detection of other biomarkers, offering a versatile platform for biosensing applications.[184]

Overall, the use of biophotonic materials in diagnostic applications in medicine demonstrates promising potential. These materials enable the detection of biomolecules, improve the sensitivity of detection methods, and facilitate the early diagnosis of diseases. Additionally, they allow for the simultaneous detection of multiple targets, thereby improving diagnostic efficiency.

4.2 Imaging

4.2.1 Optical coherence tomography (OCT). Optical coherence tomography (OCT) is an advanced imaging technique that enables high-resolution, non-invasive visualization of biological tissues. By employing a broadband light source and a fiber optic

Open Access Article. Published on 22 July 2025. Downloaded on 10/28/2025 10:32:42 AM. This article is licensed under a Creative Commons Attribution-NonCommercial 3.0 Unported Licence.

interferometer, OCT provides micrometer-scale spatial resolution. Utilizing NIR light, it can penetrate scattering media, allowing for detailed cross-sectional and three-dimensional imaging of tissue structures and functions.[153] With a high temporal resolution of less than one second, OCT has become a reliable diagnostic tool in biomedical applications; however, OCT images can sometimes exhibit low contrast.[185] To address this issue, researchers are exploring the use of contrast agents, including biophotonic materials, to enhance image quality and diagnostic capabilities. Various contrast agents have been employed to improve image quality in OCT techniques. Au NPs are notable OCT contrast agents that have been used in many studies. For instance, Jiang *et al.* utilized Au NPs as a contrast agent to prepare three-dimensional (3D) imaging by OCT, focusing on the penetration and distribution of ozone (O_3) into biological tissue. The Au NPs, in the form of triangular nanoprism, were employed for imaging the anterior chamber of an isolated crucian carp eye. The results showed that using Au as a contrast agent in OCT allowed for the imaging of the penetration and distribution of O_3 in the eye at a depth of 311 μm over 172 minutes.[186]

Bismuth Selenide (Bi_2Se_3) is a material commonly used in various applications, including photonics and electronics. Yao *et al.* employed Bi_2Se_3 nanostructures as a contrast agent for OCT. These nanostructures exhibited a desert rose-like morphology, producing an OCT signal comparable to that of Au nanostructures. The nanoclusters, tested in an intralipid medium, were evaluated in tissue phantoms. When the nanoclusters were injected into the tissue phantom, the OCT intensity increased by two to fourfold in the regions where the clusters were located. The clusters enabled imaging of the tissue at a depth of 1 mm.[187] The advancement in nanomaterials has introduced novel options for OCT imaging. Recently, innovative materials have been utilized for this purpose. For instance, intralipid, a nutrient solution for patients unable to eat normally, was introduced as a contrast agent for OCT bioimaging due to its favorable optical properties and excellent biocompatibility.[188]

Geng *et al.* used intralipid modified with DSPE-PEG2000-COOH (P-INT) as a contrast agent for OCT (Fig. 7). This contrast agent was employed to monitor changes in the vascular network of the ear site, the cerebral cortex and tumors. These contrast agents, based on NIR-II imaging, allowed for imaging at depths of up to 3 mm. The OCT imaging results not only provided images of the vascular network but also enabled calculations of blood flow. Additionally, P-INT was used for neuroimaging of the mouse brain at depths of 1–3 mm. This approach successfully imaged the blood vessels of melanoma tumors in mice, whereas other optical imaging methods, such as fluorescence and photoacoustic imaging, face challenges in visualizing melanoma vessels.[185]

Upconversion particles are another class of novel materials that have gained immense interest in the field of bioimaging due to their unique optical properties. Maurya *et al.* introduced an OCT contrast agent based on UCNPs using chicken tissue. The upconversion NPs, specifically $NaGdF_4:Er^{3+}/Yb^{3+}$, were stabilized by polyvinylpyrrolidone and oleic acid. Under 976 nm diode laser, the UCNPs exhibited spectra with three dominant emission bands at 521, 540, and 645 nm. The NPs provided a quantum yield of 4.92 ± 0.10% and 2.70 ± 0.10% at moderate power. They also exhibited good biocompatibility, with over 75% cell viability observed for HeLa and HEK293 cells. These contrast agents provided high-contrast OCT images of chicken breast tissue at significant depths of penetration.[189] Therefore, UCNPs exhibited potential biophotonic properties as OCT agents.

4.2.2 Photoacoustic imaging (PAI). Photoacoustic imaging (PAI) is a widely used biomedical imaging modality due to its several advantages, including non-invasiveness, non-ionizing radiation, and real-time imaging. In this technique, three-dimensional (3D) imaging is achieved through sound waves generated by the irradiation of near infrared (NIR) light on tissues. Under NIR laser light at 757 nm, tissue undergoes rapid thermal expansion, leading to the generation of sound waves. The performance of photoacoustic imaging depends on the light absorption coefficient of the imaged tissue and the contrast agents used in this technique. Since contrast agents in PAI interact with NIR light, they could be considered as biophotonic materials.[190]

So far, various biophotonic materials have been used as contrast agents in PAI, including metallic nanomaterials, carbon-based nanomaterials, organic molecules, and semiconducting NPs.[191] Although widely used in biomedicine, PAI has limitations like low contrast that need to be solved. To address this issue, Sun *et al.* fabricated Au nanorods modified with an azide compound, called as gas-generating laser-activatable nanorods for contrast enhancement (GLANCE). Under 815 nm NIR irradiation, the Au nanorods acted as a catalytic agent, generating nitrogen (N_2) gas bubbles from the azide compounds. This process enhanced the intensity of the ultrasound signal and improved the performance of PAI in targeted tissues. The GLANCE-modified Au nanorods exhibited significantly greater contrast enhancement compared to unmodified Au NPs.[192] In another study by Kim *et al.*, it was reported that Au nanospheres arranged in chains (Au sphere chains, or GSCs) significantly enhanced the efficiency of PAI compared to Au nanorods. The GSCs exhibited a high PAI signal *in vivo*, with mice receiving GSCs showing a 300% higher intensity of the PAI signal compared to those receiving a saline solution.[193] Using NIR-II laser irradiation can improve the efficiency of PAI due to its good penetrating biological tissue. Some organic dyes can act as contrast agents in the NIR range.

4.2.3 Luminescence (fluorescence) imaging. Luminescence imaging is a cutting age approach for studying biological species and their underlying processes, offering advantages such as non-invasiveness, real-time monitoring, and high sensitivity and selectivity. The success of this technique is attributed to speed development of its imaging instrument a fluorescent prob.[194] Fluorescent probs as biophotonic materials play a crucial role in improving luminescence imaging performance. These probes encompass a range of materials, including organic, inorganic, and hybrid types.[195] Among them, Au NPs have gained prominence as luminescent probes. Particularly, ultrasmall Au NPs have shown great potential in

 © 2025 The Author(s). Published by the Royal Society of Chemistry

Open Access Article. Published on 22 July 2025. Downloaded on 10/28/2025 10:32:42 AM.
This article is licensed under a Creative Commons Attribution-NonCommercial 3.0 Unported Licence.

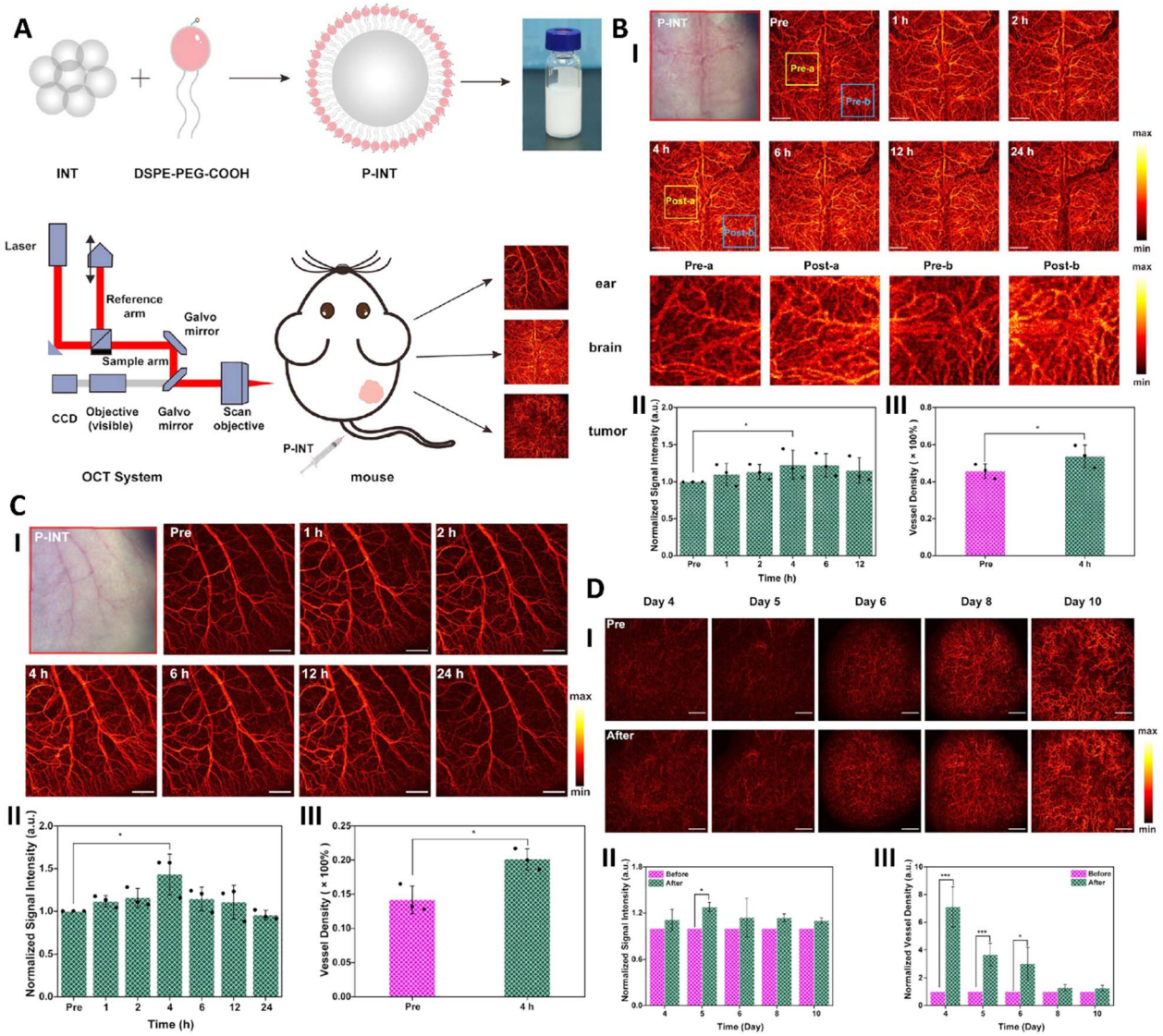

Fig. 7 (A) Schematic synthesis and mechanism of P-INT for OCT imaging. (B) OCT imaging (I) signal intensity (II) blood vessel density at 0 and 4 hours after injection of P-INT (III) for brain blood vessels. (C) OCT angiography imaging (I) signal intensity (II), blood vessel density 0 and 4 hours after injection of P-INT (III) of ear of mouse. (D) Monitoring tumor angiogenesis (I) quantification of signal intensity before and after injection of P-INT (II) tumor blood vessel density at different times after injection (III). Reprinted from 185 under CC-BY 4.0 license. Copyright 2024, American Chemical Society.

enhancing luminescence performance, especially in the NIR-II spectral window, which overcomes challenges such as limited tissue penetration and poor temporal resolution.[195]

Zhou *et al.* developed ultrasmall AuNPs as a nanoprobe for NIR-II luminescence. The AuNPs, with a size of approximately 1.93 nm, assembled through an etching process to form a unique Au(0) core/Au(1) shell structure (Fig. 8A). Their surface was functionalized by a series of mercaptoalkyl acids with different carbon chain lengths, including 6-mercaptohexanoic acid (MHA) and 8-mercaptooctanoic acid (MUA) (Fig. 8B). These NPs exhibited excellent NIR-II luminescence peak at 370 nm and a green fluorescence emission at 549 nm, providing a high quantum yield of 3.0%, which is higher than that of the majority of previously reported NIR-II emitting Au NPs (Fig. 8C). The ultrasmall Au NPs were biocompatible, with over 95% cell viability observed for HUVECs using the CCK-8 method. The MUA-capped NPs showed an intense NIR-II luminescence in the liver when injected into mice, with negligible emission in the kidney. The intense of emission reached its maximum within 1 h after injection and was retained for 48 h (Fig. 8D). ICP results confirmed that the content of MUA-capped NPs (1.0 ± 0.1% ID g^{-1}) in the kidney was significantly lower than that of MHA-capped Au (18.8 ± 1.1% ID g^{-1}), while the content of MUA-capped Au (82.0 ± 3.1% ID g^{-1}) in the liver was significantly higher than that of MHA-capped Au (30.6 ± 2.1% ID g^{-1}), providing prolong retention of MUA-capped Au in the liver for a week (Fig. 8E and D).[196]

In another study, the luminescence performance of Au NPs was enhanced when they were assembled with lanthanides. Li *et al.* employed ultrasmall Au nanoclusters to improve

Open Access Article. Published on 22 July 2025. Downloaded on 10/28/2025 10:32:42 AM.
This article is licensed under a Creative Commons Attribution-NonCommercial 3.0 Unported Licence.

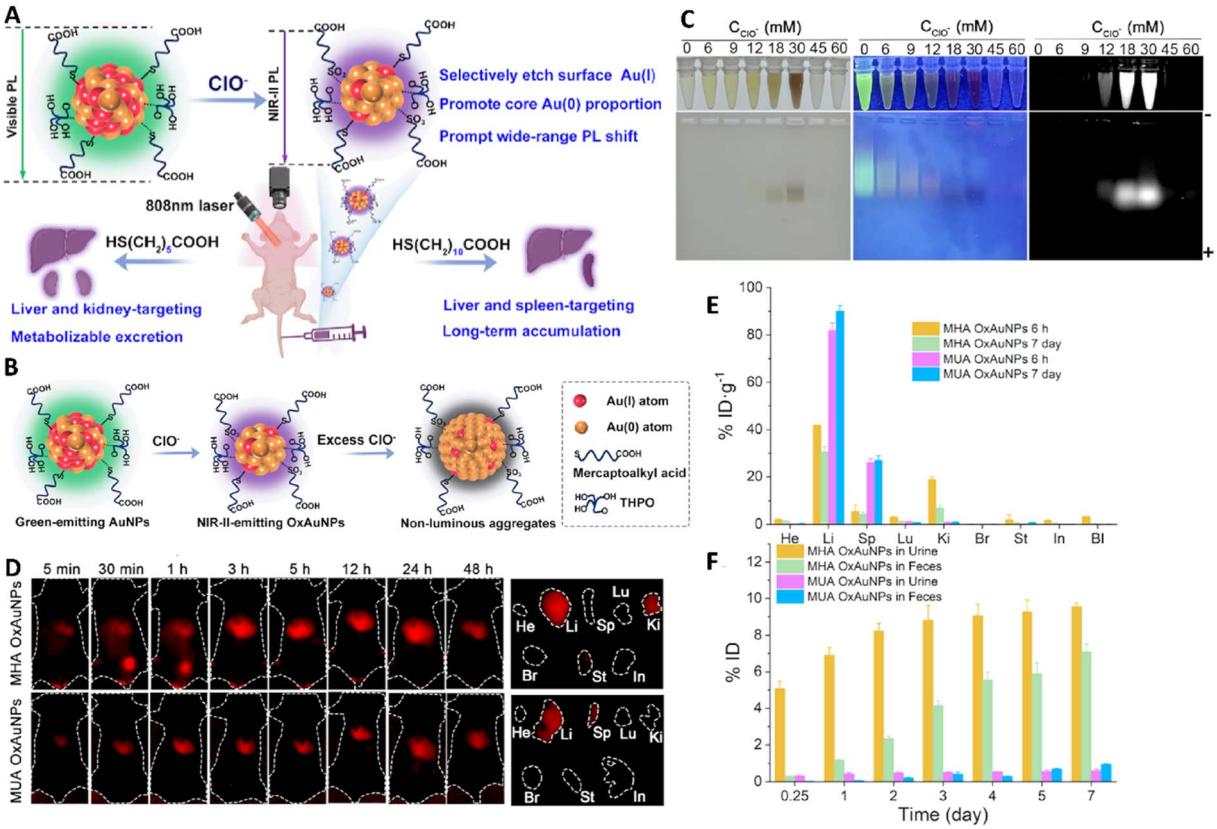

Fig. 8 (A) Schematic illustration of the acting mechanism of Au NPs. (B) Schematic illustration of the synthesis of Au NPs. (C) Optical characteristic of MUA Au NPs, left: bright field, middle: visible fluorescence, and right: NIR-II fluorescence. (D) Imaging performance of Au nanostructures *in vivo* at different times. (E) Biodistribution of Au capped MUA in main organs. (F) Body clearance at different times. Reprinted with permission from 196. Copyright 2024, American Chemical Society.

luminescence performance in *in vivo* NIR-II imaging of H_2S molecules. Au NPs with size of 2 nm were assemble with erbium (Er^{3+})-doped lanthanide NPs to create a core-satellite structure (Ln@AuNCs). These nanostructures provided strong NIR-II luminescence; under 808 nm laser irradiation, Ln@AuNCs demonstrated dual emission at 1100 nm and 1500 nm, with an intensity approximately 2.5-fold greater than that of Au nanoclusters. This approach enabled imaging of H_2S molecules with a limit of detection of 1.6 μM in mouse body, demonstrating a high selectivity. Furthermore, it allowed for liver-targeted and real-time imaging of H_2S.[197]

Using metals as hybrid materials has been employed as probes for luminescence. Wanas *et al.* developed a hybrid nanostructure integrating graphene oxide and zinc oxide for luminescence imaging of cancer. These graphene-based nanomaterials provided dual-mode emissions and targeted imaging *via* folic acid. The nanocomposite exhibited both up-conversion and down-conversion luminescence properties. The resulting spectra for down-conversion luminescence showed two characteristic emission peaks at 485 nm and 538 nm, while the up-conversion luminescence exhibited different characteristic emission peaks in the blue and green regions. Bioimaging of tumor-bearing mice injected with the nanocomposite demonstrated targeted luminescence at the tumor site.[198]

Utilizing natural compounds as luminescence probes can offer many advantages. Curcumin, as a natural compound, provides not only therapeutic benefits, such as anti-inflammatory and antioxidant effects, but also exhibits unique optical properties that make it suitable as a fluorescence probe. Wang *et al.* employed encapsulated in poly(D, L-lactide-*co*-glycolic) acid NPs (Cur@PLGA-NPs) for luminescence cell imaging. These NPs exhibited superior optical performance, achieving quantum yields of 23.78% in solution and 21.52% in solid state. The luminescence emission spectra showed a characteristic peak at 483 nm for the solution state and 537 nm for the solid state. The CT26 cells treated with Cur@PLGA-NPs demonstrated luminescence emission that was dependent on the concentration of the NPs.[199]

Some studies utilizing biophotonic nanomaterials, such as UCNPs and FRET-based NPs like cyanine fluorophore and Black Hole Quencher-3, have demonstrated high-quality imaging for the analysis of live biosystems.[200–202] For instance, a high-efficiency fluorescence imaging strategy was designed for imaging living cells and mouse bodies using biophotonic materials derived from UCNPs. This strategy included a DNA nanodevice that operated under NIR light. The nanodevice employed a self-propelled DNAzyme as a catalyst for a cascading entropy-driven mechanism in which the catalytic activity of the

 © 2025 The Author(s). Published by the Royal Society of Chemistry

Open Access Article. Published on 22 July 2025. Downloaded on 10/28/2025 10:32:42 AM. This article is licensed under a Creative Commons Attribution-NonCommercial 3.0 Unported Licence.

DNAzyme was activated *via* NIR irradiation. In this strategy, the UCNPs were modified with a triplex DNA composite, whose strands were labeled with fluorophore molecules (cyanine) and a quencher (Black Hole Quencher-3). The close spatial proximity between the cyanine and quencher led to the fluorescence quenching through FRET. Under NIR light irradiation, the UCNPs emitted UV light that cleaved the labeled triplex DNA composite, resulting in the production of a fluorescence signal for imaging applications. The modified UCNPs were loaded onto MnO_2 nanosheets, which served as a platform to facilitate the cascading entropy-driven catalysis process and provided highly effective *in vivo* imaging. Using a confocal laser scanning microscope, high-resolution images were obtained from human cells treated with the DNA nanodevice when exposed to 808 nm NIR irradiation. In the absence of NIR irradiation, the DNA nanodevice remained inactive, resulting in faint cyanine fluorescence.[200] In a similar study, the combination of a DNA device and UCNPs that were physiosorbed onto MnO_2 nanosheets were used to develop a high-quality fluorescence imaging strategy for living biosamples. In this strategy, a self-enhanced orthogonal catalytic DNA nanomachine was produced which contained a hairpin DNA structure and detached from the UCNPs under NIR irradiation. The detached hairpin initiated a catalytic process and triggered a strand displacement mechanism upon interaction with endogenous TK1 mRNA. This led to the formation of a three-stranded intermediate that contained an intact fuel chain, facilitating further catalytic cycles. The sensing target, miRNA-21, induced additional strand displacements, resulting in fluorescence recovery and enabling highly sensitive detection of biomolecular interactions.[201] These innovative approaches demonstrate the potential of using UCNPs and DNA nanomachines for real-time biosensing and imaging applications in living systems.

Biophotonic materials hold significant potential in imaging applications for medicine. They improve imaging resolution, allowing for detailed visualization of cellular and tissue structures. One advantage of biophotonic materials is their ability to facilitate real-time monitoring of bio-samples. In addition to enhancing imaging resolution, they serve as contrast agents, increasing the visibility of specific biological targets during imaging. Furthermore, these materials provide high-resolution images of living cells and organisms.

4.3 Therapy

Biophotonic materials have emerged as innovative tools in therapeutic applications due to their ability to interact with light in unique and precise ways. These materials, including nanostructures like Au NPs, UCNPs, and QDs, enable advanced treatment modalities such as PTT and photodynamic therapy (PDT). They can target diseased tissues, such as cancer cells, and interact with light to produce thermal effects, free radicals, or triggered chemical reactions that help eliminate diseased cells. Additionally, biophotonic materials have shown potential in wound healing and regenerative medicine by promoting controlled light delivery to stimulate tissue repair and angiogenesis. Their ability to be engineered for specific wavelengths and biocompatibility makes them a promising platform for next-generation therapeutic strategies.[203]

4.3.1 Photothermal therapy (PTT). PTT is a widely used method in treatment that relies on converting NIR light into heat using photosensitizer agents. The effectiveness of PTT is largely determined by the photothermal converting agents that generate hyperthermia after interacting with light and can be classified as biophotonic structures. Different types of photothermal agents have been used to date, including inorganic materials, organic materials, and hybrid of them. Noble metals including Ag, Au, palladium (Pd), and platinum (Pt) belong to the class of inorganic materials.[204]

Noble metals exhibit strong optical properties and relatively efficient photothermal conversion. They demonstrate an intriguing optical phenomenon known as Localized Surface Plasmon Resonance (LSPR), which involves the oscillation of electrons on the surface of metals due to light excitation. Photothermal conversion in noble metals occurs when photons are absorbed and converted into heat through the LSPR effect, resulting in outstanding photostability.[204,205] The efficiency of the photothermal effect in noble metals can be enhanced by optimizing their shape, size, and composition. For instance, studies have shown that gold nanostructures in rod shapes exhibit significant photothermal effects, and the LSPR is improved as the aspect ratio of the gold nanorods increases.[204,206] However, while gold nanorods possess excellent photothermal properties, they face biocompatibility challenges that limit their biological applications.[207]

Zengin *et al.* synthesized biocompatible Au nanorods (AuNRs) as a photothermal agent using a novel method. Cetyltrimethylammonium bromide (CTAB) is a common surfactant used in the synthesis of Au NPs; however, it is toxic to biological systems. In this study, a novel method was introduced to improve the biocompatibility of Au nanorods while preserving their photothermal efficiency. Consequently, CTAB was replaced with two biopolymers: Bovine Serum Albumin (BSA) and Dextran. The biocompatibility of AuNRs was enhanced while maintaining their photothermal efficiency. At a concentration of 200 μg mL^{-1} of CTAB@AuNR, the cell viability of the L929 cell line decreased to below 20%. In contrast, at the same concentration of biopolymer@AuNR, cell viability was above 78%. Notably, under 808 nm NIR irradiation, the photothermal efficiency of both nanostructures showed negligible differences.[208]

Another category of inorganic materials used in photothermal therapy as biophotonic structures includes carbon-based nanomaterials, owing to their unique optical properties and excellent thermal behavior.[204] Carbon-based nanomaterials can absorb a broad spectrum of light, including visible, ultraviolet (UV), and infrared (IR) wavelengths. They exhibit remarkable thermal stability, high thermal conductivity, and extensive chemical modifiability, which make them excellent candidates for use as photothermal therapy agents.[209] These materials typically convert light into heat through a non-radiative relaxation pathway. In this mechanism, upon light irradiation, electrons in the valence band of carbon atoms become excited and, as they return to the ground state, the

Open Access Article. Published on 22 July 2025. Downloaded on 10/28/2025 10:32:42 AM.
This article is licensed under a Creative Commons Attribution-NonCommercial 3.0 Unported Licence.

energy is released in the form of heat.[204] Interestingly, it has also been reported that some carbon-based nanomaterials, such as graphene, exhibit photothermal conversion based on LSPR effects, especially when modified or structured at the nanoscale.[210] Various types of carbon-based materials are employed as biophotonic agents for photothermal therapy, such as carbon dots, carbon nanotubes, and graphene. Khajuria *et al.* developed a photothermal agent using multiwalled carbon nanotubes specifically targeted for breast cancer cells. These carbon nanotubes were functionalized with an aptamer and possessed MRI imaging capabilities. Under UV-visible light irradiation, the nanotubes generated heat *via* the photothermal effect. At a light intensity of 62.5 mW cm^{-2}, the heat output was approximately 19.91 W g^{-1}.[211]

MXenes, a category of inorganic biophotonic materials, have shown promising potential for use as photothermal agents. MXenes are two-dimensional materials derived from transition metal carbides, nitrides, or carbonitrides. They share several properties with carbon-based nanomaterials, especially graphene, such as high electrical conductivity, tunable surface chemistry, and strong light absorption.[210] Their layered architecture and electronic structure make them effective broadband absorbers, capable of absorbing light in both visible and NIR regions.[209] Like graphene, MXenes exhibit photothermal effects, which are attributed to LSPR phenomena resulting from the presence of transition metals in their structure.[210] Due to their ease of surface engineering and the abundance of functional groups, MXenes can be tailored for specific biomedical applications. This versatility is particularly beneficial for addressing

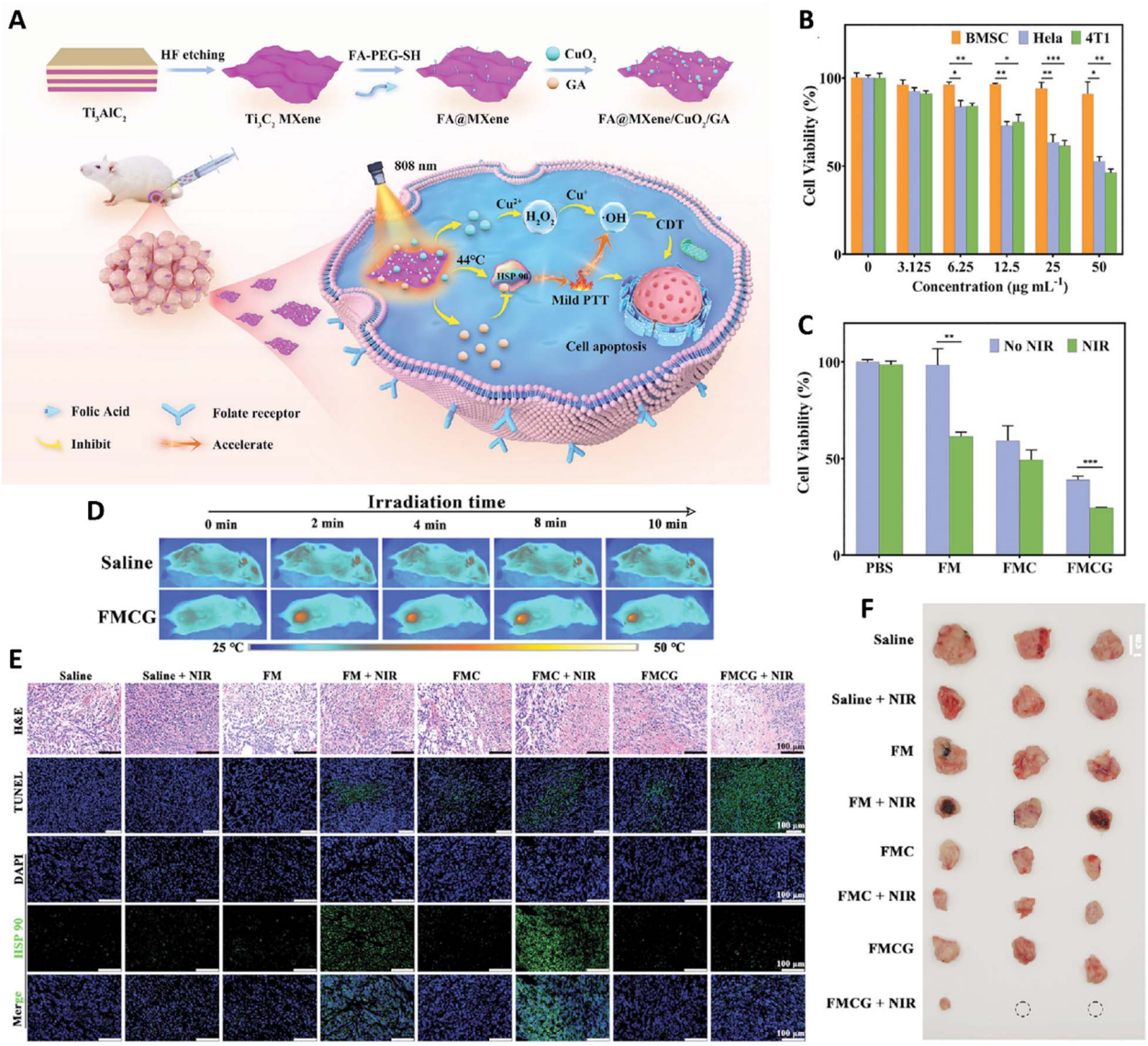

Fig. 9 (A) Schematic illustration of the nanocomposite: synthesis and mechanism. (B) *In vitro* cytotoxicity of different NPs. (C) Cell viability of normal and cancer cells at different concentration of FMCG. (D) Thermal infrared imaging in mice. *In vivo* anti-tumor effect of FMCG (E) immunofluorescence investigation in tumor tissue, including H & E staining, tunnel assay, and HSP90 immunofluorescence staining. (F) Tumor volume at the end of the experiments. Reprinted with permission from 212. Copyright 2024, Wiley.

 © 2025 The Author(s). Published by the Royal Society of Chemistry

Open Access Article. Published on 22 July 2025. Downloaded on 10/28/2025 10:32:42 AM. This article is licensed under a Creative Commons Attribution-NonCommercial 3.0 Unported Licence.

critical challenges such as cytotoxicity, targeted therapy, and enhanced photothermal conversion efficiency.[209] Xiong *et al.* synthesized a MXene nanocomposite as a photothermal agent for mild photothermal therapy (Fig. 9A). This nanocomposite was composed of Ti_3C_2 MXene, copper oxide (CuO_2) nanodots, and Gambogic acid (GA), which were functionalized with folic acid (FA) to create FA@MXene/CuO_2/GA (FMCG) as a targeting agent for tumor sites. FMCG not only served as a photothermal agent but also acted as a chemodynamic therapy agent due to the presence of CuO_2. The nanocomposite exhibited photothermal properties with an efficiency of 29.40% under NIR irradiation. In tumor-bearing mice, these nanocomposites were able to inhibit tumor growth (Fig. 9E and F); under 808 nm NIR irradiation, the temperature at the tumor site rapidly rose to over 40 °C and was maintained below 45 °C (Fig. 9D). Furthermore, FMCG exhibited good biosafety, with no observed adverse systemic effects during treatment (Fig. 9B and C).[212]

Besides the inorganic materials mentioned above, many organic materials have been used as photothermal agents, including semiconducting polymers such as polypyrrole, polydopamine, polythiophene, and polyaniline, as well as small molecules like porphyrin, BODIPY, cyanine, and phthalocyanine.[204] Conductive polymers are gaining attention as photothermal agents due to their lower cost compared to noble metals, as well as their photostability and biocompatibility. They exhibit photothermal effects through non-radiative relaxation processes, in which the π-conjugated system within the polymers absorbs photons under light irradiation, promoting electrons to excited states. These excited electrons then relax back to the ground state through vibrational and phonon interactions, releasing the absorbed energy as heat. Conductive polymers can be readily tuned *via* molecular design to achieve maximum absorption in the desired light region. As organic materials, polymers generally exhibit lower toxicity compared to inorganic counterparts.[213] Chen *et al.* synthesized conjugated polymer nanomaterials based on porphyrin and diketopyrrolopyrrole for cancer photothermal therapy. These nanomaterials exhibited a photothermal effect in the NIR-II window. Under 940 nm laser irradiation, a photothermal conversion efficiency of 86.21% was achieved, which was able to kill 78% of cancer cells *in vitro* at a concentration of 40 μg mL^{-1}. Additionally, tumor growth was almost completely inhibited in mice injected with the nanocomposite due to the photothermal effect.[214]

4.3.2 Photodynamic therapy (PDT). For the first time, the term "photodynamic action" was introduced in the 20th century, which laid the foundation for PDT.[215] PDT relies on the dynamic interaction between a biophotonic agent (photosensitizer (PS), light, and molecular oxygen. Upon light irradiation, the PS becoms activated and converts molecular oxygen into ROS, triggering a cascade of biochemical events that lead to damage to the target tissue.[216] Photoactivation of the PS can be achieved using various light sources, including ultraviolet (UV), visible, or NIR light, initiating a series of photochemical reactions. Under light exposure, the electron in the ground state absorbs the energy and becomes excited to a singlet state (^{1}PS*). Due to its short lifetime, ^{1}PS* tends to return to the ground state *via* radiative emission (fluorescence). Alternatively, ^{1}PS* can undergo intersystem crossing to reach the more stable triplet excited state (^{3}PS*), which has a longer lifetime. Upon returning to the ground state, ^{3}PS* may emit light through phosphorescence. PDT mechanisms are classified into two types based on the pathway followed during the return of ^{3}PS* to the ground state:

Type I: ^{3}PS* undergoes electron or hydrogen transfer with nearby molecules, especially molecular oxygen, leading to the formation of ROS such as superoxide anion ($O_2^{\bullet-}$) and hydroxyl radical ($^\bullet$OH).

Type II: ^{3}PS* transfers its energy directly to ground-state molecular oxygen ($^3O_2$), converting it into singlet oxygen ($^1O_2$), a highly reactive and cytotoxic form of oxygen.

The ROS generated during PDT ultimately lead to cancer cell death through both direct and indirect mechanisms. Direct mechanisms include biological processes such as necrosis, autophagy, and apoptosis, while indirect effects involve damage to the tumor vasculature, thereby restricting the supply of nutrients and oxygen to the tumor. Given the pivotal role of the PS in ROS generation, its properties significantly affect the efficacy of PDT. Desirable characteristics of an effective PS are including biocompatibility, suitable excitation wavelength, and chemical and photostability.[205] The first-generation PS was a porphyrin derivative that had several limitations, including poor water solubility, requirement for visible light excitation (which limits tissue penetration), low molar extinction coefficient, and challenges in purification. Since then, PDT has evolved significantly, with the development of newer generations of PSs that can be excited by NIR light, are water-soluble, and exhibit improved biocompatibility.[205,215] Today, the goal is to design PSs as advanced biophotonic materials that are biocompatible, easily synthesized, capable of efficiently generating ROS through both Type I and Type II PDT mechanisms under NIR irradiation, and selectively targeted to the intended tissue.

Au NPs have been reported as PS for PDT. Moloudi *et al.* synthesized a nanoformulation by combining berberine and Au NPs in a liposome platform (Lipo@AuNPs@BBR) as a PS for lung cancer photodynamic therapy. The hypothesis was that berberine and Au NPs would provide a synergistic PDT effect. The results confirmed this hypothesis; under 405 nm laser irradiation, the morphology of A549 cells treated with Lipo@AuNPs@BBR showed shrinkage and dissociation, while cells treated with Au NPs and berberine alone exhibited no changes in morphology. Additionally, the nanocomposite demonstrated greater efficacy in killing lung cancer cells compared to Au NPs and berberine alone when the treated cells were exposed to laser irradiation.[217] Besides noble metals, transition metal sulfides can also act as photosensitizer agents for PDT. Recent studies reported that hollow copper sulfide (CuS) can function as a photosensitizer and generate ROS under NIR irradiation.[218]

Chen *et al.* developed hollow copper sulfide platinum(IV) NPs loaded with platinum(IV) complexes as a photosensitizer for PDT, combined with chemo/photothermal therapy. These NPs were modified with polyethylene glycol (CuS@Pt (IV)@PEG NPs) to improve biocompatibility. Hollow CuS NPs and CuS@Pt (IV) @PEG NPs exhibited the ability to generate ROS, producing

Open Access Article. Published on 22 July 2025. Downloaded on 10/28/2025 10:32:42 AM.
This article is licensed under a Creative Commons Attribution-NonCommercial 3.0 Unported Licence.

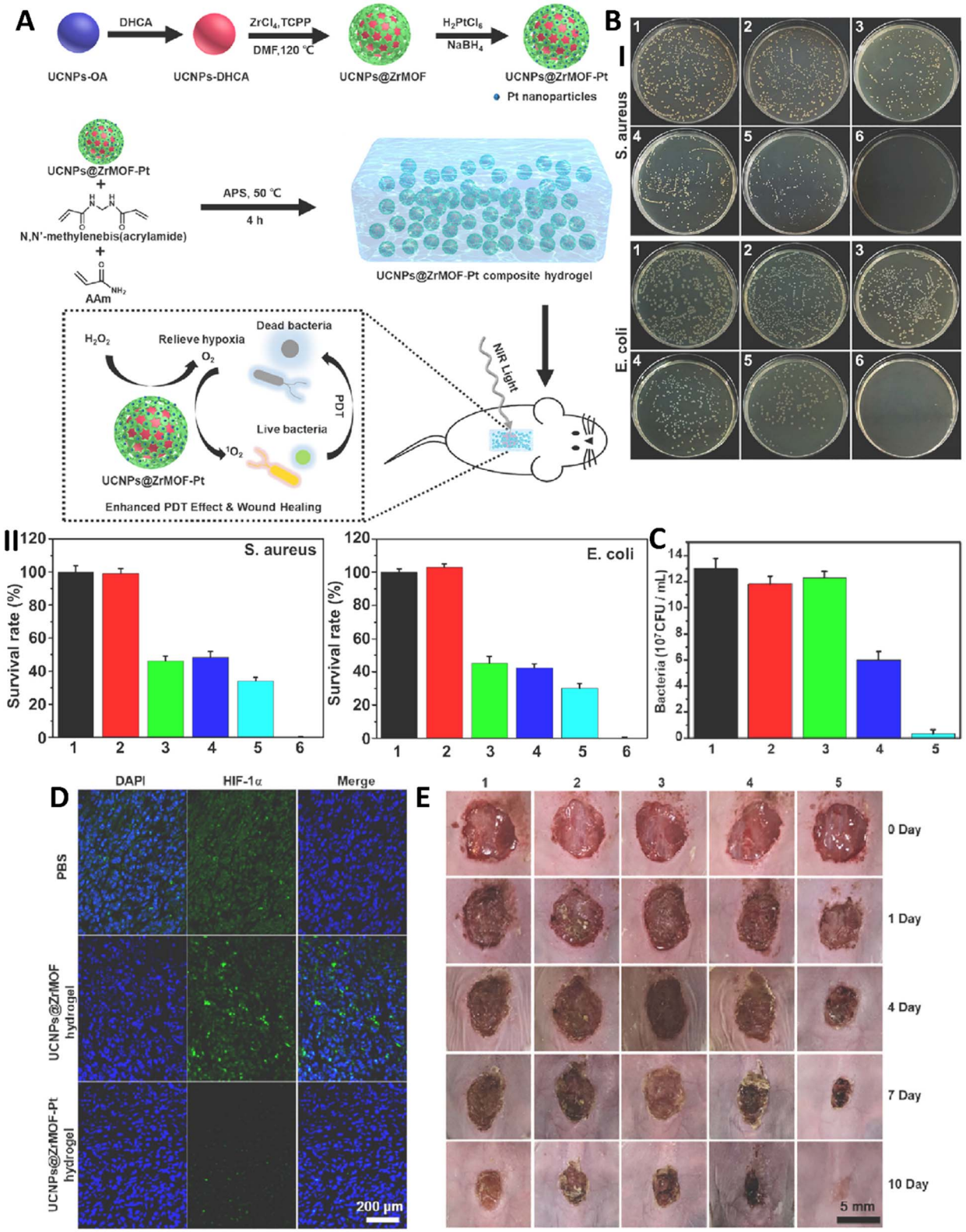

Fig. 10 (A) Schematic illustration of the synthesis and wound healing process of the UCNPs@ZrMOF-Pt hydrogel. (B) Antibacterial efficacy of the nanocomposite *in vitro* against *S. aureus* and *E. coli*: photograph of colony counter test (I), corresponding counted number of surviving bacteria (II) for different treatments including: (1) PBS, (2) UCNPs@ZrMOF-Pt hydrogel, (3) UCNPs@ZrMOF + laser, (4) UCNPs@ZrMOF-Pt + laser, (5) UCNPs@ZrMOF + H_2O_2+ laser, (6) UCNPs@ZrMOF-Pt + H_2O_2+ laser. (C) Counted number of survival bacteria in the wound after treatment. (D) Fluorescent image of immunofluorescence staining showing hypoxia level in the wound of mice. (E) Healing process of the wound in mice under different treatments: (1) PBS, (2) laser, (3) UCNPs@ZrMOF-Pt hydrogel, (4) UCNPs@ZrMOF hydrogel + laser, (5) UCNPs@ZrMOF-Pt hydrogel + laser. Reprinted with permission from 222. Copyright 2023, Elsevier.

 © 2025 The Author(s). Published by the Royal Society of Chemistry

Open Access Article. Published on 22 July 2025. Downloaded on 10/28/2025 10:32:42 AM. This article is licensed under a Creative Commons Attribution-NonCommercial 3.0 Unported Licence.

a strong 2′,7′-dichlorofluorescein (DCF)fluorescence peak under NIR irradiation. Additionally, platinum(IV) could enhance PDT performance by consuming glutathione. ROS were produced in HeLa cells incubated with CuS@Pt (IV)@PEG under 808 nm NIR irradiation, as indicated by the remarkable green fluorescence illumination from DCF. CuS@Pt (IV)@PEG significantly suppressed tumor growth in tumor-bearing mice injected with the NPs under NIR irradiation.[219]

MXenes have been reported as materials that possess excellent infrared light absorption capabilities at tumor sites. Furthermore, MXenes can serve as an ideal PS in PDT. They enhance the efficiency of PDT by integrating type I and type II mechanisms.[220] Zheng *et al.* utilized MXenes to combine type I and type II PDT for cancer treatment. The heterojunction formed by Ti_3C_2 MXene and cerium dioxide (CeO_2@MXene) exhibits Schottky junction properties, making it suitable for both type I and type II PDT. This system is capable of generating superoxide ions, hydroxyl radicals, singlet oxygen, and hydrogen peroxide. Under NIR irradiation, the viability of 143B cells treated with the heterojunction increased gradually with higher concentrations. In contrast, without laser irradiation, the cell viability reached 100%. Moreover, the heterojunction demonstrated efficient PDT *in vivo*, as the tumor volume in tumor-bearing mice treated with CeO_2@MXene under NIR irradiation was the smallest.[221]

Biophotonic structures, when used as PDT agents, offer promising antibacterial applications in tissue engineering. A novel composite hydrogel (UCNPs@ZrMOF-Pt) dressing incorporating UCNPs ($NaEr_{99.5\%}F_4$:$Tm_{0.5\%}$@$NaYF_4$) has been created to accelerate wound healing while showing remarkable antibacterial efficacy (Fig. 10A). This hydrogel dressing features a nanostructure coated with a porphyrin-based metal–organic framework and modified with platinum, serving as a catalyst for converting hydrogen peroxide to oxygen, thus addressing hypoxia. When exposed to NIR light, the porphyrin helps convert environmental oxygen to singlet oxygen, enabling photodynamic antibacterial action. This hydrogel was biocompatible, as evidenced by achieving a cell viability of over 90%. The composite demonstrated excellent antibacterial efficacy *in vitro*, eradicating 100% of bacterial colonies (Fig. 10B(I and II)). The hydrogel also decreased hypoxia levels *in vivo*, as shown by the lower intensity of immunofluorescence staining compared to other groups (Fig. 10C). Moreover, the nanocomposite facilitated wound healing, with the UCNPs@ZrMOF-Pt hydrogel achieving 100% wound closure under laser irradiation (980 nm, 10 min, 1.5 Wcm^{-2}) (Fig. 10D). Additionally, the nanocomposite's excellent antibacterial efficacy was confirmed *in vivo* by completely eradicating bacterial colonies in wounds (Fig. 10E). This nanocomposite provides an efficient strategy for antibacterial effects, enhancing the generation of singlet oxygen to improve antibacterial action and promote wound healing.[222]

Biophotonic nanostructures play a crucial role in advancing medical applications by enhancing therapeutic interventions. They improve the effectiveness of PDT and PTT in treating diseases such as cancer and bacterial infections. These nanostructures can be designed to be targeted and controllable, allowing for more precise treatment methods. Additionally, they enable the development of smart drug delivery systems that provide temporal-spatial control over drug release. The effectiveness of light irradiation in PTT and PDT can be further enhanced. For instance, biophotonic nanomaterials like UCNPs can improve the penetration depth of NIR light, increasing treatment efficacy. Thus, these materials exhibit great potential in therapeutic applications.

4.3.3 Advanced therapeutic applications

4.3.3.1. 3D-printing. Today, light-based 3D printing technology has gained popularity due to its spatial resolution, pattern fidelity, and fabrication speeds. This technology employs light to crosslink or solidify photosensitive bio-inks. Given the light-based nature of this technology, the use of biophotonic materials is crucial in the development of bio-inks. In this strategy, the interaction of light-sensitive bio-inks containing biophotonic materials with light initiates the photopolymerization process. These reactions are characterized by rapid curing rates, even under low light intensity, short exposure times, and negligible heat generation. Additionally, these reactions can be conducted under physiologic conditions without harsh cytotoxic reagents. These features facilitate application of biophotonic nanostructures on large-scale and are favorable for cell-based bioprinting applications, where maintaining biocompatibility is essential.[223]

Using biophotonic materials in three-dimensional (3D) printing technology enhances its functionality and potential applications. This led to the fabrication of a NIR light-responsive, 3D-printed scaffold for bone regeneration. This scaffold was composed of polydopamine-coated hydroxyapatite NPs and collagen, in which polydopamine-coated hydroxyapatite acted as a photothermal agent that responded to NIR light, enabling controlled drug release through heat generation. The scaffold was loaded with pargyline, an osteogenic drug, which was released in a controlled and on-demand manner under NIR irradiation. Upon NIR light exposure, the scaffold exhibited a photothermal effect, generating heat up to 48 °C. Drug release was adjustable under NIR irradiation, with an average release increase of approximately 10.38%, attributed to the photothermal effect. The biocompatible scaffold demonstrated osteogenic potential, as evidenced by the upregulation of osteogenesis-related gene expression, confirming its effectiveness in bone tissue engineering.[224]

In addition, biophotonic materials can impart valuable functionalities-such as photo-crosslinking to 3D-printed scaffolds. In this context, an aerogel scaffold was developed using photo-crosslinking-assisted 3D printing for applications in cancer therapy and tissue engineering. The scaffold was fabricated *via* self-assembly of silk fibroin methacrylate (SF-MA), as the primary biopolymeric matrix, incorporated with bismuth sulfide methacrylate (Bi_2S_3-MA) nanobelts, serving as photothermal agents. This composite mixture functioned as a bio-ink for 3D printing and was solidified through light-induced crosslinking. The scaffold was loaded with sorafenib, a chemotherapeutic agent, which was released upon localized heating triggered by the photothermal effect. Under 808 nm NIR irradiation for 2–3 min, the scaffold temperature increased up to 47–50 °C, enabling effective photothermal ablation of tumor

Open Access Article. Published on 22 July 2025. Downloaded on 10/28/2025 10:32:42 AM. This article is licensed under a Creative Commons Attribution-NonCommercial 3.0 Unported Licence.

tissue and controlled drug release. This platform achieved a 40% reduction in cancer cell viability after 20 min irradiation. These findings underscore the potential of biophotonic materials in advancing next-generation 3D-printed scaffolds for combined cancer therapy and regenerative applications.[225]

4.3.3.2. Self-assembly. Controlled self-assembly is an important topic in biological and nanotechnological applications and is widely used in diagnostic and therapeutic studies. RGD is a peptide that binds specifically to integrin $\alpha_v\beta_3$, which is overexpressed on cancer cells and associated with cell adhesion and migration behavior. Engineering the self-assembly of RGD peptides can help regulate the metastatic behavior of cancer cells. To this aim, a light-triggered self-assembly system was fabricated using RGD peptides to modulate peptide behavior. It was a platform composed of RGD, 3-methylene-2-(quinolin-8-yl) isoindolin-1-one, as a light-responsive unit, and a hydrogen-bonding peptide segment. Upon light irradiation, the platform transformed from nonfunctional NPs into functional nanofibers within living cells. While nanofibers were not internalized by cells, the NP conformation allowed cellular uptake. The light-induced self-assembly occurred rapidly, with a rate constant of up to 0.17 min^{-1}. A cell scratch healing assay was used to assess cell adhesion, revealing that cells treated with the nanoplatform under light irradiation achieved 76% closure, significantly higher than the untreated group (14%) and the group treated without light (17%). Therefore, the light-triggered self-assembly of RGD peptides can modulate cellular adhesion and holds potential for regulating biological behaviors in biosystems.[226]

Light-triggered self-assembly can control the size, shape, surface chemistry, and long-term stability of nanostructures, influencing their cellular internalization ability and clinical safety. Self-assembly can also affect selective biocompatibility; altering the shape of nanostructures can induce selective cytotoxicity. For instance, transforming from a spherical form to a fibrous form under light irradiation can target specific cells, or releasing drugs from self-assembled prodrugs that can induce selective toxicity for target cells.[227] In a study by Wang *et al.*, self-assembled platinum(II) complexes were synthesized as anticancer theranostic agents that exhibited varying levels of cytotoxicity before and after self-assembly. These complexes were a series of planar cyclometalated platinum(II) complexes with a main ligand containing enlarged aromatic rings, which enabled phosphorescence emission and self-assembly into linear nanoparticles. With an increase in the number of rings, both lipophilicity and selective cytotoxicity for cancer cells increased.[228] In addition, self-assembly is a bottom-up fabrication strategy that supports the scalable production of nanostructures. Compared to conventional techniques such as lithography, self-assembly is more cost-effective and offers a flexible approach for controlling interparticle spacing in assembled structures.[229] Specifically, light-triggered self-assembly can further reduce costs, as light serves as a non-invasive initiator of the assembly process. Moreover, the use of light enables the application of this technique under biologically relevant conditions.[230]

4.3.3.3. Wearable device. Biophotonic materials offer a transformative approach for the next generation of wearable health devices due to their unique optical and physical properties. These materials enable highly sensitive and rapid monitoring, support the simultaneous tracking of multiple health signals, and are less susceptible to electromagnetic interference compared to traditional electrically based wearable devices. Additionally, they facilitate non-invasive health monitoring. Technological advancements critical to enabling continuous health monitoring include the development of highly flexible and biocompatible materials (*e.g.*, polydimethylsiloxane (PDMS), polyurethane (PU), graphene, molybdenum disulfide (MoS_2)), integration of nanoscale optical sensors capable of functioning under dynamic physiological conditions, and incorporation of self-powered systems through mechanisms like solar energy harvesting. These features enhance comfort, long-term wearability, and uninterrupted data collection. Despite their advantages, biophotonic materials also face certain limitations compared to conventional electronic materials. These include higher production costs, complex manufacturing processes, and sensitivity to environmental factors such as variations in ambient light and the opacity of biological tissues. Additionally, ensuring reliable data transmission, device miniaturization, and compatible integration with existing digital health platforms remains a key challenge.[231]

This section presents examples of innovative applications involving the integration of biophotonic materials into wearable devices. Using biophotonic materials in wearable devices introduces innovative and valuable properties for medical applications. Transparency, defogging functionality, and self-healing are beneficial features that increase the efficiency of light-responsive wearable devices. These features enhance optical clarity, prevent fog formation on optical surfaces, and reduce the need for frequent replacements. For instance, a wearable composite film was fabricated in a study with the capability of efficient photothermal healing. This transparent composite film was composed of plasmonic Ag NPs embedded in covalent-organic framework (COF) nanosheets and exhibited defogging functionality. The composite film was then integrated into a waterborne elastic polyurethane (PU) matrix. By integrating AgNPs, with strong plasmonic properties, and COFs, as photothermal agents, the researchers achieved a synergistic photothermal effect, resulting in a rapid temperature increase to 80 °C under NIR irradiation. This localized temperature rise enabled efficient self-healing, with a recovery rate exceeding 98%. Additionally, after 12 h of NIR irradiation, the composite film maintained a high transmittance of 96.2%. The composite film was successfully tested on human skin, confirming its practical potential as a transparent, self-healing, defogging, and solar-powered wearable material.[232]

Integrating biophotonic materials with wearable electronics also offers a promising approach for developing patient-friendly diagnostic tools. This led to the fabrication of a wearable on-eye contact lens system *via* embedding ultrathin organic light-emitting diodes (OLEDs) into contact lenses for electroretinography (ERG), aimed at diagnosing retinal diseases. The OLED was encapsulated within a dual two-dyad multilayer structure to ensure both durability and biocompatibility. This

 © 2025 The Author(s). Published by the Royal Society of Chemistry

Open Access Article. Published on 22 July 2025. Downloaded on 10/28/2025 10:32:42 AM.
This article is licensed under a Creative Commons Attribution-NonCommercial 3.0 Unported Licence.

system incorporated wireless power transfer operating at a resonance frequency of 433 MHz, enabling smartphone-controlled energy delivery. Preclinical testing on rabbits demonstrated that the device could generate a robust ERG signal of approximately 60 μV during 10 Hz flicker stimulation at a luminance of 126 nits. By integrating biophotonic components into a wearable medical platform, this system provided a portable, point-of-care solution for retinal diagnostics.[233]

5 Challenges

Despite the tremendous advancements in biophotonic nanostructures, several technical, material, and translational challenges exist that hinder their full potential in biomedical and industrial applications. These challenges range from issues in material compatibility and device fabrication to integration with complex biological systems and scalability for clinical translation. Addressing these challenges needs a multidisciplinary approach combining innovations in material science, engineering, and biology, alongside advancements in fabrication techniques and regulatory frameworks.

5.1 Biocompatibility and biodegradability

The biocompatibility and biodegradability of materials remain a cornerstone challenge for biophotonic nanostructures, particularly for *in vivo* applications. Conventional materials such as silica, glass, and metal NPs offer superior optical properties but often fail to meet the stringent requirements for biological safety.[234] Metal-based materials, including Au and Ag NPs, frequently accumulate in tissues, posing risks of cytotoxicity and long-term inflammation. Similarly, polymeric materials, though versatile, often lack sufficient biodegradability, necessitating removal or leading to chronic adverse effects.[234,235] Emerging biologically derived materials, such as silk fibroin, DNA, and polysaccharides, offer promising alternatives due to their inherent biocompatibility and natural degradation in biological environments.[236] For instance, silk-based photonic devices have shown exceptional promise in optical sensing while minimizing immunogenic responses.[237,238] However, these materials often require optimization to achieve the same level of optical performance and stability as traditional synthetic materials. Advancing composite materials that combine the optical superiority of synthetic materials with the biocompatibility of biological ones is a promising pathway. Another pressing issue is the limited environmental sustainability of current nanofabrication methods, which often involve hazardous chemicals and high energy consumption.[239] The development of greener, more sustainable materials and synthesis approaches is essential for addressing these concerns.

5.2 Device scalability and fabrication

Achieving scalable and reproducible fabrication of biophotonic nanostructures is a persistent challenge that significantly impacts their commercial and clinical viability. Traditional fabrication methods such as electron-beam lithography, colloidal synthesis, and template-assisted assembly, while precise, are time-consuming, costly, and impractical for mass production. These methods often face difficulties in maintaining uniformity and reproducibility across large-scale production, where even slight variations in size, shape, or composition can drastically alter optical properties and device performance. Microfluidic technologies have emerged as a transformative solution for addressing these challenges. By leveraging the precise control over fluid dynamics at the microscale, microfluidic systems enable the scalable synthesis of nanostructures with exceptional uniformity and reproducibility. For instance, droplet-based microfluidic platforms allow for the production of monodisperse NPs and microbeads, which are critical for applications such as plasmonic sensing and fluorescence imaging. The ability to control reaction kinetics and mixing efficiency in microfluidic channels ensures consistent particle properties across batches.[240–242] Additionally, microfluidics facilitates the integration of multiple fabrication steps, such as synthesis, functionalization, and assembly, into a single automated platform. This approach reduces manufacturing complexity and cost while enhancing throughput. For instance, microfluidic systems have been utilized to create multilayered photonic crystals and hybrid nanostructures, combining diverse optical functionalities for advanced applications in imaging and sensing.[243] Advancements in additive manufacturing techniques, such as 3D printing, have also opened new avenues for the scalable fabrication of biophotonic devices. 3D printing allows for the rapid prototyping of customizable nanostructures with complex geometries, paving the way for patient-specific medical devices and tailored therapeutic solutions. However, ensuring the optical precision and material compatibility of 3D-printed biophotonic devices remains a critical area for further research.[244]

5.3 Integration with biological systems

Biophotonic nanostructures are designed to operate in complex biological environments, where their performance can be significantly influenced by factors such as optical scattering, tissue absorption, and dynamic biological processes. Achieving effective integration with living systems requires precise control over bio-nano interactions, including cellular uptake, immune responses, and long-term stability. Surface functionalization strategies, such as ligand attachment and polymer coatings, have been developed to improve the targeting and biocompatibility of nanostructures. Despite these advancements, challenges remain in ensuring uniform interactions across diverse biological environments. For instance, tissue heterogeneity and variations in pH, temperature, and enzymatic activity can alter the behavior of biophotonic devices, reducing their efficacy.[245–247] Adaptive nanostructures that respond dynamically to environmental stimulus, such as temperature or pH changes, offer a promising solution. These stimuli-responsive materials can enhance the specificity and functionality of biophotonic devices in real-time applications, such as targeted drug delivery and responsive imaging.[248,249]

5.4 Challenges of clinical translation

Bridging the gap between research and clinical application is one of the most significant hurdles in biophotonics. Regulatory

Open Access Article. Published on 22 July 2025. Downloaded on 10/28/2025 10:32:42 AM.
This article is licensed under a Creative Commons Attribution-NonCommercial 3.0 Unported Licence.

frameworks for medical devices require rigorous testing for safety, efficacy, and reliability, often necessitating extensive preclinical and clinical studies. The high cost and time required for these processes can delay the translation of innovative technologies from the lab to the clinic.[250,251] Agencies like the FDA or EMA require extensive safety, efficacy, and manufacturing data, which are costly and time-consuming to generate. Nanostructures often do not fit neatly into existing regulatory categories, leading to ambiguity and delays. Moreover, the lack of standardized testing protocols for nanomaterials hampers approval processes. Biocompatibility issues are at the core of regulatory concerns. The interaction of nanostructures with biological systems is complex and not fully understood. Factors like immune activation, cytotoxicity, and potential genotoxicity must be thoroughly investigated. Surface modifications intended to improve stability or targeting can introduce new risks, such as unforeseen immune responses or toxicity. Long-term biodistribution and clearance also remain poorly characterized, raising doubts about accumulation and chronic effects. Moreover, the integration of biophotonic devices into existing diagnostic and therapeutic workflows requires compatibility with established medical infrastructure.[252] For instance, imaging devices must seamlessly integrate with hospital imaging systems, and biosensors must align with laboratory protocols for sample preparation and analysis. Standardization of operating procedures, device calibration, and data interpretation is critical for achieving widespread clinical adoption. The future of biophotonic nanostructures lies in overcoming existing challenges through interdisciplinary innovation and the adoption of emerging technologies. One promising direction is the development of hybrid nanostructures that combine the strengths of multiple materials.[253–255] For instance, integrating plasmonic NPs with bio-inspired polymers can yield devices with enhanced optical properties and improved biocompatibility. Artificial intelligence (AI) and machine learning (ML) are poised to revolutionize the design, fabrication, and application of biophotonic devices. AI-driven algorithms can optimize nanostructure designs for specific applications, while ML-based tools can analyze complex optical signals for enhanced diagnostic accuracy. These technologies can also facilitate the development of adaptive systems that learn and respond to environmental changes, improving the performance of biophotonic devices in dynamic biological settings.[256–258] Sustainability is another critical frontier for biophotonics. Indeed, the development of renewable, biodegradable materials and energy-efficient fabrication methods aligns with global efforts to reduce environmental impact. Exploring the use of bio-waste and naturally abundant materials for constructing photonic devices represents a promising step toward eco-friendly innovation. Additionally, phototoxicity arises when light-based therapies induce damage to healthy tissues due to reactive oxygen species or thermal effects. This is a concern in photodynamic therapy and other light-activated treatments using nanostructures, requiring careful control of light dose and NP properties to minimize adverse effects. Understanding and mitigating phototoxic effects are critical for safe clinical application, especially when NPs enhance light absorption or generate reactive species.

6 Conclusion

Recent advancements in biophotonic nanostructures have significantly enhanced the capabilities of optoelectronic devices. Innovations in materials science and engineering have led to the development of highly efficient LEDs, photodetectors, and various other photonic devices that leverage the unique optical properties of nanostructures. By manipulating light at the nanoscale, researchers have improved functionality, resulting in devices with better performance metrics, such as increased sensitivity and reduced energy consumption. These advancements expand the applications of optoelectronics into diverse fields, including telecommunications and environmental monitoring, but perhaps most notably, biomedicine. In this context, the ability to create more sensitive and accurate diagnostic tools has paved the way for earlier disease detection and better patient management, ultimately improving health outcomes. Despite the progress made in biophotonic nanostructures, several challenges hinder their widespread application in biomedicine. One significant concern involves the design and synthesis of nanostructures that are not only effective but also safe for clinical use. Issues related to biocompatibility, stability, and reproducibility must be thoroughly addressed to ensure the successful translation of these technologies from the laboratory to clinical settings. Additionally, the variability in patient responses to nanostructured materials complicates the development of universally applicable solutions. Furthermore, regulatory hurdles and the need for comprehensive clinical trials can slow down the implementation of biophotonic innovations, as these processes require extensive validation to ensure safety and efficacy. Looking ahead, the future of biophotonics and its applications in biomedicine appears promising. We can expect a new generation of biophotonic devices that are more efficient, versatile, and capable of addressing complex medical challenges. The integration of artificial intelligence and machine learning with biophotonic technologies may further enhance their diagnostic and therapeutic capabilities by enabling real-time data analysis and decision-making. By harnessing these advanced computational tools, clinicians could receive timely insights, improving patient outcomes through personalized treatment strategies. Additionally, as our understanding of biological systems deepens, biophotonic nanostructures can be tailored for specific medical applications, fostering personalized medicine approaches that cater to individual patient needs.

Data availability

No data was used for the research described in the article.

Author contributions

Masoomeh Amoozadeh: writing – review & editing; Amirali Hariri: writing – review & editing; Atefeh Zarepour: writing –

 © 2025 The Author(s). Published by the Royal Society of Chemistry

Open Access Article. Published on 22 July 2025. Downloaded on 10/28/2025 10:32:42 AM. This article is licensed under a Creative Commons Attribution-NonCommercial 3.0 Unported Licence.

review & editing; Arezoo Khosravi: writing – review & editing, visualization; Siavash Iravani: supervision, conceptualization, writing – review & editing; Ali Zarrabi: supervision, writing – review & editing.

Conflicts of interest

Author(s) declare no conflict of interest.

References

1 M. A. Iqbal, M. Malik, N. Anwar, S. Bakhsh, S. Javeed, S. S. Maidin, K. Morsy, R. Y. Capangpangan, A. C. Alguno and J. R. Choi, *Arabian J. Chem.*, 2023, **16**, 105040.
2 W. S. Lam, W. H. Lam, P. F. Lee and S. H. Jaaman, *Heliyon*, 2023, **9**, e23011.
3 Q. Luo, *Sci. China:Life Sci.*, 2020, **63**, 1771–1775.
4 S. Zhang, C. L. Wong, S. Zeng, R. Bi, K. Tai, K. Dholakia and M. Olivo, *Nanophotonics*, 2020, **10**, 259–293.
5 S. Khan and I. Sharma, in *Photonic Materials: Recent Advances and Emerging Applications*, 2023, pp. 141–159.
6 S. Dasgupta and K. Ray, *Front. Chem.*, 2024, **12**, 1407561.
7 M. A. Iqbal, N. Ashraf, W. Shahid, M. Awais, A. K. Durrani, K. Shahzad and M. Ikram, in *Nonlinear Optics - Nonlinear Nanophotonics and Novel Materials for Nonlinear Optics*, ed. B. I. Lembrikov, 2021, pp. 17–39.
8 K. Agarwal, H. Rai and S. Mondal, *Mater. Res. Express*, 2023, **10**, 062001.
9 M. Criado-Gonzalez, C. Marzuoli, L. Bondi, E. Gutierrez-Fernandez, G. Tullii, P. Lagonegro, O. Sanz, T. Cramer, M. R. Antognazza and D. Mecerreyes, *Nano Lett.*, 2024, **24**, 7244–7251.
10 S. Gandhi, S. K. Awasthi and A. H. Aly, *RSC Adv.*, 2021, **11**, 26655–26665.
11 A. S. Firouzjaei, S. S. Afghahi and A.-A. E. Valmoozi, in *Recent Advances and Trends in Photonic Crystal Technology*, IntechOpen, 2024, pp. 27–55.
12 P. Steglich, G. Lecci and A. Mai, *Sensors*, 2022, **22**, 2901.
13 A. Guglielmelli, F. Pierini, N. Tabiryan, C. Umeton, T. J. Bunning and L. De Sio, *Adv. Photonics Res.*, 2021, **2**, 2000198.
14 K. Yang, Y. Chen, S. Yan and W. Yang, *Heliyon*, 2023, **9**, e16598.
15 J. Chen and K. Rong, *Mater. Chem. Front.*, 2021, **5**, 4502–4537.
16 Y.-R. Wang, I. S. Han and M. Hopkinson, *Nanophotonics*, 2023, **12**, 1469–1479.
17 M. Ghoumazi and A. Hocini, *Int. J. Sens. Wirel. Commun. Control.*, 2021, **11**, 216–224.
18 M. He, Z. Zhang, C. Cao, Y. Qiu, X. Shen, G. Zhou, Z. Cai, X. Sun, X. He and L. Xu, *PhotoniX*, 2022, **3**, 25.
19 Y. Zhou, Y. Lu, Y. Liu, X. Hu and H. Chen, *Biosens. Bioelectron.*, 2023, **228**, 115231.
20 F. Peng, S. Jeong, A. Ho and C. L. Evans, *Cytometry, Part A*, 2021, **99**, 1067–1078.
21 Y. Zhang, M. Zhao, J. Wang, W. Liu, B. Wang, S. Hu, G. Lu, A. Chen, J. Cui and W. Zhang, *Sci. Bull.*, 2021, **66**, 824–838.
22 N. Li, C. P. Ho, I.-T. Wang, P. Pitchappa, Y. H. Fu, Y. Zhu and L. Y. T. Lee, *Nanophotonics*, 2021, **10**, 1437–1467.
23 B. A. Taha, I. A. Al-Tahar, A. J. Addie, A. B. Mahdi, A. J. Haider, Y. Al Mashhadany, V. Chaudhary and N. Arsad, *Appl. Mater. Today*, 2024, **38**, 102229.
24 P. Sarbadhikary, B. P. George and H. Abrahamse, *Theranostics*, 2022, **12**, 7335.
25 A. S. Gomes, L. d. S. Menezes and H. P. de Oliveira, in *Modern Luminescence from Fundamental Concepts to Materials and Applications*, Elsevier, 2023, pp. 275–312.
26 P. Pallavi, P. Sharmiladevi, V. Haribabu, K. Girigoswami and A. Girigoswami, *Curr. Nanosci.*, 2022, **18**, 675–689.
27 X. Liu, J. Yuan, D. Wu, X. Zou, Q. Zheng, W. Zhang and H. Lei, *Nanophotonics*, 2020, **9**, 611–622.
28 Q. Lu, Y. Sun, Z. Liang, Y. Zhang, Z. Wang and Q. Mei, *ACS Nano*, 2024, **18**(22), 14123–14144.
29 B. J. Barros and J. P. Cunha, *Front. Neurosci.*, 2024, **18**, 1382341.
30 C. Sun, L. Yang, B. Li, W. Shi, H. Wang, Z. Chen, X. Nie, S. Deng, N. Ding and A. Zhang, *Opt. Lett.*, 2021, **46**, 5699–5702.
31 W. Redjem, Y. Zhiyenbayev, W. Qarony, V. Ivanov, C. Papapanos, W. Liu, K. Jhuria, Z. Al Balushi, S. Dhuey and A. Schwartzberg, *Nat. Commun.*, 2023, **14**, 3321.
32 H. Wang, Z. Chen, C. Sun, S. Deng, X. Tang, L. Zhang, R. Jiang, W. Shi, Z. Chen and Z. Li, *Opt. Lett.*, 2021, **46**, 286–289.
33 J. Chang, J. Gao, I. Esmaeil Zadeh, A. W. Elshaari and V. Zwiller, *Nanophotonics*, 2023, **12**, 339–358.
34 H. Y. Lee and S. Kim, *Nanophotonics*, 2022, **11**, 2571–2582.
35 T. Pan, D. Lu, H. Xin and B. Li, *Light: Sci. Appl.*, 2021, **10**, 124.
36 N. Liu, *Nano Lett.*, 2020, **20**, 8430–8431.
37 L. Dai, P. Liu, X. Hu, X. Zhao, G. Shao and Y. Tian, *Analyst*, 2021, **146**, 1807–1819.
38 X. Zhou, S. Lin and H. Yan, *J. Nanobiotechnol.*, 2022, **20**, 257.
39 V. E. Bochenkov, E. M. Lobanova, A. M. Shakhov, A. A. Astafiev, A. M. Bogdanov, V. A. Timoshenko and A. V. Bochenkova, *Nanomaterials*, 2020, **10**, 2563.
40 G. Heesink, C. Caron, K. van Leijenhorst-Groener, R. Molenaar, T. W. Gadella Jr, M. M. Claessens and C. Blum, *J. Phys. Chem. B*, 2022, **126**, 7906–7915.
41 J. D. Pajović, R. J. Dojčilović, S. Kaščáková, M. Réfrégiers, D. K. Božanić and V. Djoković, *Colloids Surf., B*, 2023, **227**, 113340.
42 X. Liu, J. Liu, X. Zhao, D. Zhang and Q. Wang, *Opt. Express*, 2022, **30**, 34918–34931.
43 R. Rajasekaran, E. Brindha, G. Bharanidharan, B. G. Manaye, P. Aruna and S. Ganesan, *Optical Biopsy XXII: Toward Real-Time Spectroscopic Imaging and Diagnosis*, 2024, vol. 12836, pp. 102–105.
44 S. Bannur Nanjunda, V. N. Seshadri, C. Krishnan, S. Rath, S. Arunagiri, Q. Bao, K. Helmerson, H. Zhang, R. Jain and A. Sundarrajan, *Nanophotonics*, 2022, **11**, 5041–5059.
45 Z. Jakšić, M. Obradov and O. Jakšić, *Biomimetics*, 2022, **7**, 222.

Open Access Article. Published on 22 July 2025. Downloaded on 10/28/2025 10:32:42 AM.
This article is licensed under a Creative Commons Attribution-NonCommercial 3.0 Unported Licence.

46 Z. Jakšić, S. Devi, O. Jakšić and K. Guha, *Biomimetics*, 2023, **8**, 278.
47 H. Y. Jeong, E. Lee, S.-C. An, Y. Lim and Y. C. Jun, *Nanophotonics*, 2020, **9**, 1139–1160.
48 H. Yu, Y. Peng, Y. Yang and Z.-Y. Li, *npj Comput. Mater.*, 2019, **5**, 45.
49 J. Liu, H. He, D. Xiao, S. Yin, W. Ji, S. Jiang, D. Luo, B. Wang and Y. Liu, *Materials*, 2018, **11**, 1833.
50 H. S. Naher, B. A. H. Al-Turaihi, S. H. Mohammed, S. M. Naser, M. A. Albark, H. A. Madlool, H. A. M. Al-Marzoog and A. T. Jalil, *J. Drug Delivery Sci. Technol.*, 2023, **80**, 104175.
51 W. He, M. Wang, P. Cheng, Y. Liu and M. You, *TrAC, Trends Anal. Chem.*, 2024, **176**, 117735.
52 S. Jin, Y. Hu, Z. Gu, L. Liu and H.-C. Wu, *J. Nanomater.*, 2011, **2011**, 834139.
53 H. Chen, J. Wei, F. Pan, T. Yuan, Y. Fang and Q. Wang, *Adv. Mater. Technol.*, 2025, **10**, 2400865.
54 A. Starczewska and M. Kępińska, *Materials*, 2024, **17**, 1196.
55 F. Baldini, K. Dholakia, P. French, O. Guntinas-Lichius, A. Kohler, W. Mäntele, L. Marcu, R. Sroka, S. Umapathy and J. Popp, *J. Biophot.*, 2025, **18**, e202500148.
56 N. N. Joshi, J. Narayan and R. Narayan, *Mater. Adv.*, 2024, **5**, 9160–9174.
57 C. Allarà, A. Orlando, G. Ciccone, S. Krik, M. Pompilio, A. Pedrielli, A. Gaiardo, P. Lugli, L. Petti and F. Cacialli, *Adv. Electron. Mater.*, 2025, 2500073.
58 K. Yadav, K. Chaturvedi, A. Singhwane and S. Verma, in *MXene-Based Emerging 2D Materials for Biomedical Applications*, ed. S. Verma, 2025, pp. 50–69.
59 M. Ragaei, M. Abdel-Raheem, M. Hala and H. Huda, *Afr. J. Biomed. Res.*, 2024, **27**, 7130–7138.
60 K. Saito, Y. Nemoto and Y. Ishikawa, *Nano Lett.*, 2024, **24**, 12840–12848.
61 K. D. Devi, A. Sharma, S. Ojha, J. Parkash, A. Mishra and F. Singh, *Mater. Today Commun.*, 2024, **40**, 109488.
62 M. A. Fakhri, B. G. Rasheed, M. J. Abd-Alhussain, E. T. Salim, A. S. Azzahrani, A. Basem and S. C. Gopinath, *Plasmonics*, 2024, 1–11.
63 N.-B. Trinh, T. A. Nguyen, S.-H. L. Truong and K. Q. Vo, *Soft Matter*, 2025, **21**, 948–969.
64 S. Atta, Y. Zhao, S. Sanchez, D. Seedial, J. P. Devadhasan, A. J. Summers, M. A. Gates-Hollingsworth, K. J. Pflughoeft, J. Gu and D. C. Montgomery, *ACS Appl. Mater. Interfaces*, 2024, **16**, 54907–54918.
65 K. El-Boubbou, E. Ximendes, F. J. Teran, R. Marin, Á. Artiga, D. H. Ortgies and D. Jaque, *ACS Appl. Nano Mater.*, 2024, **7**, 13959–13972.
66 A. A. Rempel, O. V. Ovchinnikov, I. A. Weinstein, S. V. e. Rempel', Y. V. Kuznetsova, A. V. Naumov, M. S. Smirnov, I. Y. e. Eremchev, A. S. Vokhmintsev and S. S. Savchenko, *Usp. Khim.*, 2024, **93**, 1–62.
67 M. H. Karami, M. Abdouss, A. Rahdar and S. Pandey, *Inorg. Chem. Commun.*, 2024, **161**, 112032.
68 D. Gaikwad, R. Bobade, V. Suryawanshi, U. Nakate, S. Shaikh, A. M. Al-Enizi, N. Dabke, B. Lokhande and R. C. Ambare, *J. Mater. Sci.: Mater. Electron.*, 2024, **35**, 363.
69 S. Rahayu and M. Lee, *J. Phys.: Conf. Ser.*, 2024, **2733**, 012028.
70 R. McGonigle, J. Glasgow, C. Houston, I. Cameron, C. Homann, D. J. Black, R. Pal and L. E. MacKenzie, *Commun. Chem.*, 2025, **8**, 1–7.
71 A. Drozdowski, D. Poelman, M. Runowski, H. Hemmerich, F. Rivera-López and T. Grzyb, *J. Mater. Chem. C*, 2024, **12**, 13040–13049.
72 S. Wang, H. Liang, Z. Yang, Z. Wang, B. Yang and C. Lu, *RSC Adv.*, 2024, **14**, 17350–17354.
73 B. Mahto, B. Mahanty, S. Hait and S. Hussain, *Mater. Sci. Eng.*, 2024, **304**, 117386.
74 H. Liu, X. Zhong, Q. Pan, Y. Zhang, W. Deng, G. Zou, H. Hou and X. Ji, *Coord. Chem. Rev.*, 2024, **498**, 215468.
75 F. R. U. Cortes, E. Falomir, C. Doñate-Buendía and G. Mínguez-Vega, *J. Phys. Chem. C*, 2025, **129**, 10378–10414.
76 A. Lakmal, P. B. Thombre and C. E. Shuck, *Acc. Chem. Res.*, 2024, **57**, 3007–3019.
77 Z. U. D. Babar, V. Iannotti, G. Rosati, A. Zaheer, R. Velotta, B. Della Ventura, R. Álvarez-Diduk and A. Merkoçi, *Chem. Soc. Rev.*, 2025, **54**, 3387–3440.
78 M. Naguib, M. W. Barsoum and Y. Gogotsi, *Adv. Mater.*, 2021, **33**, 2103393.
79 K. C. Chan, X. Guan, T. Zhang, K. Lin, Y. Huang, L. Lei, Y. Georgantas, Y. Gogotsi, M. A. Bissett and I. A. Kinloch, *J. Mater. Chem. A*, 2024, **12**, 25165–25175.
80 Y. Wei, P. Zhang, R. A. Soomro, Q. Zhu and B. Xu, *Adv. Mater.*, 2021, **33**, 2103148.
81 Z. Y. Pan, C. Z. Huang, L. Zhan and J. Zhou, *TrAC, Trends Anal. Chem.*, 2023, **164**, 117090.
82 J. Z. Wu, S. A. Ghopry, B. Liu and A. Shultz, *Micromachines*, 2023, **14**, 1393.
83 A. Pakravan, M. Azizi, F. Rahimi, F. Bani, F. Mahmoudzadeh, R. Salehi and M. Mahkam, *Cancer Nanotechnol.*, 2021, **12**, 1–26.
84 Y.-B. Guo, J. Zhu, G.-J. Weng, J.-J. Li and J.-W. Zhao, *Opt. Commun.*, 2024, **562**, 130562.
85 S. Mitra and M. Basak, *Mater. Today*, 2022, **57**, 225–261.
86 N. M. Ngo, H.-V. Tran and T. R. Lee, *ACS Appl. Nano Mater.*, 2022, **5**, 14051–14091.
87 B. Karadza, H. Van Avermaet, L. Mingabudinova, Z. Hens and Y. Meuret, *Photonics Res.*, 2021, **10**, 155–165.
88 H. S. Shim, M. Ko, S. Jeong, S. Y. Shin, S. M. Park, Y. R. Do and J. K. Song, *J. Phys. Chem. C*, 2021, **125**, 9965–9972.
89 Y. Lv, Y. Yuan, N. Hu, N. Jin, D. Xu, R. Wu, H. Shen, O. Chen and L. S. Li, *ACS Appl. Nano Mater.*, 2021, **4**, 2855–2865.
90 D. Roy, C. K. De, S. Ghosh, S. Mukherjee, S. Mandal and P. K. Mandal, *Phys. Chem. Chem. Phys.*, 2022, **24**, 8578–8590.
91 S. M. Click, PhD thesis, Vanderbilt University, 2023.
92 A. M. Wagner, J. M. Knipe, G. Orive and N. A. Peppas, *Acta Biomater.*, 2019, **94**, 44–63.
93 S. Lamon, H. Yu, Q. Zhang and M. Gu, *Light: Sci. Appl.*, 2024, **13**, 252.
94 M. K. Mahata, R. De and K. T. Lee, *Biomedicines*, 2021, **9**, 756.

 © 2025 The Author(s). Published by the Royal Society of Chemistry

Open Access Article. Published on 22 July 2025. Downloaded on 10/28/2025 10:32:42 AM.
This article is licensed under a Creative Commons Attribution-NonCommercial 3.0 Unported Licence.

95 F. Huang, N. Bagheri, L. Wang, H. Ågren, J. Zhang, J. Widengren and H. Liu, *J. Alloys Compd.*, 2023, **936**, 168149.
96 W. Wei, Y. Zhang, R. Chen, J. Goggi, N. Ren, L. Huang, K. K. Bhakoo, H. Sun and T. T. Y. Tan, *Chem. Mater.*, 2014, **26**, 5183–5186.
97 T. Zhou, Q. Cheng, L. Zhang, D. Zhang, L. Li, T. Jiang, L. Huang, H. Xu, M. Hu and S. Jing, *Chem. Eng. J.*, 2022, **438**, 135637.
98 X. Lin, X. Chen, W. Zhang, T. Sun, P. Fang, Q. Liao, X. Chen, J. He, M. Liu and F. Wang, *Nano Lett.*, 2018, **18**, 948–956.
99 J. Yang, H. Miao, J. Jing, Y. Zhu and W. Choi, *Appl. Catal., B*, 2021, **281**, 119547.
100 I. Shtepliuk, V. Khranovskyy and R. Yakimova, *Phys. Chem. Chem. Phys.*, 2017, **19**, 30445–30463.
101 S. Hu, A. Trinchi, P. Atkin and I. Cole, *Angew. Chem., Int. Ed.*, 2015, **54**, 2970–2974.
102 H. Nie, M. Li, Q. Li, S. Liang, Y. Tan, L. Sheng, W. Shi and S. X.-A. Zhang, *Chem. Mater.*, 2014, **26**, 3104–3112.
103 M.-H. Jang, S. H. Song, H. D. Ha, T. S. Seo, S. Jeon and Y.-H. Cho, *Carbon*, 2017, **118**, 524–530.
104 S. R. Singamaneni, J. van Tol, R. Ye and J. M. Tour, *Appl. Phys. Lett.*, 2015, **107**, 212402.
105 T. Kulahava, N. Belko, M. Parkhats, A. Bahdanava, S. Lepeshkevich, V. Chizhevsky and D. Mogilevtsev, *J. Photochem. Photobiol., B*, 2023, **248**, 112800.
106 F. Shahzad, A. Iqbal, H. Kim and C. M. Koo, *Adv. Mater.*, 2020, **32**, 2002159.
107 D. Xu, Z. Li, L. Li and J. Wang, *Adv. Funct. Mater.*, 2020, **30**, 2000712.
108 H. Wang, X. Li, B. Luo, K. Wei and G. Zeng, *Energy*, 2021, **227**, 120483.
109 T. Zhu, Q. Tang, Y. Zeng, S. Chen, Y. Yang, H. Wang, J. Chen, L. Guo and L. Li, *Spectrochim. Acta, Part A*, 2023, **293**, 122474.
110 T. M. Veloso, A. de Souza da Fonseca and G. Costa dos Santos, *F. Photon.*, 2022, **3**, 1018773.
111 S. Lee, C. H. Park, J. K. Kim, K. Ahn, H. Kwon, J. K. Kim, S. U. Park and H. J. Yeo, *Antioxidants*, 2023, **12**, 1686.
112 T. Pan, D. Lu, H. Xin and B. Li, *Light: Sci. Appl.*, 2021, **10**, 124.
113 W. A. Wan Mahari, W. A. Wan Razali, K. Waiho, K. Y. Wong, S. S. Foo, A. S. Kamaruzzan, C. J. C. Derek, N. L. Ma, J.-S. Chang, C.-D. Dong, Y. Chisti and S. S. Lam, *Chem. Eng. J.*, 2024, **485**, 149619.
114 D. C. Mukunda, J. Rodrigues, V. K. Joshi, C. R. Raghushaker and K. K. Mahato, *Biosens. Bioelectron.*, 2022, **209**, 114230.
115 J. A. Hagen, W. Li, A. Steckl and J. Grote, *Appl. Phys. Lett.*, 2006, **88**, 171109.
116 K.-W. Lee, Y. Wan, Z. Huang, Q. Zhao, S. Li and C.-S. Lee, *Adv. Mater.*, 2024, **36**, 2306492.
117 Y.-Y. Pei, J.-T. Wang, L. Yuan, Y. Luo, X.-Y. Niu, X. Rong, L. Jin and Q.-F. Li, *Int. J. Biol. Macromol.*, 2023, **235**, 123865.
118 J. Xu, H. Zhang, Z. Guo, C. Zhang, H. Tan, G. Gong, M. Yu and L. Xu, *Int. J. Biol. Macromol.*, 2023, **230**, 123195.
119 M. Hirano, R. Ando, S. Shimozono, M. Sugiyama, N. Takeda, H. Kurokawa, R. Deguchi, K. Endo, K. Haga and R. Takai-Todaka, *Nat. Biotechnol.*, 2022, **40**, 1132–1142.
120 L. Niklaus, S. Tansaz, H. Dakhil, K. T. Weber, M. Pröschel, M. Lang, M. Kostrzewa, P. B. Coto, R. Detsch, U. Sonnewald and A. Wierschem, *Adv. Funct. Mater.*, 2017, **27**, 1601792.
121 E. Delamarche, I. Pereiro, A. Kashyap and G. V. Kaigala, *Langmuir*, 2021, **37**, 9637–9651.
122 C. F. Aguino, M. Lang, V. Fernández-Luna, M. Pröschel, U. Sonnewald, P. B. Coto and R. D. Costa, *ACS Omega*, 2018, **3**, 15829–15836.
123 S. Sadeghi, R. Melikov, D. Conkar, E. N. Firat-Karalar and S. Nizamoglu, *Adv. Mater. Technol.*, 2020, **5**, 2000061.
124 S. Kim, C. Cui, J. Huang, H. Noh, D. H. Park and D. J. Ahn, *Adv. Mater.*, 2020, **32**, 2005238.
125 R. J. Mazuski, S. A. Díaz, R. E. Wood, L. T. Lloyd, W. P. Klein, D. Mathur, J. S. Melinger, G. S. Engel and I. L. Medintz, *J. Phys. Chem. Lett.*, 2020, **11**, 4163–4172.
126 D. Chen, T. Xu, Y. Dou and T. Li, *ACS Nano*, 2024, **18**, 21873–21885.
127 B. Mizaikoff, *Chem. Soc. Rev.*, 2013, **42**, 8683–8699.
128 B. Tian and C. M. Lieber, *Chem. Rev.*, 2019, **119**, 9136–9152.
129 P. A. Belov, Y. Hao and S. Sudhakaran, *Phys. Rev. B: Condens. Matter Mater. Phys.*, 2006, **73**, 033108.
130 K. Boeneman, D. E. Prasuhn, J. B. Blanco-Canosa, P. E. Dawson, J. S. Melinger, M. Ancona, M. H. Stewart, K. Susumu, A. Huston and I. L. Medintz, *J. Am. Chem. Soc.*, 2010, **132**, 18177–18190.
131 S. Lu, J. Yang, H. Xing, Y. Chang, J. Sun, C. Guo and X. Yang, *Biosens. Bioelectron.*, 2023, **224**, 115080.
132 T. Zhang, X. Sun, X. Chen, W. Chen, H. Tang and C.-Y. Li, *Biosens. Bioelectron.*, 2024, **259**, 116412.
133 F. Nicoli, A. Barth, W. Bae, F. Neukirchinger, A. H. Crevenna, D. C. Lamb and T. Liedl, *ACS Nano*, 2017, **11**, 11264–11272.
134 H. Lv, N. Xie, M. Li, M. Dong, C. Sun, Q. Zhang, L. Zhao, J. Li, X. Zuo, H. Chen, F. Wang and C. Fan, *Nature*, 2023, **622**, 292–300.
135 S. A. Díaz, Y. C. Kim, P. D. Cunningham, D. Mathur, I. L. Medintz, D. L. Kellis, B. Yurke, W. B. Knowlton and J. S. Melinger, *ACS Appl. Opt. Mater.*, 2024, **3**, 494–506.
136 A. K. Adamczyk, T. A. Huijben, K. Kolataj, F. Zhu, R. Marie, F. D. Stefani and G. P. Acuna, *arXiv* preprint arXiv:2402.06292, 2024.
137 N. Martino, S. J. Kwok, A. C. Liapis, S. Forward, H. Jang, H.-M. Kim, S. J. Wu, J. Wu, P. H. Dannenberg and S.-J. Jang, *Nat. Photonics*, 2019, **13**, 720–727.
138 K. Kikuchi, L. D. Adair, J. Lin, E. J. New and A. Kaur, *Angew. Chem.*, 2023, **135**, e202204745.
139 J. Li, *Sens. Actuators Rep.*, 2020, **2**, 100018.
140 H. Lu, O. Alkhazragi, Y. Wang, N. Almaymoni, W. Yan, W. H. Gunawan, H. Lin, T.-Y. Park, T. K. Ng and B. S. Ooi, *npj Nanophoton.*, 2024, **1**, 9.
141 X. Fan and S. H. Yun, *Nat. Methods*, 2014, **11**, 141–147.
142 Y. C. Chen and X. Fan, *Adv. Opt. Mater.*, 2019, **7**, 1900377.
143 M. Humar and S. H. Yun, *Optica*, 2017, **4**, 222–228.

Open Access Article. Published on 22 July 2025. Downloaded on 10/28/2025 10:32:42 AM.
This article is licensed under a Creative Commons Attribution-NonCommercial 3.0 Unported Licence.

144 Q. Chen, X. Zhang, Y. Sun, M. Ritt, S. Sivaramakrishnan and X. Fan, *Lab Chip*, 2013, **13**, 2679–2681.
145 Z. Yuan, X. Tan, X. Gong, C. Gong, X. Cheng, S. Feng, X. Fan and Y.-C. Chen, *Nanoscale*, 2021, **13**, 1608–1615.
146 A. K. Jaiswal, A. Hokkanen, V. Kumar, T. Mäkelä, A. Harlin and H. Orelma, *ACS Appl. Mater. Interfaces*, 2021, **13**, 25346–25356.
147 Y. Zhang, C. Zhang, Y. Fan, Z. Liu, F. Hu and Y. S. Zhao, *ACS Appl. Mater. Interfaces*, 2021, **13**, 19187–19192.
148 T. Van Nguyen, N. Van Pham, H. H. Mai, D. C. Duong, H. H. Le, R. Sapienza and V.-D. Ta, *Soft Matter*, 2019, **15**, 9721–9726.
149 X. Gong, S. Feng, Z. Qiao and Y.-C. Chen, *Anal. Chem.*, 2021, **93**, 5823–5830.
150 Y. Yang, G. Mao, X. Ji and Z. He, *J. Mater. Chem. B*, 2020, **8**, 9–17.
151 C. Gong, X. Yang, S.-J. Tang, Q.-Q. Zhang, Y. Wang, Y.-L. Liu, Y.-C. Chen, G.-D. Peng, X. Fan and Y.-F. Xiao, *Light: Sci. Appl.*, 2023, **12**, 292.
152 X. Gong, Z. Qiao, P. Guan, S. Feng, Z. Yuan, C. Huang, G.-E. Chang and Y.-C. Chen, *Adv. Photonics Res.*, 2020, **1**, 2000041.
153 J. Conde, J. Rosa, J. C. Lima and P. V. Baptista, *Int. J. Photoenergy*, 2012, **2012**, 619530.
154 X. Zhu, Y. Zhang, M. Liu and Y. Liu, *Biosens. Bioelectron.*, 2021, **171**, 112730.
155 G. Janith, H. Herath, N. Hendeniya, D. Attygalle, D. Amarasinghe, V. Logeeshan, P. Wickramasinghe and Y. Wijayasinghe, *J. Pharm. Biomed. Anal.*, 2023, 100019.
156 H. Liu, Y. Wang, S. Huang, J. Tai, X. Wang, X. Dai, C. Qiu, D. Gu, W. Yuan and H.-P. Ho, *Anal. Chem.*, 2024, **96**, 8791–8799.
157 J. Lv, J. Wang, L. Yang, W. Liu, F. Haihao, P. K. Chu and C. Liu, *Sens. Diagn.*, 2024, **3**, 1369–1391.
158 V. Kravets, R. Jalil, Y.-J. Kim, D. Ansell, D. Aznakayeva, B. Thackray, L. Britnell, B. Belle, F. Withers and I. Radko, *Sci. Rep.*, 2014, **4**, 5517.
159 Y. V. Stebunov, D. I. Yakubovsky, D. Y. Fedyanin, A. V. Arsenin and V. S. Volkov, *Langmuir*, 2018, **34**, 4681–4687.
160 W. Li, Y. Qiu, L. Zhang, L. Jiang, Z. Zhou, H. Chen and J. Zhou, *Biosens. Bioelectron.*, 2016, **79**, 500–507.
161 M. Azharuddin, G. H. Zhu, D. Das, E. Ozgur, L. Uzun, A. P. Turner and H. K. Patra, *Chem. Commun.*, 2019, **55**, 6964–6996.
162 Y. Fang, L. Jiang, Y. Zhou and S. Jin, *ACS Appl. Nano Mater.*, 2024, **7**, 10648–10659.
163 W. Wen, W. Qiong, R. Sheng-Nan, L. Zhuo and C. Fang-Fang, *Chin. J. Inorg. Anal. Chem.*, 2022, **50**, 13–18.
164 Q. Wu, N. Li, Y. Wang, Y. Xu, J. Wu, G. Jia, F. Ji, X. Fang, F. Chen and X. Cui, *Anal. Chem.*, 2020, **92**, 3354–3360.
165 M. Chen, Y. Xie and M. Li, *Nano Lett.*, 2024, **24**, 11520–11528.
166 R. Boudries, H. Williams, S. Paquereau–Gaboreau, S. Bashir, M. Hojjat Jodaylami, M. Chisanga, L.-É. Trudeau and J.-F. Masson, *ACS Nano*, 2024, **18**, 22620–22647.
167 C. Lin, Y. Li, Y. Peng, S. Zhao, M. Xu, L. Zhang, Z. Huang, J. Shi and Y. Yang, *J. Nanobiotechnol.*, 2023, **21**, 149.
168 W. Wu, J. C. Ranasinghe, A. Chatterjee and S. Huang, *Mater. Chem. Phys.*, 2024, **318**, 129281.
169 J. Mi, Y. Yuan, X. Hao, Y. Lin and J. Shi, *ACS Appl. Nano Mater.*, 2024, **7**, 13664–13671.
170 M. Wang, K. Zhang, L. Yue, X. Liu, Y. Lai and H. Zhang, *ACS Appl. Nano Mater.*, 2024, **7**, 13672–13680.
171 Z. Wu, M. Sha, D. Ji, H. Zhao, L. Li and Y. Lei, *ACS Appl. Nano Mater.*, 2024, **7**, 11–31.
172 W. M. Pazin, L. N. Furini, D. C. Braz, M. Popolin-Neto, J. D. Fernandes, C. J. Leopoldo Constantino and O. N. Oliveira Jr, *ACS Appl. Nano Mater.*, 2024, **7**, 2335–2342.
173 Z. Wang, J. Ye, K. Zhang, L. Ding, T. Granzier-Nakajima, J. C. Ranasinghe, Y. Xue, S. Sharma, I. Biase and M. Terrones, *ACS Nano*, 2022, **16**, 6426–6436.
174 C.-Y. Xi, M. Zhang, L. Jiang, H.-Y. Chen, J. Lv, Y. He, M. E. Hafez, R.-C. Qian and D.-W. Li, *Sens. Actuators, B*, 2022, **369**, 132264.
175 H. Sohrabi, R. Mahmoudi-Maleki, M. R. Majidi, F. Oroojalian, A. A. Mokhtarzadeh and M. de la Guardia, *TrAC, Trends Anal. Chem.*, 2024, **176**, 117753.
176 D. A. Hastman, S. Hooe, M. Chiriboga, S. A. Díaz, K. Susumu, M. H. Stewart, C. M. Green, N. Hildebrandt and I. L. Medintz, *ACS Sens.*, 2023, **9**, 157–170.
177 N. Ma, J. Zhang, J. Kong and X. Zhang, *Anal. Chem.*, 2024, **96**, 8450–8457.
178 Y. K. Park, W. Y. Jung, M. G. Park, S. K. Song, Y. S. Lee, H. Heo and S. Kim, *MedChemComm*, 2017, **8**, 2228–2232.
179 L.-M. Zhang, Q.-X. Gao, J. Chen, B. Li, M.-M. Li, L. Zheng, J.-X. Chen and W.-J. Duan, *Anal. Chim. Acta*, 2022, **1192**, 339382.
180 M. Jiang, J. Zhou, Y. Chai and R. Yuan, *Anal. Chem.*, 2024, **96**, 9866–9875.
181 V. Lamberti, M. Dolci and P. Zijlstra, *ACS Nano*, 2024, **18**, 5805–5813.
182 Y. Ma, M. Song, L. Li, X. Lao, Y. Liu, M.-c. Wong, M. Yang, H. Chen and J. Hao, *Biosens. Bioelectron.*, 2024, **243**, 115778.
183 J. Zhu, S. Xu, L. Zhou, Q. Zeng, Y. Wang, M. Yan and H. Liu, *Anal. Chem.*, 2024, **96**, 12584–12592.
184 L. P. Cao, Y. Wang, Y. Bai, Y. J. Jiang, C. M. Li, H. Zuo, Y. F. Li, S. J. Zhen and C. Z. Huang, *ACS Appl. Nano Mater.*, 2021, **4**, 2849–2854.
185 X. Geng, X. Liang, Y. Liu, Y. Chen, B. Xue, X. Wei and Z. Yuan, *ACS Nano*, 2024, **18**, 9187–9198.
186 X. Jiang, P. Tang, P. Gao, Y. S. Zhang, C. Yi and J. Zhou, *Anal. Chem.*, 2017, **89**, 2561–2568.
187 J. Yao, T. Muñoz-Ortiz, F. Sanz-Rodríguez, E. Martin Rodriguez, D. H. Ortgies, J. García Solé, D. Jaque and R. Marin, *ACS Photonics*, 2022, **9**, 559–566.
188 Y. Liu, Z. Wang, Z. Xu and F. Lin, *ACS Appl. Nano Mater.*, 2023, **6**, 17691–17697.
189 S. K. Maurya, M. Mohan, R. Poddar, D. Senapati, S. Singh, A. Roy, A. K. Munirathnappa, J. C. G. E. da Silva and K. Kumar, *J. Phys. Chem. C*, 2020, **124**, 18366–18378.
190 Q. Fu, R. Zhu, J. Song, H. Yang and X. Chen, *Adv. Mater.*, 2019, **31**, 1805875.

 © 2025 The Author(s). Published by the Royal Society of Chemistry

Open Access Article. Published on 22 July 2025. Downloaded on 10/28/2025 10:32:42 AM. This article is licensed under a Creative Commons Attribution-NonCommercial 3.0 Unported Licence.

191 E. Alchera, M. Monieri, M. Maturi, I. Locatelli, E. Locatelli, S. Tortorella, A. Sacchi, A. Corti, M. Nebuloni and R. Lucianò, *Photoacoustics*, 2022, **28**, 100400.
192 I.-C. Sun, D. S. Dumani and S. Y. Emelianov, *ACS Nano*, 2024, **18**, 3575–3582.
193 M. Kim, K. P. Kubelick, D. Vanderlaan, D. Qin, J. Lee, A. Jhunjhunwala, M. Cadena, R. J. Nikolai, J. Kim and S. Y. Emelianov, *Nano Lett.*, 2024, **24**, 7202–7210.
194 L. C.-C. Lee and K. K.-W. Lo, *Chem. Rev.*, 2024, **124**, 8825–9014.
195 T. Zhou and Z. Li, *Sci. China Mater.*, 2024, **68**, 86–104.
196 T. Zhou, C. Hu, K. He and Z. Li, *Anal. Chem.*, 2024, **96**, 17840–17849.
197 S. Li, Q. Ma, C. Wang, K. Yang, Z. Hong, Q. Chen, J. Song, X. Song and H. Yang, *Anal. Chem.*, 2022, **94**, 2641–2647.
198 W. Wanas, S. A. Abd El-Kareem, S. Ebrahim, M. Soliman and M. Karim, *Sci. Rep.*, 2023, **13**, 27.
199 R. Wang, L. Zou, Z. Yi, Z. Zhang, M. Zhao and S. Shi, *Int. J. Pharm.*, 2023, **639**, 122944.
200 X. Chen, Z. Chen, T. Zhang, W. Chen, H. Tang and C.-Y. Li, *Chem. Eng. J.*, 2024, **496**, 154268.
201 W.-L. Chen, Z. Chen, X.-X. Chen, T.-T. Zhang, H.-W. Tang and C.-Y. Li, *Anal. Chem.*, 2024, **96**, 14020–14027.
202 M.-K. Xin, X. Sun, H.-W. Tang and C.-Y. Li, *Anal. Chem.*, 2024, **96**, 7101–7110.
203 J. Son, G. Yi, J. Yoo, C. Park, H. Koo and H. S. Choi, *Adv. Drug Delivery Rev.*, 2019, **138**, 133–147.
204 X. Qi, Y. Xiang, E. Cai, X. Ge, X. Chen, W. Zhang, Z. Li and J. Shen, *Coord. Chem. Rev.*, 2023, **496**, 215426.
205 S. Barik, P. K. Namdeo and R. K. Sharma, *ChemistrySelect*, 2024, **9**, e202400587.
206 J. Chen, C. Ning, Z. Zhou, P. Yu, Y. Zhu, G. Tan and C. Mao, *Prog. Mater. Sci.*, 2019, **99**, 1–26.
207 M. L. Taylor, R. E. Wilson Jr, K. D. Amrhein and X. Huang, *Bioengineering*, 2022, **9**, 200.
208 Y. Zengin, D. Kelle and B. Iyisan, *Macromol. Rapid Commun.*, 2024, **45**, 2400497.
209 X. Yu, S. Fan, B. Zhu, S. I. El-Hout, J. Zhang and C. Chen, *Green Energy Environ.*, 2024, DOI: 10.1016/j.gee.2024.09.002.
210 M. Saqlain, M. A. Baqir and P. K. Choudhury, *IEEE Trans. Nanotechnol.*, 2024, **23**, 652–657.
211 A. Khajuria, H. K. Alajangi, A. Sharma, H. Kaur, P. Sharma, S. Negi, L. Kumari, M. Trivedi, A. K. Yadav and R. Kumar, *Discover Nano*, 2024, **19**, 145.
212 P. Xiong, X. Wei, L. Zhou, W. Zhou, M. Li, Y. Ge, J. Zou, S. Peng, L. Jiang, L. Tian and Y. Liu, *Adv. Funct. Mater.*, 2024, **34**, 2405124.
213 L. Xiao, X. Chen, X. Yang, J. Sun and J. Geng, *ACS Appl. Polym. Mater.*, 2020, **2**, 4273–4288.
214 L. Chen, X. Li, M. Xiong, Y. Zhao, S. Liu, C. Li and K. Wang, *Mater. Des.*, 2023, **225**, 111532.
215 X. Li, S. Kolemen, J. Yoon and E. U. Akkaya, *Adv. Funct. Mater.*, 2017, **27**, 1604053.
216 J. H. Correia, J. A. Rodrigues, S. Pimenta, T. Dong and Z. Yang, *Pharmaceutics*, 2021, **13**, 1332.
217 K. Moloudi, H. Abrahamse and B. P. George, *Mater. Adv.*, 2024, **5**, 6185–6195.
218 M. Li, Y. Wang, H. Lin and F. Qu, *Mater. Sci. Eng., C*, 2019, **96**, 591–598.
219 Q.-B. Chen, M. Qi, M. Yang, Z.-Q. Luo, Q. Yuan, T. Peng, J. Wang, T. Zou and H. Wang, *Colloids Surf., B*, 2024, **242**, 114076.
220 F. Duan, Q. Jia, G. Liang, M. Wang, L. Zhu, K. J. McHugh, L. Jing, M. Du and Z. Zhang, *ACS Nano*, 2023, **17**, 11290–11308.
221 B. Zheng, R. Zhang, F. Kuang, T. Hui, C. Fu, L. Zhang, C. Zhou, M. Qiu and B. Yue, *J. Mater. Chem. B*, 2024, **12**, 1816–1825.
222 Y. Chen, D. Li, Y. Zhong, Z. Lu and D. Wang, *Int. J. Biol. Macromol.*, 2023, **235**, 123683.
223 C. Yu, J. Schimelman, P. Wang, K. L. Miller, X. Ma, S. You, J. Guan, B. Sun, W. Zhu and S. Chen, *Chem. Rev.*, 2020, **120**, 10695–10743.
224 D. Qinyuan, W. Zhuqing, L. Qing, L. Yunsong, Z. Ping, Z. Xiao, N. Yuting, L. Hao, Z. Yongsheng and L. Longwei, *Biomater. Adv.*, 2024, **159**, 213804.
225 N. Al-Jawuschi, S. Chen, N. Abie, T. Fischer, S. Fare and H. H. Maleki, *Langmuir*, 2023, **39**, 4326–4337.
226 S. Sun, H.-W. Liang, H. Wang and Q. Zou, *ACS Nano*, 2022, **16**, 18978–18989.
227 L. Qiao, H. Yang, S. Gao, L. Li, X. Fu and Q. Wei, *J. Mater. Chem. B*, 2022, **10**, 1908–1922.
228 W. Wang, P. Wang, X. Liao, B. Yang, C. Gao and J. Yang, *J. Med. Chem.*, 2023, **66**, 13103–13115.
229 L. Zhang, L. Dai, Y. Rong, Z. Liu, D. Tong, Y. Huang and T. Chen, *Langmuir*, 2015, **31**, 1164–1171.
230 C. S. Sia, B. T. Tey and L. E. Low, *Adv. Funct. Mater.*, 2024, **34**, 2314278.
231 T. Park, J. W. Leem, Y. L. Kim and C. H. Lee, *Adv. Mater.*, 2025, 2418705.
232 G. Chen, Y. Lou, J. Li, L. Chen, Z. Xing, T. Zhang, D. Gu, Y. Peng and H. Wu, *ACS Mater. Lett.*, 2024, **6**, 648–655.
233 J. H. Sim, H. Chae, S.-B. Kim, S. B. Shin, H. K. Hong, H. Cho, Y. H. Jung, D. Lee, M. Kim and S. Hahn, *ACS Nano*, 2025, **54**, 3441–3474.
234 N. Ya, D. Zhang, Y. Wang, Y. Zheng, M. Yang, H. Wu and G. Oudeng, *Nanoscale*, 2024, **16**, 13784–13801.
235 K. Hamad-Schifferli, in *Trends in Biosensing Research: Advances, Challenges and Applications*, ed. F. Lisdat and N. Plumeré, Springer International Publishing, Cham, 2024, pp. 185–221.
236 S.-C. Chuang, S.-A. Yu, P.-C. Hung, H.-T. Lu, H.-T. Nguyen and E.-Y. Chuang, *Photonics*, 2023, **10**, 1124.
237 Y. Wang, M. Li and Y. Wang, *Chin. Opt. Lett.*, 2020, **18**, 080004.
238 C. He, L. Yu, L. Ding, H. Yao, Y. Chen and Y. Hao, *Biomaterials*, 2020, **255**, 120181.
239 S. Sharma, S. Das, B. Soni and M. Sabir, in *Artificial Intelligence and Edge Computing for Sustainable Ocean Health*, ed. D. De, D. Sengupta and T. A. Tran, Springer Nature Switzerland, Cham, 2024, pp. 359–385.

Open Access Article. Published on 22 July 2025. Downloaded on 10/28/2025 10:32:42 AM.
This article is licensed under a Creative Commons Attribution-NonCommercial 3.0 Unported Licence.

240 C. Adamopoulos, H.-S. Oh, S. Buchbinder, P. Zarkos, P. Bhargava, A. Gharia, A. M. Niknejad, M. Anwar and V. Stojanović, *IEEE J. Solid-State Circuits*, 2024, **59**, 2907–2921.
241 T. Kurdadze, F. Lamadie, K. A. Nehme, S. Teychené, B. Biscans and I. Rodriguez-Ruiz, *Sensors*, 2024, **24**, 1529.
242 M. Zhou, S. Jiang, X. Yang, Q. Li, B. Jiang, L. Zhou and L. Zhang, *J. Mater. Res. Technol.*, 2024, **33**, 874–883.
243 Y. Li, Y. Guo, H. Chen, X. Xiao, F. Long, H. Zhong, K. Wang, Z. Guo, Z. Zhuang and Z. Liu, *ACS Photonics*, 2024, **11**, 613–625.
244 Y. Kang, J. Zhao, Y. Zeng, X. Du and Z. Gu, *Small*, 2024, **20**, 2403525.
245 P. Kaur, N. Nazeer, V. Gurjar, R. Tiwari and P. K. Mishra, *Drug Discovery Today*, 2024, **29**, 104086.
246 R. Prasad, R. Kumari, R. Chaudhari, R. Kumar, G. C. Kundu, S. Kumari, G. Roy, M. Gorain and P. Chandra, *ACS Appl. Mater. Interfaces*, 2024, **16**, 53393–53404.
247 D. Sourvanos, T. C. Zhu, A. Dimofte, T. M. Busch, W. Yang, J. Burrell, R. Neiva, T. Schoenbaum, Z. Chen and K. I. Ko, *Biophotonics and Immune Responses XIX*, 2024, vol. 128, pp. 19–29.
248 T. Guo, Z. Zhang, Z. Lin, J. Tian, Y. Jin, J. Evans, Y. Xu and S. He, *Nat. Nanotechnol.*, 2024, **19**, 1635–1643.
249 F. Wang, X. Wang, X. Lu and C. Huang, *Biosensors*, 2024, **14**, 39.
250 P. K. Mishra and R. Shandilya, *Nanomedicine*, 2020, **15**, 1541–1544.
251 E. N. Gerasimova, L. I. Fatkhutdinova, I. I. Vazhenin, E. I. Uvarov, E. Vysotina, L. Mikhailova, P. A. Lazareva, D. Kostyushev, M. Abakumov and A. Parodi, *Nanophotonics*, 2024, **13**, 4111–4125.
252 L. Egen, G. S. Demmel, M. Grilli, A. Studier-Fischer, F. Nickel, C. M. Haney, J. Mühlbauer, F. O. Hartung, H. S. Menold and P. Piazza, *Eur. Urol. Focus.*, 2024, **9**, 248–258.
253 Á. Barreda, F. Vitale, A. E. Minovich, C. Ronning and I. Staude, *Adv. Photonics Res.*, 2022, **3**, 2100286.
254 E. Adibnia, M. Ghadrdan and M. A. Mansouri-Birjandi, *Sci. Rep.*, 2024, **14**, 21094.
255 M. Zhu, S. Abdollahramezani, C. Li, T. Fan, H. Harutyunyan and A. Adibi, *Nanophotonics*, 2022, **11**, 2727–2735.
256 D. Gostimirovic, D.-X. Xu, O. Liboiron-Ladouceur and Y. Grinberg, *ACS Photonics*, 2022, **9**, 2623–2633.
257 D. Gostimirovic, Y. Grinberg, D.-X. Xu and O. Liboiron-Ladouceur, *ACS Photonics*, 2023, **10**, 1953–1961.
258 A. Mirza, A. Shafiee, S. Banerjee, K. Chakrabarty, S. Pasricha and M. Nikdast, *IEEE Trans. Nanotechnol.*, 2022, **21**, 763–771.

 © 2025 The Author(s). Published by the Royal Society of Chemistry